ASSESSMENT OF SEQUENTIAL EXTRACTIONS: IMPLICATIONS FOR ISOTOPIC COMPOSITION OF AUTHIGENIC OXIDES AND DETRITAL RESIDUES AS PALEOCEANOGRAPHIC PROXIES

A Dissertation

by

CLAIRE CECELIA MCKINLEY

Submitted to the Office of Graduate and Professional Studies of
Texas A&M University
in partial fulfillment of the requirements for the degree of

DOCTOR OF PHILOSOPHY

Chair of Committee, Deborah Thomas
Committee Members, Franco Marcantonio
Leah LeVay
Jessica Fitzsimmons
Head of Department, Shari Yvon-Lewis

August 2018

Major Subject: Oceanography

ABSTRACT

Constraints on characteristics of past oceans-- ocean circulation, sedimentation processes, and sources of dissolved trace metals-- are vital because they contribute to our understanding of heat transport, atmospheric conditions, and productivity. Proxies that record information about these processes in marine sediment are key to understanding the ocean's role in past climate. This dissertation looks in depth at how the Neodymium (Nd) and Lead (Pb) isotopic composition (IC) of fish debris, sequentially extracted oxide coatings, and "detrital" residues are used as proxies for ocean circulation and sediment composition.

We first present a reconstruction of ocean circulation in the Cenozoic Pacific Ocean employing Neodymium IC of fossil fish Debris and oxide coatings based on Deep Sea Drilling Program (DSDP), Ocean Drilling Program (ODP), and Integrated Ocean Drilling Program (IODP) sites spanning the North and South Pacific. The South Pacific becomes slowly less radiogenic, after 35Ma as the gradient between the North and South Pacific increases. This, combined with the North Pacific becoming more radiogenic (seemingly because of non-conservative mixing of Nd) indicates that there is a fundamental transition in the North Pacific from surface ventilated deep-water formation to circulation dominated by sluggish diffusive mixing.

There are two main results from The South Pacific becomes slowly less radiogenic, after 35Ma the gradient between the North and South Pacific increases. This indicates a fundamental transition in the North Pacific from surface ventilated deep-water formation to circulation dominated by sluggish diffusive mixing.

Then I preform an assessment of the fidelity and reproducibility of the leaching procedure we use to isolate the Fe-Mn oxyhydroxide coatings.. Our procedure entails a two-step leach with a Hydroxylamine-Hydrochloride mixture: Leach 1 targets the Fe-Mn oxide coatings and is 1 hour, and Leach 2, is 24 hours designed to remove remaining Fe-Mn oxides from the detrital residue. In order to analyze leach reproducibility we performed replicate analysis of a USGS certified reference material (MAG-1) and an in house internal standard from the central Atlantic (INTL-STD-A). We also performed an assessment of the geochemistry of two sites (IODP Sites 1149 and U1370) from the Pacific.

Finially we evaluate which geochemical phases are mobilized by each step of our sequential leaching procedure at Site 1149 and U1370. We utilize a novel multivariate statistical assessment of major, trace and rare earth elements to identify their sources and the sources relationship with the Nd and Pb isotopic composition.

DEDICATION

To my Grandma Elizabeth “Anne” Jackets, who instilled in me the importance of education and reproductive rights for women, and who went back to school when her oldest was in High School and eventually became an English Professor. To my Grandma Eleanor “Pat” McKinley whose kindness, thoughtfulness and joy has permeates throughout the McKinley Family.

ACKNOWLEDGEMENTS

The culmination of this work would not have been possible if not for the support of my family, community and mentors. I would specifically like to thank my advisor Dr. Debbie Thomas for supporting me and allowing me to follow where my research and curiosity lead, for helping me to build a project that combined paleoceanography and geochemistry in a way that played to my strengths and developed my skills. This dissertation was supervised with considerable help from Dr. Rachel Scudder, a Thomas Lab Post Doc, and my dissertation committee: Dr. Leah LeVay, Dr. Franco Marcantonio, and Dr. Jessica Fitzsimmons. I would also like to acknowledge Rick Murrary, Rob Pokalany, Brent Miller, Suzanne O'Connell and Gloria Lima. Who have been my mentors and friends.

Dr. Rachel Scudder, my friend and mentor has played an instrumental role in my success as a scientist. It was on a trip to College Station to sample at IODP December of my senior year of college that we talked at length about the possibility of grad school. It has been extreamly helpful to be able to see Rachel go through the process of defending, and becoming an early carrer scientist.

The Multnomah County Education Service District's Outdoor School Program instilled a love of science in me. I attented Collins Outdoor School with my 6th grade class, and I discovered my love of teaching when I volunteered at Namanu outdoor school as a highschool student. I am extremely proud to have been on staff at Angelos Outdoor School with some of the brightest and kindest human beings on the planet. I would not have become a scientist if Outdoor School had not been a part of my life. Finially I would like to acknowledge the Namanu Outdoor School staff from 2015 to present. They have welcomed me into their community and created a

space where I (and countless High School Mentees) have been able to find a footing closer to the person I want to be, closer to my best self. They truly are the best placed based science educators in the game and I would not have perserveared through the PhD with out their love and support.

I would also like to thank my family for constanly showing up for me, and everyone in their communities. They are truly good citizens and community members and I am so greatful for their example. Robert “Bear” Levine my partner has unwavering confidenice in me. He has also done most of the cooking since October of 2017, and most importantly makes me laugh.

Maya Reimi who defended this spring as well has been my accountability and dissertation buddy. There is a story in my family about my Grandpa Bob and his best friend Jonnny falling in the Icicile River while fishing. Neither of them could swim, and my Grandpa Bob had a bad leg, and so they took turns pushing off eachother, and bobbing up for air. They seesawed like that all the back to the shore (and lost a new fishing rod). Maya and I have been trading having our heads underwater and leading on the other person for five years, she is generous with her time and dedicated to her community. I am endlessly impressed with her grace, and grateful for her friendship.

I would not have made it this far without the Graduate students in the Thomas Lab Group: Zach Rolewicz, Ty Cobb, and Jenna Patten. Everyone who has lived in the house on Richards has become a member of my family, and made my time in College Station feel like home: Ali Snell, Monica Barbery, Chelsea Berry, Natalie Zelinski, Stephanie Durkacz, and Mike Evans. My paper reading group Ann Dunlea, Emily Estes, Chloe Anderson and Rachel Scudder. They are smart, kind and generous women who elevate the work that I do.

Finially, take care of youself in gradschool is a challenge. I have worked very hard to maintain my health, and be open about how much work it takes to do so. I would like to thank

my health care team, finding a good doctor, dentist, eye doctor and hair cutter was the first time I thought to myself “I am going to make it in this place”. So thank you to Dr. Amy Hinton, Dr. Tiffany Skaggs, Dr. Belinda Dobson, Willimas family dentistry, Dr, Nancy Welsh, Dr, Kerry Hope, Everyone in the Maturae Aggie Women Group, Pete Rosencranz and Shelly Strom.

CONTRIBUTORS AND FUNDING SOURCES

Contributors

This dissertation was supervised by Dr. Debbie Thomas with considerable help from Dr. Rachel Scudder, a Thomas Lab Post Doc, and my dissertation committee: Dr. Leah LeVay, Dr. Franco Marcantonio, and Dr. Jessica Fitzsimmons.

This work was designed by Claire C. McKinley, Debbie Thomas and Rachel Scudder. The samples were collected on several IODP legs and we sampled them ourselves at the Gulf Coast Core Repository. Christina Stubt wrote the Thomas lab group lab manual and Zach Rolewiz trained Claire McKinley in the radiogenic geochemical methods. Throughout time several undergraduate students (Alyssa Schultz, Jonathan Tybur, Samantha Bowers, and Calli Provenza) contributed to the sample preparation and column chemistry. We could not have performed the lab work a without the help of Luz Romero, and we could not have prerormed the analysis on the Thermal Ionization Mass Spectrometer with out Dr. Brent Miller.

Funding Sources

Claire McKinley has been funded by the Louis and Elizabeth Scherck Graduate Fellowship, for the Fall of 2013. She was also supported as an International Ocean Discovery Program Graduate Assistant Researcher from 2014 to 2015. Claire has also been supported in part by NSF S-STEM Grant Number DUE0806926 and DUE135580, and by an Ocean Drilling and Sustainable Earth Sciences (**ODASES**) fellowship. Additionally, Claire has been funded by several Oceanography and College of Geosciences scholarships including the Mr. and Mrs. Kenneth P. Pipes Scholarship (2016-2017), the Joe and Doris Watson Endowed Fellowship (2017-2018), and the Louis & Elizabeth Scherck Scholarship (2016-2017 and 2017-2018)

TABLE OF CONTENTS

Page

LIST OF FIGURES

Page

LIST OF TABLES

Page

1. INTRODUCTION

Characterizing deep-water circulation and its effect on global heat transport is critical for understanding the dynamics of past climate and predicting future climate. Global overturning circulation in the modern ocean is broadly dominated by air-sea heat exchange in high latitudes, leading to the convection and formation of the major water masses responsible for ~1/4 of the global heat transport system. In addition, this operating mode of overturning circulation influences global nutrient transport and carbon cycling (Talley, 2013). Modern global overturning circulation is characterized by surface ventilated (sourced) North Atlantic Deep-water and Antarctic Bottom Water, as well as diffusively formed Indian Deep-water and Pacific Deep-water (Talley, 2013). Given the importance of overturning circulation in modern heat transport, nutrient distributions, and carbon cycling, it is widely presumed that any changes in the operating mode of overturning circulation through time would have an impact on those processes. Thus understanding changes in ocean overturning patterns and, ideally, rates should provide valuable constraints on our understanding of the causes and consequences of variations in Earth's climate. For example, modern observations indicate a decrease in surface water salinity attributed to melting of the Greenland Ice sheet (Cesar et al., 2018; Rahmstorf et al., 2015). This trend is expected to cause, or may have already started to cause a decrease in the flux of North Atlantic Deep-water (NADW) and consequently a diminished rate of Atlantic Meridional Overturning Circulation (Thornalley et al., 2018). However, oceanographers and climate scientists are constrained by the short time-scales over which we have instrumental data to observe these trends. Establishing an accurate and spatially/temporally comprehensive

reconstruction of past overturning circulation variations and environmental conditions can provide context for the changes we are observing in the present.

One proxy widely applied to studies of paleocean-circulation exploits the marine geochemistry of Neodymium (Nd) and Lead (Pb). These radiogenic isotope tracers exploit several unique characteristics of Nd and Pb in the marine environment, and while both elements share some similarities in this regard they also have some important differences that also yield useful paleoceanographic information. The foundation of using Nd and Pb as paleocean-circulation tracers are based on five presumptions: 1) The dominant source of dissolved Nd and Pb to the oceans is presumed to be fluvial inputs; 2) Other sources of Nd and Pb to the oceans have been presumed negligible 3) The isotopic composition of the fluvial inputs reflects the regional geology drained by those fluvial systems – hence there is a relationship to provenance; 4) Both have short residence times in the oceans and thus have regional applicability; 5) Several sedimentary phases record and retain the composition of the dissolved Nd and Pb at the seafloor .

Recent studies and advances in sampling suggest that all of the presumed characteristics listed above may oversimplify the marine geochemical cycling of Nd and Pb, complicating their application as a water mass proxy. The concentration of Nd in the ocean follows the profile of a nutrient element, with low concentrations in the surface, and increasing concentration with depth (Bruland et al, 2014). However, the isotopic composition of Nd in the water column appears to behave quasi-conservatively, and "tag" water masses at their origin. The origin of the marine Nd has long been thought to be fluvial inputs. Water masses gain their signature from fluvial inputs near their origin and are slowly modified by mixing with other water masses and their distinct signatures. Water masses in the modern oceans have distinct Nd isotopic compositions from one another, consistent with established hydrographic water mass characteristics presumably due to

the short residence time of Nd. For instance a vertical profile sampling Antarctic Intermediate Water, North Atlantic Deep-water and Antarctic Bottom Water indicates that all retain distinct isotopic signatures throughout their transit in the Atlantic basins.

There is difficultly in reconciling the apparent conservative behavior of the isotopic composition of Nd with an increase in concentration of Nd along the path of ocean circulation. This mismatch between the concentration of Nd and the isotopic composition is called "The Nd Paradox" (Goldstein and Hemming, 2003). Some non-conservative source or behavior is required to the explain mismatch between the behavior of the concentration of Nd and this isotopic composition throughout the ocean.

Until recently other potential sources of Nd have been assumed negligible. In addition to fluvial inputs, dissolution of dust is another established source of Pb to the oceans (Grousset and Biscaye, 2005; Jones et al., 1994). However, dust had been ruled out as a major source of Nd to the oceans (Jones et al., 2000). Hydrothermal inputs also had been ruled out as a major contributor of Nd and Pb to the oceans (Frank et al., 2002). Limitations in sampling and analyzing the low concentrations of Rare Earth Elements (REE) in the water column have hindered research in this area and sources and sinks are not well understood. Some models of Nd marine cycling suggest that up to 95% of the sources of the Nd to the ocean are not constrained (Arozue et al., 2008). There have been several non-conservative pathways proposed recently to explain Nd isotopic composition and concentration throughout the oceans (Haley et al., 2017), including a "bottom up" pore water derived source (Abbott et al., 2015), submarine ground water discharge and reversible scavenging overprinting the Nd signature from the top down. Specifically, recent work by Abbott et al., (2015) has established that pore water fluxes of REE

in the ocean are a source of REE to the ocean and are potentially a dominant ($10 \times 10^6 - 110 \times 10^6$ mol Nd /yr) source of Nd.

The modern distribution of Pb isotopes are more difficult to study because they are pervasively complicated by anthropogenic inputs from leaded gas, coal combustion, and myriad other industrial processes. However, Pb is often used as a tracer of weathering and dust inputs into the ocean, especially in the geologic past (Basak and Martin 2011; Jones et al., 1994; Wilson et al., 2017). Therefore, we hope to combine Pb isotopes with the Nd isotopes to provide more context for changes in Nd isotopic composition, and to bolster our evaluation of the sources of Nd.

The paleoceanographic interpretations are based on the observation that water masses maintain quasi-conservative Nd isotopic signatures as they move away from their location of formation as detailed above. The $^{143}Nd/^{144}Nd$ isotopic ratio of Nd is measured, and the distinct signatures depend on the age or the rocks at formation. The difference in ratios is so small they are expressed as deviations in parts per ten thousand from the chondritic uniform reservoir (CHUR) ($\varepsilon_{Nd} = ([^{143}Nd/^{144}Nd]_0/[^{143}Nd/^{144}Nd]_{CHUR(t)} - 1) \times 10^4$). The isotope ^{147}Sm decays to ^{143}Nd and overtime the young rocks that are enriched in via differentiation in the mantel ^{147}Sm become enriched in ^{143}Nd. We refer to young rocks that are enriched in ^{147}Sm and ^{143}Nd as radiogenic. Conversely old continental crust rocks are depleted in parent ^{147}Sm, and thus daughter ^{143}Nd, and we refer to them as un-radiogenic. The distinct rock types and/ or ages impart a distinct signature when they weather into the ocean. The North Atlantic has the most negative, non-radiogenic values, which is thought to be caused by drainage off ancient Canadian rocks into the Labrador Sea (ε_{Nd} ~-18; Pipegras & Wasserburg, 1987) and the Norwegian-Greenland Sea (ε_{Nd} ~-8 to -11; Lacan & Jeandel, 2004). In contrast, young arc terrains impart the most radiogenic values on

North Pacific waters. The Pacific that has an ε_{Nd} signature ranging from -2.9 to -3.7 (Goldstein & Jacobson, 1988). ε_{Nd} values of surface waters of the modern Pacific range from ~0 to -4 (Piepgras & Jacobsen, 1988). Southern Ocean waters (Antarctic Intermediate and Bottom Waters) have an ε_{Nd} signature of -8 to -9. This signature is generally thought to reflect a mixture of nonradiogenic NADW and radiogenic Pacific surface waters (Basak et al., 2015; Molina-Kasher et al., 2016 and Pipegras & Jacobsen, 1998). North Atlantic Deep-water, Indian Deep-water and Pacific Deep-water are major constituents of Circumpolar Deep-water. A homogenization of these sources potentially explains a portion of this signature. However, the Antarctic continent also contributes weathered material with highly variable ε_{Nd} values and cannot be discounted as a potential source as well. For example, in detrital sediments off the Adelie Land Coast ε_{Nd} have been shown to range from -5.9 to -14.7 within a 2 myr interval (Cook et al., 2013). In the South Pacific, the Ross Sea Bottom Water (RSBW) has a distinct signature (ε_{Nd} = -7; Basak et al., 2015) and slowly mixes with Lower Circumpolar Deep-water as it moves into the Pacific Ocean. Thus, this signature may show variation over time due not only to changes in circulation, but also due to change in weathering inputs from Antarctica.

Concurrent with the proposed potential regional sources of Nd above, there is new evidence of overprinting of the ε_{Nd} bottom water via pore water fluxes. Abbott et al., (2015) show alterations of the ε_{Nd} along margin of California and Oregon. This indicates that fluvial inputs and mixing are not the only controls on the Nd isotopic composition of water masses.

Another relatively new potential explanation for the "Nd Paradox" is boundary exchange: a process that yields exchange between margins and water masses (Lecan and Jeandel 2005). The most likely mechanism by which this exchange could occur is dissolved / particulate exchange where trace metals are remobilized via diagenesis and Nd is subsequently adsorbed

back into particulate form, while altering the isotopic composition of the water mass (Lecan and Jeandel, 2005). In this dissertation we present major, trace and rare earth elements in conjunction with Nd and Pb isotopes to try to identify sources of Nd to the sediment that are not fluvial.

The residence time the time it takes for all of a specific element in the ocean to be removed) of Pb and Nd is important to understand because their potential utility as water mass tracers depends on them having a residence time that is shorter than ocean mixing. Henderson and Maier-Raimer (2002) calculated the residence time of stable Pb in the ocean by employing a model of the sink of ^{210}Pb. Their calculations yield a global residence time of ~48 years. However, they warn that the flux of Pb out of the water column varies with productivity and the rate of transport of material to the seafloor, and so the residence time can vary by an order of magnitude depending on location and the factors that influence scavenging rate.

Calculating the residence time of Nd in the ocean is even less straight-forward. The residence time indicated by the distribution of Nd (less than 1000 years), and the residence time indicated by the Nd concentration distribution (greater than 10000 years; Goldstein and Hemming 2003; Haley et al., 2017) creates an additional layer of uncertainty, referred to as the "Nd paradox". Tachakawa et al. (2003) present the most commonly cited residence time calculations of Nd of 500-1000 years.. They make a series of assumptions including that 100% of the Nd outfluxed via particle scavenging was remineralized and calculated a global residence time of 500-1000 years using the PANDORA model, borrowed from Broker and Peng (1987). Sidell et al., (2008) confirmed the 500-1000 year estimate with a reversible scavenging model that takes the Nd paradox into account. The work that is actively being performed by the GEOTRACES community will move our understanding of the cycling of both of these elements and help us to make better interpretations of the pale-ocean with our data.

Nd is incorporated into fish debris, fish teeth, and adsorbed onto Fe-Mn oxyhydr(oxide) coatings. The Pb adsorbed in fish debris and foraminifera cannot be distinguished from Pb that has decayed from the U present in apatite and carbonate. This makes fish debris and foraminifera unsuitable recorders of Pb seawater composition. However, Pb does become adsorbed onto Fe-Mn oxyhydroxide coatings, and both are thus used in paleoceaonographic studies. Recent studies have evaluated the effects of changing conditions such as redox state on the incorporation of Rare Earth Elements into fish debris (Huck et al., 2016). Additionally, there have been evaluations of several sequential leaching procedures designed to extract Fe-Mn Oxyhydroxide coatings from sediment that indicate that the results of sequential leaching are variable depending on the lithology of the sediment, the solute to solvent ratio, and the number of steps performed on the sediment (Blaser et al., 2016; Molina-Kesher et al., 2014; Wilson et al., 2013). We see reflections of these issues in our own work in Chapter II, and so we work to identify and establish the extent of those procedural issues in Chapter III.

The goal of this research was 1) to extend the records presented in Thomas et al., (2014) from 70 to 40 million years ago forward from 40 million years ago to 15 million years ago. 2) To evaluate the use of Nd and Pb isotopes in extracted from Fe-Mn oxyhydroxide coatings as a paleoproxy in the Pacific basin, where using other circulation proxies like $\delta^{18}O$ and $\delta^{13}C$ is difficult because of the old age of the water obscuring potential gradients. The approach is geochemical in nature. I have analyzed Nd isotopes in fish debris, leach phases, and in the residue left being by leaches, in addition to Pb isotopes in leaches and residues. In this dissertation, I present the results of my work analyzing the paleoceanography of four sites spanning the North and South Pacific: 596, U1370, 464 and 1209. Additional Pb data for the sites as well as data from Site 883 are published in the appendices. I have also analyzed Pb

isotopes and major, trace and REE analyzed Nd Leach phases, in the residue left behind by leaches in Site U1370 and 1149 from the South and North Pacific respectively, in order to evaluate our leaching procedure and the full scope of its results. The dissertation is structured with three chapters in addition to the chapters containing the introduction and conclusion. All of the work presented here is being finalized for peer-reviewed journals, therefore each chapter is organized as an individual publication. The interpretations and discussions presented here will be superseded by whatever is published in the final papers.

Chapter II, which is intended for Earth and Planetary Science Letters, focuses on the paloeceanographic applications of Nd isotopes as a tracer of ocean circulation in the pacific. This chapter extends the existing paleoceanographic circulation of a quasi-north-south swath of the Pacific from 70 to 40 Ma to forward to 15 Ma. This work identifies two main results that prompt the studies that follow in Chapters III and IV. The first is that the operationally defined oxide coatings at Site 1209 in the North Pacific have variable compositions that are overall more radiogenic than their corresponding fish debris. These findings raise questions about the efficacy of the leaching procedure. The second is that after a shift from +4 to -1 from 70 to 35 Ma (Thomas et al., 2014), the North Pacific Nd isotopic composition becomes more radiogenic between 35 and 25 Ma, while the South Pacific becomes less radiogenic, which increases the gradient between the North and South Pacific. We argue that this shift marks the transition between surface ventilated deep-water formation and the modern sluggish mode. However, these findings raise questions about the systems that control the Nd isotopic composition in the North Pacific. Specifically, what is the source of this radiogenic signature and does it reflect a circulation change or a change in the source of Nd to the North Pacific?

Chapter III, which is intended for Geochemistry, Geophysics, Geosystems, focuses on establishing the reproducibility and fidelity of our leaching procedure. Briefly our procedure entails a two-step leach with a Hydroxylamine-Hydrochloride mixture: Leach 1 is 1 hour, and Leach 2 is 24 hours. Our procedure is representative of those used in similar studies (Gutjahr et al., 2007; Wilson et al., 2013) and is designed to isolate the Fe-Mn oxyhydr(oxide) fraction if the sediment. In order to analyze leach reproducibility, we performed replicate analysis of a USGS certified reference material (MAG-1) and an in house internal standard from the central Atlantic (INTL-STD-A). The residues of MAG-1 and INTL-STD-A have the lowest reproducibility, or the highest RSD. RSD is the standard deviation represented as a percentage of the mean. It is a way to examine the precision of the data in the context of the mean. The first leach of MAG-1 has the highest reproducibility, for the major, trace and Rare Earth Elements and the isotopes. There is better reproducibility of ε_{Nd} in samples with highest concentrations. Interestingly, there is no relationship the RSD of the concentrations of Pb and Nd, and the reproducibility of their isotopic compositions.

To evaluate the fidelity of the leach (how well the leach extracts its intended target) we evaluated Major, Trace and Rare Earth Elements that we expect to be associated with specific phases. We performed these tests on two sites: ODP Site 1149 and IODP Site U1370. Both sites are ideal for this study because they are representative of their regions of the ocean, and because the bulk sediment from each site has been previously geochemically characterized. Site 1149 was characterized by Scudder et al., (2009 and 2014), and Site U1370 was characterized by Dunlea et al., (2015a and 2015b).

In the first and second leach Si, Ti, and Al are all below detection limit. These are the elements we would expect to extract if the leach were "contaminated" or extracting

aluminosilicates, in the first and second leach. Mn is consistently extracted from both leaches at both sites; however, the percentage of Fe extracted is low in comparison to the total amount of Fe in each sample. The Rare Earth Element patterns at Site U1370 confirm that the first leach effectively extracts the target phase. The Rare Earth Elements also confirm that the first leach effectively extracts the target phase in the bottom 80 meters of Site 1149, whereas the top 100 meters (everything above 101.14 mbsf) reflects a signature most likely derived from a lithogenic source.

Chapter IV, which is intended for Geochemistry, Geophysics, Geosystems, is focused on identifying the sources and controls of the Major, Trace, Rare Earth Elements and isotopic compositions of all three leach phases: the first leach, the second leach, and the residue. We use the data from Sites 1149 and U1370 presented in Chapter III and combine it with Nd and Pb isotope analysis of each leached phase. We view the leaching results from three geochemical perspectives: isotopic data, elemental data, and Q-Mode factor analysis of the resulting geochemical data to identify the impact of sources and / or physiochemical controls on the elemental distribution. We hope to establish which geochemical end-members contributed to the Nd and Pb isotopic signal in the phases accessed by the operationally defined leaching.

We identified five factors that explain 99% of the data in both sites, and we describe that each phase is controlled by a different dominant source, however, there is overlap in the minor sources between the three phases that could influence the ultimate results of the isotopic analysis. This is confirmed by the isotopic results that the second leach has higher isotopic ratios than the first leach or the residue at both sites, indicating that either there are distinct sources contributing to Leach 1, Leach 2 and the Residue, or that fractionation is occurring in the sorption or leaching process.

1.1 References

Abbott, April N, Brian A Haley, and James McManus. 2016. "The impact of sedimentary coatings on the diagenetic Nd flux." *Earth and Planetary Science Letters* 449:217-227.

Basak, Chandranath, and Ellen E Martin. 2013. "Antarctic weathering and carbonate compensation at the Eocene-Oligocene transition." *Nature Geoscience* 6 (2):121-124.

Blaser, Patrick, Jörg Lippold, Marcus Gutjahr, Norbert Frank, Jasmin M. Link, and Martin Frank. 2016. "Extracting foraminiferal seawater Nd isotope signatures from bulk deep sea sediment by chemical leaching." *Chemical Geology* 439:189-204. doi: https://doi.org/10.1016/j.chemgeo.2016.06.024.

Broecker, WS, and TH Peng. 1982. "Tracers in the Sea, 690 pp." *Lamont-Doherty Geological Observatory, Palisades, NY*.

Bruland, K. W., R. Middag, and M. C. Lohan. 2014. "8.2 - Controls of Trace Metals in Seawater A2 - Holland, Heinrich D." In *Treatise on Geochemistry (Second Edition)*, edited by Karl K. Turekian, 19-51. Oxford: Elsevier.

Frank, Martin. 2002. "Radiogenic isotopes: tracers of past ocean circulation and erosional input." *Reviews of geophysics* 40 (1).

Goldstein, Steven J., and Stein B. Jacobsen. 1987. "The Nd and Sr isotopic systematics of river-water dissolved material: Implications for the sources of Nd and Sr in seawater." *Chemical Geology: Isotope Geoscience section* 66 (3–4):245-272. doi: 10.1016/0168-9622(87)90045-5.

Goldstein, S. L., and S. R. Hemming. 2003. "6.17 - Long-lived Isotopic Tracers in Oceanography, Paleoceanography, and Ice-sheet Dynamics A2 - Holland, Heinrich D." In *Treatise on Geochemistry*, edited by Karl K. Turekian, 453-489. Oxford: Pergamon.

Grousset, Francis E., and Pierre E. Biscaye. 2005. "Tracing dust sources and transport patterns using Sr, Nd and Pb isotopes." *Chemical Geology* 222 (3):149-167. doi: https://doi.org/10.1016/j.chemgeo.2005.05.006.

Gutjahr, Marcus, Martin Frank, Claudine H. Stirling, Veronika Klemm, Tina van de Flierdt, and Alex N. Halliday. 2007. "Reliable extraction of a deepwater trace metal isotope signal from Fe–Mn oxyhydroxide coatings of marine sediments." *Chemical Geology* 242 (3):351-370. doi: https://doi.org/10.1016/j.chemgeo.2007.03.021.

Haley, Brian A., Jianghui Du, April N. Abbott, and James McManus. 2017. "The Impact of Benthic Processes on Rare Earth Element and Neodymium Isotope Distributions in the Oceans." *Frontiers in Marine Science* 4 (426). doi: 10.3389/fmars.2017.00426.

Henderson, Gideon M., and Ernst Maier-Reimer. 2002. "Advection and removal of 210Pb and

stable Pb isotopes in the oceans: a general circulation model study." *Geochimica et Cosmochimica Acta* 66 (2):257-272. doi: 10.1016/s0016-7037(01)00779-7.

Huck, Claire E, Tina van de Flierdt, Francisco J Jiménez-Espejo, Steven M Bohaty, Ursula Röhl, and Samantha J Hammond. 2016. "Robustness of fossil fish teeth for seawater neodymium isotope reconstructions under variable redox conditions in an ancient shallow marine setting." *Geochemistry, Geophysics, Geosystems*.

Jones, Charles E, Alex N Halliday, David K Rea, and Robert M Owen. 1994. "Neodymium isotopic variations in North Pacific modern silicate sediment and the insignificance of detrital REE contributions to seawater." *Earth and Planetary Science Letters* 127 (1-4):55-66.

Jones, Charles E., Alex N. Halliday, David K. Rea, and Robert M. Owen. 2000. "Eolian inputs of lead to the North Pacific." *Geochimica et Cosmochimica Acta* 64 (8):1405-1416. doi: https://doi.org/10.1016/S0016-7037(99)00439-1.

Kryc, KA, RW Murray, and DW Murray. 2003. "Elemental fractionation of Si, Al, Ti, Fe, Ca, Mn, P, and Ba in five marine sedimentary reference materials: results from sequential extractions." *Analytica Chimica Acta* 487 (1):117-128.

Molina-Kescher, Mario, Martin Frank, and Ed Hathorne. 2014. "South Pacific dissolved Nd isotope compositions and rare earth element distributions: Water mass mixing versus biogeochemical cycling." *Geochimica et Cosmochimica Acta* 127:171-189. doi: https://doi.org/10.1016/j.gca.2013.11.038.

Molina-Kescher, Mario, Martin Frank, and Ed C. Hathorne. 2014. "Nd and Sr isotope compositions of different phases of surface sediments in the South Pacific: Extraction of seawater signatures, boundary exchange, and detrital/dust provenance." *Geochemistry, Geophysics, Geosystems* 15 (9):3502-3520. doi: 10.1002/2014GC005443.

Piepgras, D. J., and G. J. Wasserburg. 1987. "Rare earth element transport in the western North Atlantic inferred from Nd isotopic observations." *Geochimica et Cosmochimica Acta* 51 (5):1257-1271. doi: 10.1016/0016-7037(87)90217-1.

Rahmstorf, Stefan, Jason E. Box, Georg Feulner, Michael E. Mann, Alexander Robinson, Scott Rutherford, and Erik J. Schaffernicht. 2015. "Exceptional twentieth-century slowdown in Atlantic Ocean overturning circulation." *Nature Clim. Change* 5 (5):475-480. doi: 10.1038/nclimate2554

http://www.nature.com/nclimate/journal/v5/n5/abs/nclimate2554.html#supplementary-information.

Tachikawa, Kazuyo, Thomas Arsouze, Germain Bayon, Aloys Bory, Christophe Colin, Jean-Claude Dutay, Norbert Frank, Xavier Giraud, Alexandra T. Gourlan, Catherine Jeandel, François Lacan, Laure Meynadier, Paolo Montagna, Alexander M. Piotrowski, Yves Plancherel, Emmanuelle Pucéat, Matthieu Roy-Barman, and Claire Waelbroeck. 2017. "The large-scale evolution of neodymium isotopic composition in the global modern and Holocene ocean revealed from seawater and archive data." *Chemical Geology* 457:131-

148. doi: http://dx.doi.org/10.1016/j.chemgeo.2017.03.018.

Talley, L.D. 2013. "Closure of the Global Overturning Circulation Through the Indian, Pacific, and Southern Oceans: Schematics and Transports." *Oceanography* 26. doi: doi.org/10.5670/oceanog.2013.07.

Thomas, Deborah J, Robert Korty, Matthew Huber, Jessica A Schubert, and Brian Haines. 2014. "Nd isotopic structure of the Pacific Ocean 70–30 Ma and numerical evidence for vigorous ocean circulation and ocean heat transport in a greenhouse world." *Paleoceanography* 29 (5):454-469.

Wilson, David J, Alexander M Piotrowski, Albert Galy, and Josephine A Clegg. 2013. "Reactivity of neodymium carriers in deep sea sediments: Implications for boundary exchange and paleoceanography." *Geochimica et Cosmochimica Acta* 109:197-221.

Wilson, David J., Tina van de Flierdt, and Jess F. Adkins. 2017. "Lead isotopes in deep-sea coral skeletons: Ground-truthing and a first deglacial Southern Ocean record." *Geochimica et Cosmochimica Acta* 204:350-374. doi: https://doi.org/10.1016/j.gca.2017.01.052.

2. NEODYMIUM ISOTOPIC STRUCTURE OF THE PACIFIC OCEAN 35–15 MA: EVIDENCE FOR THE REORGANIZATION OF DEEP NORTH PACIFIC OCEAN CIRCULATION BETWEEN 35 AND 25 MA

2.1 Introduction

The oceanic meridional overturning circulation (MOC) is a crucial component of the climate system, influencing heat transport, nutrient transport, and global carbon cycling. The operating mode of the MOC is responsible for a significant contribution of poleward heat transport in the modern climate system. Thus, changes in the pattern and strength of the MOC are considered to have played a large role in past climate variations. In order to assess the relationship between climate and ocean circulation in the past, we must constrain the characteristics of past ocean circulation. This in turn relies on our ability to identify and employ proxies from marine sediments that record and preserve information about these processes.

One such proxy is the Neodymium (Nd) isotopic composition of seawater, a robust tracer of ancient water mass composition that is widely applied to timescales spanning the past ~400 million years [e.g., Frank, 2002]. Nd isotope records constructed with fossil fish debris and with analyses of authigenic oxide minerals (crusts and within sediments) suggest that the operating mode of the MOC was significantly different during the last major greenhouse climate interval during the Late Cretaceous and early Paleogene 70-35 Ma (e.g., Hague et al., 2012; Thomas, 2004; Thomas et al., 2014; Via & Thomas, 2006). A compilation of ancient Pacific Ocean Nd isotope data from deep-sea drill cores and Fe-Mn crusts indicates a geographic gradient in water mass composition with radiogenic (high) Nd isotope values in the deep North Pacific and unradiogenic (low) values in the deep South Pacific from ~70 to 40 Ma (e.g., Thomas et al.,

2014). All drill sites and Fe-Mn crust records derived from low and mid latitudes recorded Nd isotope values between the North and South Pacific values (Huck et al., 2017; Le Houdec et al., 2016; Ling et al., 1997; van de Flierdt et al 2004). These results were interpreted to indicate bipolar circulation in the Pacific. Specifically, the Nd isotopic gradient indicates surface ventilated radiogenic North Pacific Deep-water during the latest Cretaceous through early Paleogene in addition to deep-water formation in the pacific quadrant of the southern ocean. This reconstruction is supported by fully coupled GCM simulations indicating that the "age" of deep-waters in the Pacific increased from high to low latitudes in both the South Pacific and North Pacific (Hague et al., 2012).

The hypothesized reconstruction of Paleogene overturning circulation differs from the modern mode of overturning, in which deep-water is formed via diffusive North Pacific Deep-water formation (Talley et al., 2013). Therefore the Nd isotopic composition of the modern North Pacific bottom water must be imparted via a process other than deep-water formation, and non-conservative processes must control the Nd isotopic composition of the modern North Pacific. If the conclusions in Thomas et al. (2014) are correct, at some point after 40Ma, the overturning circulation evolved from a mode dominated by bipolar convection to the monopolar convection (AABW only) observed in the present. To test the timing of such a hypothesized transition, we extend our record of Nd isotopes to describe Pacific Ocean circulation between 40 and ~10 Ma. One advantage of Nd isotopes as a pacific paleoproxy is that it is not affected by the shallow carbonate compensation depth in the Pacific (Palike et al., 2012), and thus enables us to work with deep- and bottom-water depths.

In this study, we generated new data from an array of deep-sea drill sites to track the evolution from the bipolar Pacific "Paleogene Mode" of MOC to the modern mode, in an effort

to advance understanding of the co-evolution of the Cenozoic climate system and MOC contribution to global heat transport. The new data suggest that deep-water Nd isotope values in the North Pacific changed remarkably little throughout the entire Cenozoic, in spite of considerable climate evolution over the interval. One primary implication of this finding is that the Nd isotopic signature may not be an impartial indicator of water mass provenance. In the case of the North Pacific, the dissolved Nd isotopic composition in deep-waters may be overprinted periodically by disseminated ash with a similar signature to local weathering inputs, especially after the onset of subduction in the Northwest Pacific 50 Ma (Sharp and Clague, 2006). However, even where overprinting occurs we identify a clear transition in the mode of circulation.

2.2 Background

2.2.1 Paleoclimate and Tectonic Liinkages

Reconstructions of the Paleogene operating mode of overturning circulation patterns based on Nd isotopic above indicate bipolar meridional overturning circulation (i.e., convection in both the North and South Pacific) from ~70 to 40 Ma (Thomas et al., 2014). A reorganization of the overturning circulation to the modern monopolar mode must have occurred between ~40 Ma and 5 Ma, based on glacial-interglacial investigations of deep-water circulation patterns in the Pacific (Woodward et al., 2014).

The 40-10 Ma interval is characterized by tectonic-paced changes in the geographic configurations of the ocean basins, which are events that could have influenced the mode of ocean circulation and climate. Surface ventilated deep-water formation (water from the surface that becomes dense and subducts flowing as deepwater like in the modern formation of North Atlantic Deepwater) is established in the Pacific Sector of the Southern Ocean prior to ~30 Ma,

the opening of the Drake Passage and the onset of the Antarctic Circumpolar Current (ACC) (Huck et al., 2017; Thomas et al., 2014). However, the permanent connection between the Pacific and Atlantic and thermal isolation of Antarctica are potentially still significant to the evolution of Pacific circulation. In the Southern Ocean, the Drake Passage opened to at least shallow water by ~30 Ma (Scher and Martin et al., 2006). Subsequent subsidence of the Scotia Arc between 23 and 18 Ma enabled deep-water to circulate through the Drake Passage (Daziel et al., 2013). In the western portion of the South Pacific between 30 and 26 Ma, the Tasman-Antarctic passage opened sufficiently to align the ocean gateway with the path of the westerlies (Scher et al., 2015). Australia continued to shift north, resulting in continued expansion of the Tasman-Antarctic passage and concomitant restriction of deep flow through the Indonesian/Australian passage (Allen and Armstrong, 2008; Lyle et al., 2008). The westerly wind and deep-water flow path through the Drake Passage are both necessary for the Antarctic Circumpolar Current (ACC) to achieve its powerful and isolated circulation of today.

During the same 40- 10 Ma interval the climate system underwent a long-term shift from the Eocene Greenhouse (a period during which no major continental ice sheets existed) to the modern icehouse (a period where ice on land is present) that is punctuated by several cooling steps. Global benthic foraminifera stable isotope values during the Cenozoic indicate significant variations in circulation, interpreted to reflect different sources of deep-water with distinct nutrient ($\delta^{13}C$) and temperature ($\delta^{18}O$) characteristics. Cramer et al. (2009) identify a major transition in the interbasinal patterns of deep-water $\delta^{18}O$ and $\delta^{13}C$ at ~35 Ma. $\delta^{18}O$ and $\delta^{13}C$ were spatially homogeneous on the global scale through the early Paleogene (65-35 Ma) reflecting either diffuse upwelling and small-scale mixing or deep-water formation with similar nutrient signatures. The latter explanation better fits with ocean circulation reconstructions based on Nd.

Thomas et al. (2014) and Huck et al. (2017) both propose deep-water formation in the Pacific sector of the Southern Ocean during the Paleogene.

The Eocene-Oligocene transition (EOT or Oi-1) is an abrupt increase in global marine carbonate $\delta^{18}O$ values (Prothero et al., 2003), which is known to reflect a major increase in glaciation on Antarctica (~34 Ma; Mudelsee et al., 2014). The EOT is also marked by a concurrent change in the interbasinal patterns of $\delta^{18}O$ and $\delta^{13}C$ from the aforementioned homogeneous state to a heterogeneous spatial gradient, where there is a clear spatial gradient between the $\delta^{18}O$ and $\delta^{13}C$ of different water masses, (Cramer et al., 2009) and a switch in the carbon cycle characterized by deepening of the calcite compensation depth by 1200-1500 meters in the Pacific (Lyle et al., 2008; Palike et al., 2012). A second shift towards heavier $\delta^{18}O$, and another step towards glaciation (Mi-1) occurs at ~23 Ma across the Oligocene-Miocene transition (Miller et al., 1991). The end of our study interval contains the mid-Miocene climatic optimum (MMCO) which begins at ~17.5 Ma (Mudelsee et al., 2014). This warm period ends with the mid-Miocene climatic transition (MMCT) ~15 Ma, a transition from warm to cold recorded in $\delta^{18}O$ (Mudelsee et al., 2014). There is a substantial body of literature on the causes and consequences of these climate events: decreasing atmospheric CO_2 (DeConto and Pollard, 2003), changing Southern ocean circulation, (Sijp et al., 2001) and carbon cycling (Lyle et al., 2008 and Mudelsee et al., 2014). However, our understanding of how or if climate events are related to changes in ocean circulation and cooling deep oceans is limited by our ability to reconstruct circulation patterns. Nd isotopes are a useful tool for augmenting our understanding of the evolution of Pacific water masses through the Cenozoic.

2.2.2 Nd Isotopic Systematics

The mixing time of Nd in the oceans (500-1000 years; Tachikawa et al., 2003, 2017) is shorter than the global ocean mixing time (~1500 years; Broecker and Peng, 1982). Water masses acquire a distinct $^{143}Nd/^{144}Nd$ isotopic fingerprint from the fluvial inputs of dissolved Nd in the region of water mass sinking (Goldstein & Jacobson, 1987; 1988). This is expressed as deviations in parts per ten thousand from the chondritic uniform reservoir (CHUR).

$$(\varepsilon_{Nd} = ([^{143}Nd/^{144}Nd]_0/[^{143}Nd/^{144}Nd]_{CHUR(t)} - 1) \times 10^4, \text{ CHUR}=0.0512638)$$

Drainage off ancient Canadian rocks imparts negative, non-radiogenic values onto waters originating in the North Atlantic. In contrast, young arc terrains and volcanism impart the most radiogenic values on North Pacific waters. The short residence time combined with the diverse sources of Nd into the ocean make Nd isotopes a viable, albeit imperfect tracer of ocean circulation (Frank, 2002).

In many locations where Nd isotopic composition (IC) is controlled only by weathering inputs and mixing, water masses maintain distinct ε_{Nd} signatures. Some signatures are subsequently modified by continued continental inputs, boundary or hydrothermal exchange (Lacan and Jeandel, 2005), overprinting from dust and ash (Jones et al., 2009; Lambert et al., 2016), and pore water fluxes (Abbott et al, 2015). The extent to which they are overprinted depends on1) the magnitude of the difference between the original ε_{Nd} signature and the signature of the overprinting material, 2) the concentration of the overprinting material, and 3) the length of time the water is exposed to inputs (Abbott et al., 2015). As our understanding of contributions of Nd into the ocean evolves, careful evaluation of our assumptions is required. Identifying that the Nd IC of the bottom water is potentially influenced by non-conservative processes presents new challenges to paleoceanographic interpretations.

Where we can infer ε_{Nd} conservation, we can perform paleoceanographic studies of water mass composition, and therefore ocean circulation. We can do this with Nd incorporated into fossil fish debris (Martin and Scher, 2004), foraminifera tests (Tachikawa et al., 2014), and Fe-Mn crusts and Fe-Mn oxidehydr(oxide) coatings on sediment accessed by sequential leaching (Wilson et al., 2013). Leaching involves exposing the sediment to a reducing agent to chemically separate one phase —in this case, the Fe-Mn oxidehydr(oxide) coating— from the rest of the sediment (Tessier et al., 1979). Results vary depending on choice of reducing agents, solute to solution ratios, and leaching times (Tachakawa et al., 2017; Wilson et al., 2013). Our methods have been informed by evaluations of sequential leaching procedures (i.e. Kyrc et al., 2006; Molina-Kesher et al., 2014; Wilson et al., 2013; Ziegler et al. 2008). Because the Fe-Mn oxyhydr(oxide) phase is operationally defined we refer to this phase as the first leach. We use the same scheme for the residue left over when the Fe-Mn oxidehydr(oxides) have been removed. This phase is operationally defined as detrital (material that is rock derived, as opposed to being a precipitate from the seawater) and so we refer to that phase as the residue. We do this to avoid over interpreting the data in both cases. The isotopic composition of the residue can also be utilized to examine changes in eolian inputs, winds patterns, and sediment sources (e.g., Remi and Marcantonio, 2016).

2.2.3 Modern Distribution of Nd Isotopic Signatures

In the modern Pacific most of the Nd IC of seawater correlates well to a mixing regime confirmed by other hydrographic water mass indicators. In general, this regime mixes younger, colder southern-sourced water ($\varepsilon_{Nd}(t)$ -8), with older, warmer equatorial, and northern-sourced water (Figure 1.1; ε_{Nd} -4; Tachakawa et al., 2017). This implies that the Nd IC signature is mainly controlled by mixing between water masses (Tachakawa et al., 2017). There are locations

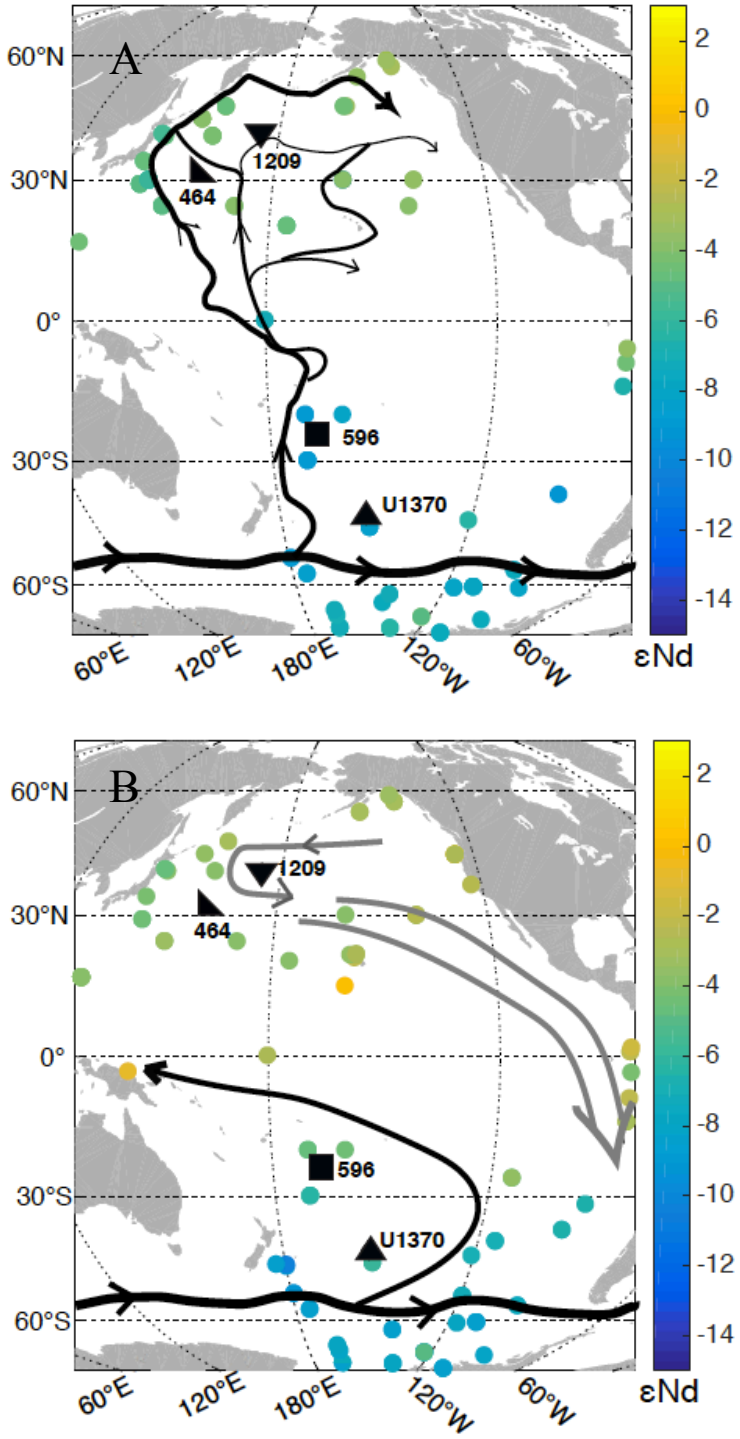

Figure 2.1: ε_{Nd} in the Pacific 3500-5000m (A) and 2000-3500m (B). Modern water column neodymium isotopic composition (Van de Flidert et al., 2016) of the 3500-5000 m (left, 1A) and 2000-3500 m (right, 1B) vertical sections of the ocean overlain with general Pacific Ocean circulation patterns modified from Kawabe et al. (2009). Site locations for this study are marked with black shapes.

including near Hawaii, off the coast of Japan, near New Zealand, and in North Central Pacific bottom water) that show offsets indicative of local or regional influence (Tachakawa et al., 2017)

Deep-water in the South Pacific originates in the Antarctic Circumpolar Current (ACC). Circumpolar deep-water with an ε_{Nd} signature of ~ -8.5 (CDW; Basak et al., 2015), undergoes complex mixing along its eastern flow path around Antarctica. Ross Sea Bottom Water (RSBW, ε_{Nd} -7; Basak et al., 2015) and Lower Circumpolar Deep-water (LCDW; ε_{Nd} -8.3; Molina-Kescher et al., 2014) flow north as bottom water into the west Pacific basin. LCDW dominates north of 60°S, as RSBW does not extend past that latitude (Basak et al., 2015). As it moves northward, LCDW becomes imprinted with an increasingly radiogenic ε_{Nd} signature and begins branching north of the equator (figure 2.1a; Kawabe et al., 2010). A portion moves east at ~15°N and upwells as North Pacific Deep-water (NPDW ε_{Nd} -4; Horikawa et al., 2011). The remaining LCDW continues north, splitting between the Hess and Shatsky Rises. One split slowly flows along the Kamchatka and Alaska Peninsulas, while maintaining the radiogenic signature seen throughout the Equatorial and North Pacific (ε_{Nd} -4). The other branch flows directly east. Both the eastern and northern branches upwell as NPDW spanning the deep and intermediate depth ranges. The majority of NPDW turns and flows south in the Eastern Pacific basin. A small portion loops back, flowing west over the Shatsky Rise as intermediate water (figure 2.1b; 1000-3000 m).

2.3 Methods

2.3.1 Sample Sites and Collection

We investigated four sites from the western basin of the Pacific (figure 2.1a). North Pacific sites include Deep Sea Drilling Project (DSDP) Site 464 (Northern Hess Rise, Paleo-water depth ~4000m) and Ocean Drilling Program (ODP) Site 1209, (TAMU Massif, Shatsky

Rise, Paleo-water depth 2000m). South Pacific sites include DSDP Site 596 (Paleowater depth ~5000m) and Integrated Ocean Drilling Program (IODP) Site U1370 (Paleo-water depth ~5000m). Samples were collected at the IODP Gulf Coast Repository. Full descriptions of each site and their age models are in apendex A.

2.3.2 Sample Digestion and Leaching

Samples were split with one portion washed and sieved so that the >63 micron size fraction could be picked for fish debris. The other portion was dried and hand pulverized with an agate mortar and pestle. We leached 0.75 g of sediment in 14 mL of 0.02 M hydroxylamine hydrochloride (HH) in 20% acetic acid, buffered to a pH 4 with sodium acetate for one hour to reduce the Fe-Mn phases, and centrifuged twice: once for 15 min to separate solids from liquid, and then the liquid again for an hour, to ensure separation of leachate from remaining solids. Note that our leaching procedure does not include a step designed to remove the carbonate material from the sediment before the reduction step, as per Wilson et al. (2013), and confirmed by Tachikawa et al. (2017). In order to analyze the residue, the remaining solids were further leached with 14 ml of HH for 24 hours. The residues were triple rinsed, dried, and re-homogenized by hand. ~0.5 g of residue was dissolved sequentially in HF-HNO_3-HCl acid.

The leachate and digested residue were converted to a nitrate matrix before column chemistry. The Rare Earth Elements (REE) of all three phases (fish debris, leachate, and residue) were dissolved in 2N Nitric acid and isolated via RE spec column chemistry following the methods outlined in Xie et al. (2012). The Nd was separated from the bulk REEs via column chemistry with Eichrom LN Spec™. In January 2016 we changed to Eichrom Tru Spec™ instead of RE Spec for the Rare Earth Element separation to improve the yield of Nd in the separation procedure.

2.3.3 Analysis

Nd isotope samples were loaded onto double rhenium filaments and analyzed on the Thermo Triton Thermal Ionization Mass Spectrometer (TIMS) at Texas A&M University. External precision based on replicate analysis of Jndi standard (n=90) was 8ppm (2σ), with a value of 0.51210124. We calculated $\varepsilon_{Nd}(t)$, which is ε_{Nd} calculated to account for the decay of ^{147}Sm with time, using the numerical ages derived from the age model for each site (please refer to apendex A), and applied a $^{147}Sm/^{144}Nd$ correction derived from measured analyses from the literature based on the phase analyzed. For fish debris we used a $^{147}Sm/^{144}Nd$ value of 0.131 (e.g., Thomas, 2004), for the first leach we used a $^{147}Sm/^{144}Nd$ value of 0.115 based on values reported for Fe-Mn crusts (Ling et al., 1997). For the residue we used a $^{147}Sm/^{144}Nd$ value of 0.109 based on upper crustal average concentrations of Sm and Nd (Taylor and McLennan, 1995) this is an assumption about the composition of the first leach and residue however, in most cases it is reasonable

2.4 Results

We analyzed samples from the North Pacific at Site 1209 over a depth range of 104.9-131.81 mbsf (15.9-38.3 Ma). Fish debris epsilon values at Site 1209 range between -3.5 and -4.9 throughout the portion of the record analyzed (Table 2.1). The first leaches at Site 1209 range between -4.4 and +1.0 $\varepsilon_{Nd}(t)$. $\varepsilon_{Nd}(t)$. Values for first leach and fish debris from the same sample are consistent within external precision for depth 114.74 mbsf (fish debris = -3.8 $\varepsilon_{Nd}(t)$ and first leach = -3.5 $\varepsilon_{Nd}(t)$); however, this does not occur at any other depths (n=2) where we have values for both the first leach and fish debris in the same sample (Table 2.1). The residues are more radiogenic in the younger, above 111 mbsf (16Ma; figure 2.2), portion of the record an average of -4 $\varepsilon_{Nd}(t)$ and are unradiogenic an average of -9.6 between 131 and 113 mbsf (38 to 30 Ma).

Leg	Site	H	Core	Type	Sec	Top	Bottom	Depth mbsf	Age (Ma)	εNd(t) Ox	143/144(t) 0.115	Std Error (2s)	εNd(t) FD	143/144(t) .131	Std Error (2s)	εNd(t) Res	143/144(t) 0.109	Std Error (2s)
91	596	*	2	H	2	41	43	5.91	8.42	-6.2	0.512311	0.000003	-	-	-	-4.6	0.512387	0.000010
91	596	*	2	H	2	20	21	7.2	11.55	-3.6	0.512436	0.000007	-	-	-	-	-	-
91	596	*	2	H	3	100	101	8	13.74	-2.9	0.512474	0.000002	-	-	-	-	-	-
91	596	*	2	H	3	100	101	9.5	18.33	-3.4	0.512440	0.000002	-	-	-	-	-	-
91	596	*	2	H	3	112	114	9.62	18.72	-4.6	0.512380	0.000008	-	-	-	-	-	-
91	596	*	2	H	3	143	144	9.92	19.72	-	-	-	-	-	-	-2.1	0.512506	0.000055
91	596	*	2	H	4	10	12	10.1	20.33	-3.8	0.512418	0.000010	-	-	-	-4.8	0.512367	0.000089
91	596	*	2	H	4	20	21	10.2	20.67	-7.3	0.512238	0.000004	-	-	-	-	-	-
91	596	*	2	H	4	22	24	10.22	20.74	-7.5	0.512225	0.000002	-7.3	0.512239	0.000005	-	-	-
91	596	*	2	H	4	100	101	11	23.49	-5.9	0.512307	0.000002	-	-	-	-	-	-
91	596	*	2	H	5	20	21	11.7	26.07	-	-	-	-	-	-	-	-	-
91	596	*	2	H	5	28	30	11.78	26.37	-5.3	0.512335	0.000025	-6.4	0.512277	0.000005	-6.3	0.512278	0.000023
91	596	*	2	H	6	100	101	12.5	29.14	-5.4	0.512326	0.000003	-	-	-	-	-	-
91	596	*	2	H	6	20	21	13.2	31.93	-4.1	0.512388	0.000002	-	-	-	-	-	-
91	596	*	2	H	6	22	24	13.22	31.90	-	-	-	-	-	-	-5.4	0.512316	0.000005
91	596	*	2	H	6	92	94	13.93	34.91	-	-	-	-	-	-	-6.2	0.512273	0.000009
91	596	*	2	H	6	100	101	14	35.23	-4.1	0.512385	0.000002	-	-	-	-	-	-
91	596	*	2	H	6	122	124	14.22	36.15	-5.6	0.512306	0.000003	-5.8	0.512297	0.000009	-4.9	0.512340	0.000016
329	1370	D	2	H	7	50	51	17.4	6.85	-7.5	0.512242	0.000003	-	-	-	-	-	-
329	1370	D	3	H	2	50	51	20.17	8.35	-7.6	0.512238	0.000007	-	-	-	-	-	-
329	1370	D	3	H	3	50	51	21.61	9.21	-7.2	0.512258	0.000004	-	-	-	-	-	-
329	1370	D	3	H	4	27	29	22.87	10.02		0.511992	0.000005	-6.7	0.512280	0.000147	-6.5	0.512292	0.000114
329	1370	D	3	H	4	50	51	23.06	10.14	-	-	-	-	-	-	-	-	-
329	1370	D	4	H	1	22	23	25.22	11.63	-5.9	0.512321	0.000005	-	-	-	-	-	-
329	1370	D	4	H	3	22	23	28.22	13.91	-6.2	0.512305	0.000004	-	-	-	-	-	-
329	1370	D	4	H	4	25	17	29.76	15.17	-	-	-	-	-	-	-	-	-
329	1370	D	4	H	4	26	28	29.86	15.26	-	-	-	-6.8	0.512268	0.000004	-	-	-
329	1370	D	5	H	1	89	91	35.61	20.58	-6.7	0.512270	0.000002	-6.9	0.512258	0.000005	-11.1	0.512041	0.000059
329	1370	D	5	H	1	145	142	35.97	20.94	-7.0	0.512255	0.000012	-6.7	0.512267	0.000009	-8.6	0.512168	0.000011
329	1370	D	5	H	3	28	30	37.79	22.83	-	-	-	-6.0	0.512302	0.000285	-	-	-
329	1370	D	5	H	4	29	31	39.3	24.46	-	-	-	-	-	-	-	-	-
329	1370	D	5	H	5	29	31	40.8	26.15	-6.6	0.512265	0.000008	-	-	-	-8.2	0.512184	0.000021
329	1370	D	6	H	1	29	31	44.3	30.33	-	-	-	-6.5	0.512265	0.000025	-	-	-
329	1370	D	6	H	2	52	54	46.03	32.51	-6.5	0.512261	0.000001	-6.0	0.512288	0.000013	-10.1	0.512077	0.000026
329	1370	D	6	H	3	96	98	48.25	35.45	-6.3	0.512269	0.000009	-	-	-	-8.0	0.512184	0.000050

Table 2.1 Nd IC of three phases of samples, including the values for the ratios, and the error.

Leg	Site	H	Core	Type	Sec	Top	Bottom	Depth mbsf	Age (Ma)	εNd(t) Ox	143/144(t) 0.115	Std Error (2s)	εNd(t) FD	143/144(t) .131	Std Error (2s)	εNd(t) Res	143/144(t) 0.109	Std Error (2s)
198	1209	A	12	H	2	97	99	105.7	16.3	-	-	-	-4.436	0.51239	5.65E-06	-4.39	0.512392	2.81E-06
198	1209	A	12	H	2	100	101	105.7	16.32	-0.973	0.512567	3.06E-06	-	-	-	-	-	-
198	1209	A	12	H	3	40	42	106.6	16.83	-4.164	0.512403	5.56E-06	-4.874	0.512367	4.45E-05	-	-	-
198	1209	A	12	H	4	40	41	108.1	17.67	-3.578	0.512432	4.49E-06	-	-	-	-	-	-
198	1209	A	12	H	4	110	111	108.8	18.35	-3.849	0.512417	5.78E-06	-	-	-	-	-	-
198	1209	A	12	H	5	60	61	109.8	20.32	-	-	-	-	-	-	-	-	-
198	1209	A	12	H	5	38	40	111.1	22.85	-3.182	0.512445	5.78E-05	-	-	-	-4.237	0.512391	2.34E-05
198	1209	A	12	H	6	40	41	111.1	22.89	-0.474	0.512584	7.56E-06	-	-	-	-3.538	0.512427	2.37E-05
198	1209	A	12	H	6	41	41	111.1	22.89	-3.692	0.512419	4.79E-06	-	-	-	-	-	-
198	1209	A	12	H	6	141	142	112.1	26.81	-2.675	0.512466	1.58E-05	-	-	-	-	-	-
198	1209	A	13	H	1	25	26	113	30.06	-2.18	0.512488	4.57E-06	-	-	-	-	-	-
198	1209	A	13	H	1	81	82	113.5	30.26	-	-	-	-	-	-	-	-	-
198	1209	A	13	H	2	24	25	114.4	30.58	-4.182	0.512384	3.08E-06	-	-	-	-	-	-
198	1209	A	13	H	2	24	26	114.4	30.58	-3.656	0.512411	6E-06	-	-	-	-9.592	0.512107	4.78E-06
198	1209	A	13	H	2	54	56	114.7	30.68	-3.585	0.512415	5E-06	-3.863	0.5124	4.96E-05	-	-	-
198	1209	A	13	H	3	25	27	116	31.11	-4.166	0.512384	3.01E-06	-	-	-	-9.586	0.512107	9.11E-06
198	1209	A	13	H	4	52	54	117.7	31.72	-4.206	0.512382	5.08E-06	-	-	-	-9.579	0.512106	4.16E-06
198	1209	A	14	H	1	41	43	122.6	33.51	-4.382	0.51237	3.85E-06	-	-	-	-9.559	0.512105	4.94E-05
198	1209	A	14	H	3	37	39	125.6	35.1	-	-	-	-5.007	0.512336	9.86E-06	-9.542	0.512104	2.57E-06
198	1209	A	15	H	1	11	13	131.8	38.28	-3.904	0.512389	3.39E-06	-3.433	0.512413	5.61E-06	-9.506	0.512101	2.91E-05
64	464	*	5	H	38	40		35.38	17.86	-	-	-	-	-	-	-10.13	0.512096	2.1E-05
64	464	*	5	H	50	52		35.51	18.2	-	-	-	-	-	-	-	-	-
64	464	*	5	H	50	52		35.51	18.2	-3.872	0.512416	2.18E-06	-	-	-	-	-	-
64	464	*	5	H	100	101		36	19.47	-4.554	0.512379	2.17E-06	-	-	-	-	-	-
64	464	*	5	H	20	21		36.7	21.3	-3.84	0.512414	5.07E-06	-	-	-	-	-	-
64	464	*	5	H	38	40		36.88	21.77	-4.744	0.512367	1.6E-05	-	-	-	-8.568	0.512171	1.92E-05
64	464	*	5	H	50	52		37	22.08	-4.673	0.51237	2.08E-06	-	-	-	-	-	-
64	464	*	5	H	100	101		37.5	23.38	-	-	-	-	-	-	-	-	-
64	464	*	5	H	50	52		38.51	23.51	-3.588	0.512424	2.94E-06	-	-	-	-	-	-
64	464	*	5	H	105	107		37.55	26.02	-4.466	0.512376	2.03E-06	-4.56	0.512371	6.94E-06	-10.02	0.512091	7.11E-06
64	464	*	5	H	105	107				-	-	-	-	-	-	-	-	-
64	464	*	5	H	100	101		39	27.29	-4.65	0.512365	2.18E-06	-	-	-	-	-	-
64	464	*	6	H	20	21		41.7	34.33	-	-	-	-	-	-	-	-	-
64	464	*	6	H	22	24		41.72	34.38	-4.262	0.512375	3.41E-06	-4.813	0.512347	2.81E-05	-	-	-
64	464	*	6	H	57	59		42.08	35.32	-4.251	0.512375	3.29E-06	-	-	-	-	-	-

Table 2.1 Continued

Leg	Site	H	Core	Type	Sec	Top	Bottom	Depth mbsf	Age (Ma)	εNd(t) Ox	143/144(t) 0.115	Std Error (2s)	εNd(t) FD	143/144(t) .131	Std Error (2s)	εNd(t) Res	143/144(t) 0.109	Std Error (2s)
64	464	*	6	H	100	101		42.5	36.41	1.4393	0.512665	9.9E-05	-	-	-	-	-	-
64	464	*	6	H	100	101		42.5	36.41	-	-	-	-	-	-	-	-	-
64	464	*	6	H	100	101		42.5	36.41	-	-	-	-	-	-	-	-	-
64	464	*	6	H	103	105		42.53	36.49	-4.381	0.512367	3.02E-06	-4.516	0.51236	2.48E-06	-	-	-
64	464	*	6	H	21	23		43.21	38.26	-5.003	0.512335	1.94E-05	-5.082	0.512331	1.94E-05	-	-	-
64	464	*	6	H	62	64		43.62	39.33	-4.159	0.512378	1.86E-05	-4.239	0.512374	1.86E-05	-7.927	0.512185	3.36E-05
64	464	*	6	H	90	91		43.9	40.06	-	-	-	-4.452	0.512363	4.88E-06	-	-	-
64	464	*	6	H	102	104				-	-	-	-	-	-	-	-	-
64	464	*	6	H	106	108		44.06	40.48	-4.321	0.51237	2.14E-06	-4.485	0.512361	3.86E-06	-5.775	0.512295	5.87E-06
64	464	*	6	H	130	131		44.3	41.11	-	-	-	-4.148	0.512376	1.25E-05	-	-	-
64	464	*	6	H	140	141		44.4	41.37	-	-	-	-3.955	0.512385	2.7E-06	-	-	-
64	464	*	6	H	10	11		44.6	41.89	-	-	-	-4.354	0.512363	1.39E-05	-	-	-
64	464	*	6	H	19	20		44.69	42.12	-	-	-	-4.017	0.51238	4.45E-06	-	-	-
64	464	*	6	H	30	31		44.8	42.41	-	-	-	-3.903	0.512385	5.71E-06	-	-	-

Table 2.1 Continued

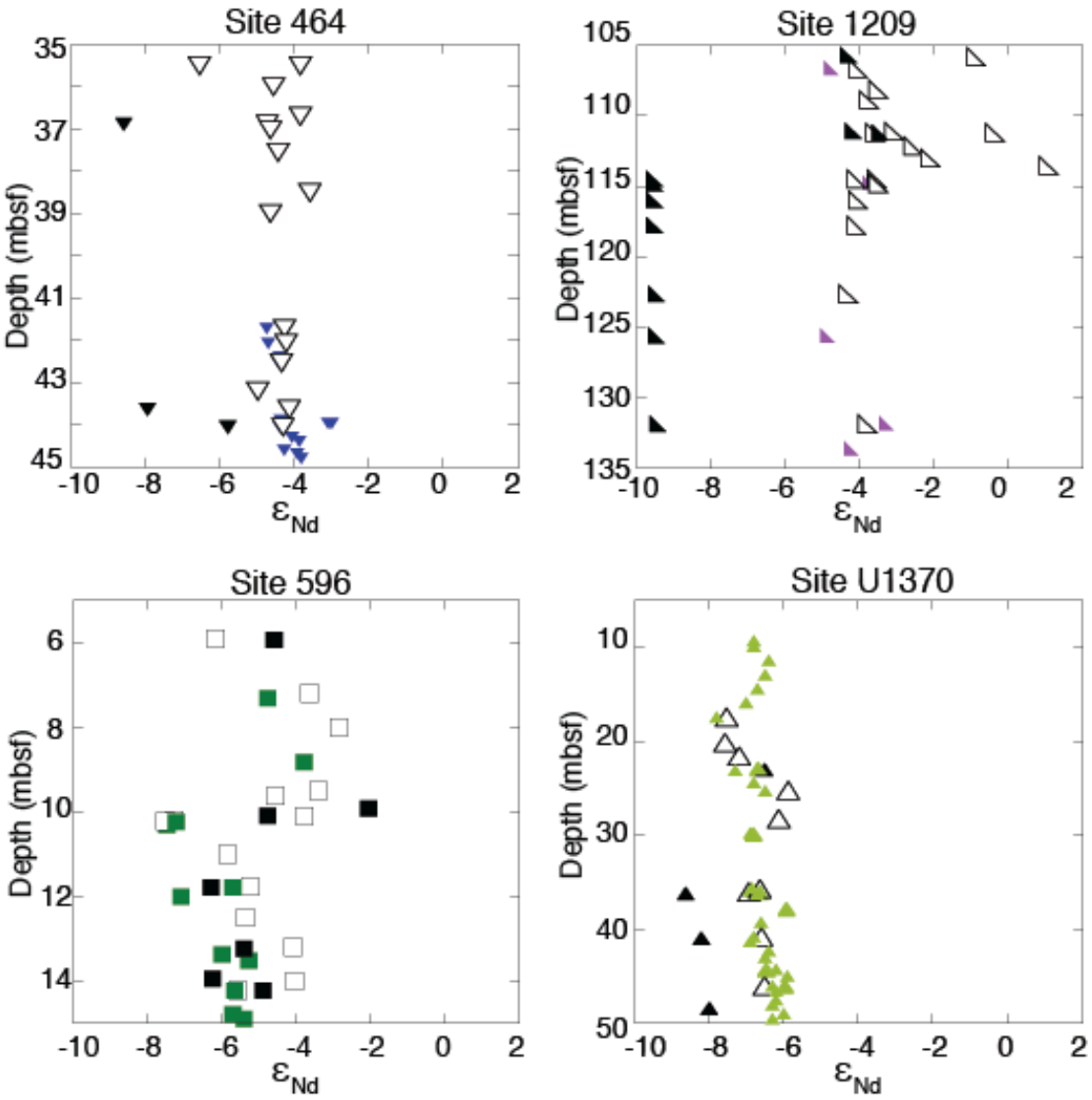

Figure 2.2 Pacific Ocean Nd isotope results data from Sites 1209, 464, 596 and U1370. Sites are plotted against depth (note y axis scale changes). Error bars for individual samples are smaller than the symbol size. Open black symbols are oxide coatings, closed symbols with color are fish debris, and closed black symbols are detrital residues.

Between 111 and 113 mbsf there was too little (less than 0.5g) residual material to analyze successfully.

We analyzed samples from the North Pacific Site 464 over a depth range of 35.51-44.8 mbsf (18-42 Ma). Fish debris epsilon values through this interval range between -3.8 and -5.0

(Fgure 2). The first leach values also stay within this range, agreeing with the first leach values at the same depth. The residue values range between -7.9 and -10 (Table 2.1). We analyzed samples from South Pacific Site 596 from 5.91-14.22 mbsf (8.40-36.1 Ma). The first leaches and fish debris over the course of the record at Site 596 range between -2.8 and -7.3 (figure 2.2). Similarly the residue values range from -2.9 to -6.3. A jump occurs from -7.54 $\varepsilon_{Nd}(t)$ at 10.2 mbsf (20.7 Ma) to -3.74 at 10.1 mbsf (20.3 Ma) in the first leaches. This jump is corroborated, in fish debris from -7.3 $\varepsilon_{Nd}(t)$ at 10.2 mbsf (20.7 Ma) to -3.4 at 9.5 mbsf (18.3 Ma) and in the residue -4.7 $\varepsilon_{Nd}(t)$ at 20.3 Ma to -2.0 at 19.7 Ma. South Pacific Site U1370 analyses span the depth range of 9.3-48.25 mbsf (3.67-35.45 Ma). First leaches and fish debris agree well over the course of the record at Site U1370 range between -5.8 and -7.6 $\varepsilon_{Nd}(t)$. The residue values range from -8.2 to -11.2 (Table 2.1).

2.5 Discussion

2.5.1 Evaluation of First Leach Values and the Leaching Process

We compared analyses of the fish debris Nd isotope values with that of the leached oxide coatings to examine the efficacy of the leaching procedure across a wide variety of lithologies and burial depths. Fish debris is broadly recognized as an impartial recorder of the isotopic composition of dissolved Nd at the seafloor because the Rare Earth Elements are incorporated into the mineral structure of apitaite, and thus used here to gauge the potential of the leached oxide coatings to record and preserve the same seawater composition because Rare Earth Elements are incoperated in or adsorbed onto the Fe oxyhydroxides and Mn oxides coating the sediment. The results of a comparison of the fish debris values with those of the leached oxide coatings in the same sample indicates the first leach and fish debris record similar values consistently in the records at Sites 464, 596 and U1370 (figure 2.2). The lithology at all three of

these is dominated by red clay. At Sites U1370 and 464 the fish debris and leached oxide values are distinct from the residues, suggesting different sources of dissolved and "detrital" Nd to those locations. At Site 596 the fish debris and leached oxide values are generally similar to those of the residues. The coincidence of values from these phases indicates that either the residue and the dissolved Nd at the seafloor had the same composition (due to a similar original source of weathering inputs or distinct sources that had similar compositions) or that the leaching procedure did not remove all the authigenic oxide coating from the residue at Site 596. The composition of sediment in the region, specifically at Site U1365, which is very close to Site 596, is well constrained (e.g. Dunlea et al 2015a; Dunlea et al 2015b). The aluminosilicate portion of the sediment, which should partition into the residue portion of the leach, is composed of an ash (rhyolite), altered basalt, and a dust component with similar composition to Post Archean Australian Average Shale (PAAS, Dunlea et al., 2015b). While we cannot be prescriptive about the method of transport for these detrital components they are more likely to be blown from Australia by the westerlies than to be transported from the Antarctic continent (Dunlea et al., 2015b), which is where the water mass at Site 596 likely originated from. Therefore the latter explanation of distinct sources of similar ε_{Nd} is more likely especially given the high (>10%) amount of authigenic material also identified at Site U1365 and nearby sites (Dunlea et al., 2015b). We tentatively consider the leached oxide values to reflect the dissolved inventory of Nd at the seafloor recorded at Site 596 and assimilate them into the paleoceanographic record with the fish debris data.

In contrast, the Site 1209 oxide and fish debris data indicate substantial differences in key portions of the record (113-105mbsf). The overall results from the sequential leaching at Site 1209 highlight how the presence of a small amount of a very radiogenic component can alter the

signature in the leached phase. This is either occurring as the radiogenic component is leached or because the radiogenic component is dissolving in the water column and becoming incorporated into all of the phases that record seawater. Given that the fish debris do not reflect the radiogenic composition found in the leached phase we conclude that our sequential leaching procedure, as identified by other studies (e.g. Wilson et al., 2013), does not work effectively on the lithology at Site 1209.

Site 1209 is unique among the study sites investigated here – it is the shallowest (paleodepths ~2300m); and more importantly it consists of at least 80 wt% carbonate throughout most of the interval from 40 to 15 Ma (Bralower et al., 2002). The isotopic composition of the residue at Site 1209 indicates two separate composition regimes. In the bottom of the record 131 to 113 mbsf (~38 to 30Ma) there is a detrital signature of ~-9.5. This indicates the presence of a dominant unradiogenic dust source, similar to Chinese Loess (e.g. Scudder et al., 2014), and is followed by a carbonate-rich regime where little to no residue was left after sequential leaching from 30 to 23Ma. Finally there is a radiogenic (-3.5), likely volcanic ash dominated, regime above 111 mbsf (23 Ma.) The shift to radiogenic values in the residue corresponds to a lithologic shift to subunit IC at 111.2 mbsf. Over this same interval the first leaches show extreme variability.

Blaser et al. (2016) determined that carbonate buffers the acid that promotes Fe reduction until the carbonate is consumed, and only then are the Fe-Mn and volcanic components dissolved. This means there is a threshold where a leach has accessed all of the carbonate and the Fe- Mn oxyhydr(oxide) coatings associated with the carbonate, and begins attacking "contaminant" phases. When this occurs Blaser et al., (2015) hypothesize that Fe-oxides and volcanic ash are easily accessed by the leachate and can overtake the signal imparted by the Fe-

Mn coatings. Blaser et al., (2016) therefore recommend using a very weak leaching procedure on sites dominated by carbonate, so as to extract the Fe- Mn oxyhydr(oxide) coatings associated with the carbonate and nothing else.

Without further analysis of the elemental composition of the leached phases it is difficult to determine if the radiogenic signature in the leach is caused by overprinting from a dissolved radiogenic source in the water, or the sequential leaching procedure extracting an aluminosilicate portion like volcanic ash. Fish debris in carbonate sediments record and retain the Nd IC of dissolved Nd of the waters at the seafloor (e.g., Scher and Martin, 2004; Tachikawa et al., 2017), and the fish debris at Site 1209 do not show the same variability as the first leaches so we rely on the fish debris data (figure 2.3), and conclude that the sequential leaching procedure extracted an aluminosilicate portion like volcanic ash and omit the first leaches for paleoceanographic interpretations at Site 1209.

2.5.2 Paleoceanographic Implications of the Nd Isotopic Records

The relatively unradiogenic signature in the South Pacific is similar to modern Southern Ocean Deep-water (ε_{Nd} -7 to -8.5; Basak et al., 2015) and supports previous models that indicate deep-water formation in the Pacific region of the Southern Ocean before the formation of the ACC (Huber et al., 2004; Thomas et al., 2014). Huck et al. (2017) identify the Nd isotopic signature of what is likely RSBW (-7.3 to 9.7) at Site 277 (paleodepth 1232m), during the middle Eocene (45 Ma). Apart from the radiogenic swing at Site 596, the bipolar circulation mode's north-south gradient published in Thomas et al. (2014) persistes after 40 Ma (figure 2.4).

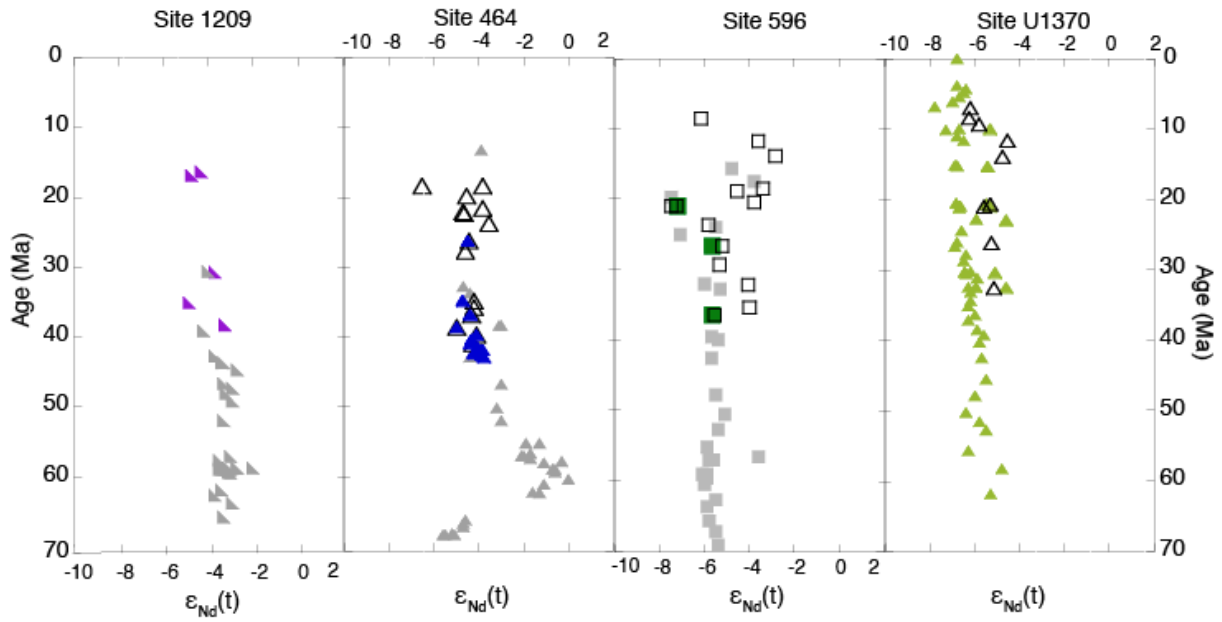

Figure 2.3 Nd isotopic composition from Sites 1209, 464, 596 and U1370 70-0Ma Error bars for individual samples are smaller than the symbol size, calculations for age models are provided in apendex A. Open black symbols are oxide coatings, closed symbols with color are fish debris, and closed grey symbols are published fish debris data (Hague et al., 2012; Thomas et al., 2004; and Thomas et al., 2014).

Our results coupled with Huck et al. (2017) conclude there was likely deepwater formation occurring in the Adelie region, or Ross Sea before the opening of the Drake and Tasman passages (figure 2.4). The South Pacific Nd IC gradient and shift are indicative of South Pacific Deep-water formation throughout the record, with an increasing influence of unradiogenic sources over time. However, the extent to which the concurrent climate changes are responses to circulation changes is unclear. The model in Sijp et al. (2014) indicate that there is cooling related to opening of Southern Ocean gateways, especially in the most recent part of the

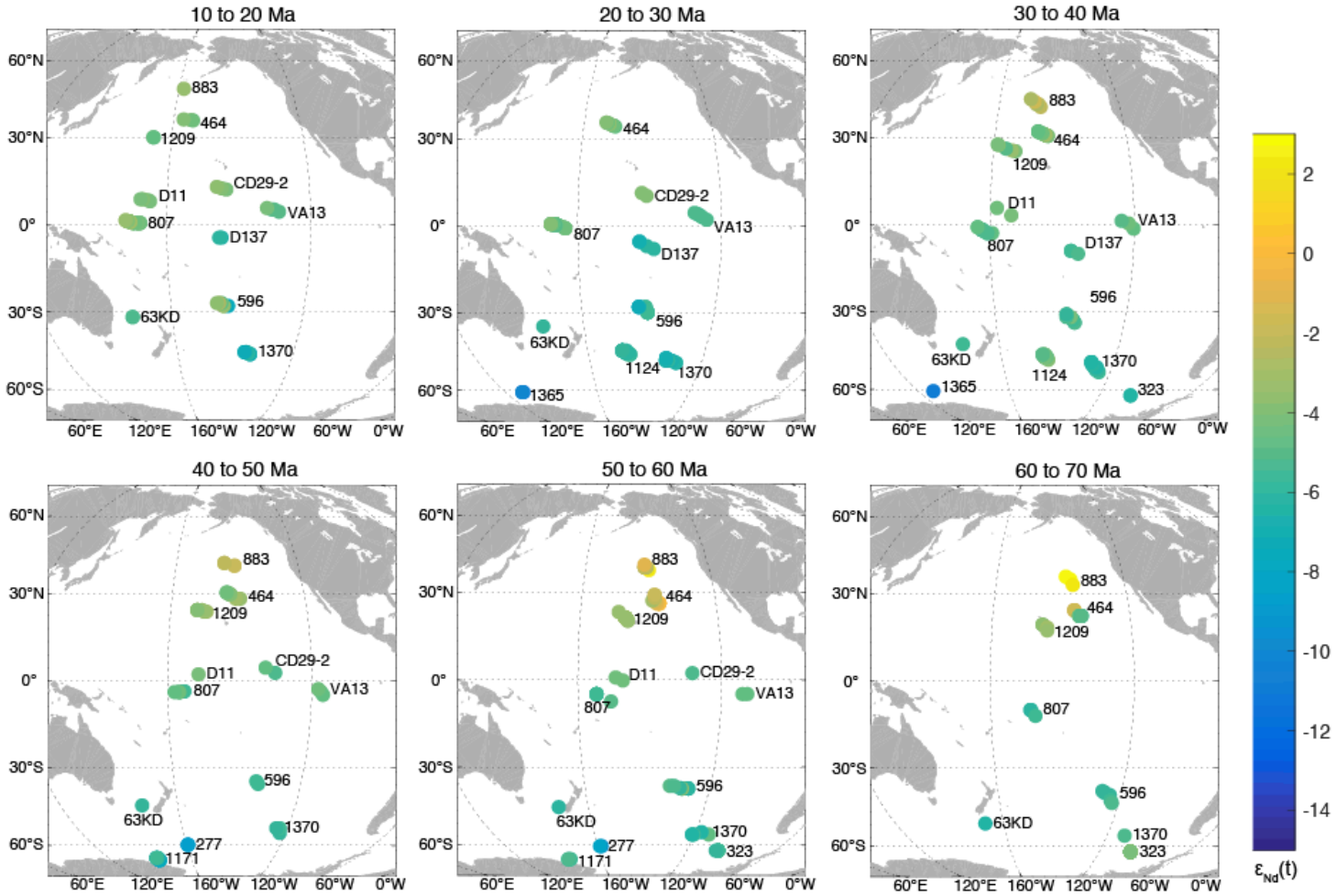

Figure 2.4 Map of the existing Nd isotopic data for the Pacific Ocean in 10 million year bins (Huck et al., 2017; Hauge et al., 2008; Le Houdec et al., 2016; Ling et al., 1997; Thomas et al., 2004; Thomas et al., 2014; van de Flierdt et al 2004). Where there is more than one data point in ten million years multiple circles are plotted with Paleo-latitude and longitude). Paleo-locations were determined in GPlates.

record (15-8Ma). The slow shift towards unradiogenic values at both Sites 596 and U1370 could reflect diminished export of radiogenic waters from the North Pacific, or increase in unradiogenic Nd via mixing within the growing circum-Antartic current system. It could also reflect a shift in the weathering sources to the Pacific sector of the Southern Ocean (e.g. Huck et al., 2017). Several lines of evidence point to the onset of permanent North Atlantic Deep-water formation beginning between 13 and 15 Ma (Blanc and Duplessy, 1982; Flower and Kennett, 1995). The increased flow of unradiogenic water to the Southern Ocean likely altered the composition of the Southern Ocean, which we would expect to eventually permeate into the signature of the water flowing North in the Pacific.

The exception to the overall slow evolution of South Pacific water mass composition is the rapid increase in values recorded at Site 596 at 20Ma (figure 2.3). This shift likely doesn't reflect a wholesale change in water mass composition because the same pattern is not evident at nearby South Pacific Site U1370 (even when we consider the limits of temporal resolution at both sites). While it seems unlikely that a radiogenic pulse of this magnitude reflects a decrease in surface ventilated bottom water coming from the North Pacific, several central Pacific sites to the north of Site 596 (Sites 807 and D11, figure 2.4) have similar at the same time. The shift could also reflect a local change in lithology of material moving into the water especially because it is reflected in all three phases of the leach (fish debris, leached and residue). The ~3 unit jump occurs within the bottom meter of Unit 1, described as a pelagic zeolitic clay spanning from 0 - 10.70 mbsf (Zhou and Kyte, 1992). Unit 2 is a metaliferous pelagic clay and zeolitic pelagic clay. The metaliferous pelagic clay could have become mobilized via bottom up processes (e.g. Abbott et al., 2015). Site 596 is oxic to basement, so there is no indication of a change in redox in the sediment, and the area below 10.70 mbsf does not reflect a radiogenic

signature that could have “bled up”. However, a rapid change in the source of sediment influencing the composition of the water from the top down water could cause a regional shift such as this one. Previous studies of the region show it receives pulses of increased volcanism that could alter the Nd IC of the water and sediment throughout time (Dunlea et al., 2015). The age of the shift at Site 596 occurs between two intervals of increased volcanism, 15 to 16 Ma and 24 to 26 Ma. It is important to note the onset of subduction in the Northwest Pacific including the initiation of volcanic island arcs occurs at 50 Ma (Seton et al., 2012). There is evidence of increased volcanic material at Site U1370, so the larger shift at Site 596 could be because it is further north, and closer to sources of terrigenous input. Dunlea et al. (2015a) model a greater portion of rhyolite (at Site U1365) in the region of Site 596, than at Site U1370 indicating that the two sites receive distinct inputs in different proportions. To the northwest of Site 596 at Site 807 on the Ontong Java plateau, Le Houedec et al. (2016) interpret radiogenic-unradiogenic “pseudo-cyclic” shifts after 40 Ma as reflecting seawater composition. They make this interpretation of their leached carbonate data on the basis of their rare earth pattern, and differentiation between the leached phase and “detrital” phase. These 7-11 Ma year “pseudo-cyclic” shifts have a similar period and magnitude to the shift at Site 596. While the interpretation in Le Houedec et al. (2016) lends validity to the interpretation that the shift at Site 596 reflects a change in seawater composition, it is equally possible that similar to our leached values at Site 1209 the leaching procedure is accessing and removing a readily reducible radiogenic component of the sediment at Site 807. Without fish debris data to compare to the leach data, it is difficult to determine if their oscillations are driven by changes in the composition of the water column or from leaching “contamination”. Either way a component that is contributed in pulses mixed well into the sediment, such as volcanic ash, could be the

radiogenic source in the cyclic shifts. Therefore, because of the regional nature of the change, the presence of similar isolated shifts in the region, and its magnitude we reason a periodic source of volcanic ash to the South Pacific is the mostly likely explanation for the jump.

The slow evolution towards increasingly unradiogenic values in the South Pacific does not translate to the North Pacific. Fish debris and first leach values from Sites 1209 and 464 have been reported from 70-40 Ma (Hague et al., 2012; Thomas, 2004). In the context of the record from 70-40Ma it is clear that the North Pacific signature remains relatively radiogenic for the entire record (figure 2.5). Site 464 values increase from -6 during the Late Cretaceous to 0 in the early Paleogene (60 Ma) before centering between -3 and -4 $\varepsilon_{Nd}(t)$ at ~50 Ma (figure 2.3); while the $\varepsilon_{Nd}(t)$ record at Site 1209 follows a similar pattern to 464 and increases from -4 to -2 between 60 and 70 Ma. The North Pacific signature at Sites 1209 and 464 remain steady (~-4) between 40 and 15 Ma.

2.5.3 Reconciling the North Pacific Trends in Nd Isotopic Composition

The new results presented in this study contribute to a growing body of data that demonstrates the slow evolution of water mass composition and circulation patterns in the South Pacific throughout the Cenozoic. As discussed above, much of this evolution can be attributed to the movement of tectonic gateways. The North Pacific's isotopic composition seems to change independently of the evolution of the South Pacific. Across the Cenozoic the North Pacific is very unradiogenic from 70 to 50Ma, and then has a relatively consistent composition of ~ -4 until 20Ma, where the signature becomes more radiogenic and the gradient between the North and South Pacific begins to increase. It is a challenge to reconcile these three stages of the North Pacific isotopic composition with theories of how the operating mode of circulation evolved throughout the Cenozoic, particularly in the subtropical regions where the mixing of NPDW and

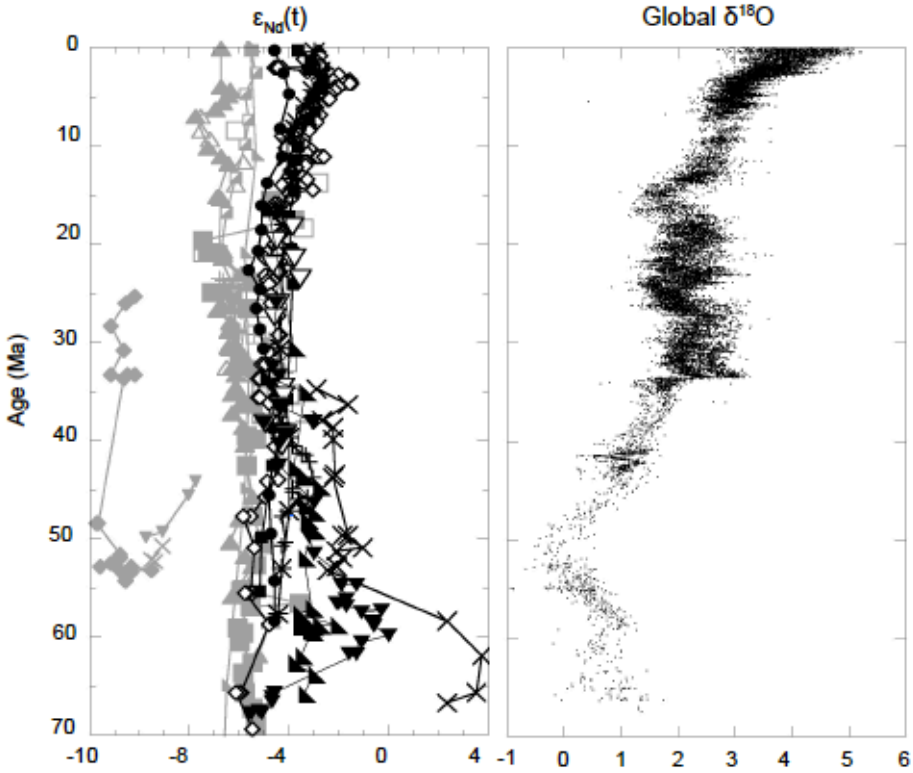

Figure 2.5 Nd isotopic composition from sites plotted in Figure 4 (Huck et al., 2017; Hague et al., 2008; Le Houdec et al., 2016; Ling et al., 1997; Thomas et al., 2004; Thomas et al., 2014; van de Flierdt et al 2004). The open symbols indicate oxide coatings, closed symbols are fish debris. Grey and black symbols indicate South and North Pacific regions, respectively. B: Global $\delta^{18}O$ of benthic foraminifera (Zachos et al., 2008)

Site	Symbol	Water Depth (m)	Location	Data Type	Citation
277	✖	1232	52°13'S 166°11'E	Fish Teeth	Huck et al., 2017
1171	●	2150	48°29'S , 149°6'E	Fish Teeth	Huck et al., 2017
D137	◪	7219	01°08'S, 168°04'W	Fe-Mn Crust	Van de Flierdt et al., 2004
1124	+	3967.5	39°29'S, 176°31'W	Fish Teeth	Scher at al., 2015
U1356	◆	4003	63°18'S , 135°59'E	Fish Teeth	Huck et al., 2017
63KD	◣	1700	28°34'S, 163°00'E	Fe-Mn Crust	Van de Flierdt et al., 2004
1370	▲	5084.7	41°51'S, 153°6'W	Fish teeth & Leach	This paper
596	■	5614	23° 51'S, 167° 39'W	Fish teeth & Leach	This paper, Thomas t al., 2014
CD29	■	2300	16°42'N, 168°14'W	Fe-Mn Crust	Ling et al., 1997
865	+	1518	18°26.'N, 179°33'W	Fish Debris	Thomas et al., 2014
D11	✕	1800	11°38'N,161°40'E,	Fe-Mn Crust	Ling et al., 1997
807	◇	2800	3°36'N, 156°3'E	Leach	Le Houdec et al., 2016
VA13	●	4800	9°18'N, 146°03'W	Fe-Mn Crust	Ling et al., 1997
883	×	2394	51°10'N, 167° 46'E	Fish Teeth	Thomas et al., 2014
1209	◣	2398.3	32°38'N, 158°30'E	Fish teeth & Leach	This paper, Thomas et al., 2014
464	▼	4670	39° 51'N, 173°53'E	Fish teeth & Leach	This paper, Thomas et al., 2014

Table 2.2 Table of locations, data type, data origin, water depth and symbol for sites plotted in Figures 4 & 5.

SPDW should have waned as NPDW convection ended and SPDW formation intensified (Thomas et al., 2014).

In order to put the gradient changes and patterns from our sites in context we compare them here with existing records from the Pacific (figure 2.5; Huck et al., 2017; Ling et al., 1997; Scher et al., 2014; Thomas et al., 2014; Van de Flierdt et al., 2004). Overall the north-south gradient in the Pacific remains consistent with very radiogenic values in the north and unradiogenic values in the south (figures 2.4, 2.5). However, the magnitude of these differences changes through time. In the center of the North Pacific the signature at Sites 1209, 464 and 883 decreases from +4 to about -4 over the course of the interval from 70 to 35 Ma. The Equatorial Pacific records (807, D11, CD29; figure 2.5, Table 2.2) center on -4 until 35 Ma and then begin to become more radiogenic between 35 and 25 Ma, increasing the gradient between the South and central Pacific. The divergence in the Nd IC gradient between the North Equatorial Pacific (807, D11, CD29) and South Pacific records (U1370, 596, D137, 63KD) between 35 and 25 Ma is likely because of slowing circulation in the region, allowing for a radiogenic signature to overprint the signature from the water mass. This explanation is confirmed by a shift from homogeneity to heterogeneity across the EOT measured in stable isotopes (Cramer et al., 2009), if the circulation from North to South decreased or stopped with would increase the heterogeneity of the stable isotopes. We posit that after 35Ma the central Pacific sites are dominated by overprinting from a radiogenic source, and this marks the transition between the formation of surface ventilated deep-water in the North Pacific and the modern sluggish-diffusive circulation state.

While eolian ash and dust inputs have previously been ruled out as major contributors of Nd to the North Pacific Ocean (Jones et al., 1994), recent research suggests volcanic ash may

impact the inventory of dissolved Nd in the water column (Scudder et al., 2014, Scudder et al., 2016, Wilson et al., 2013). Up to 50% of the marine sediment in the North Pacific region is composed of dispersed ash (Scudder et al., 2014). Dispersed ash is defined as volcanic ash material that is mixed throughout the bulk sediment and is altered to authigenic clay or is very fine grained (Scudder et al., 2016). The alteration to fine-grained material means ash present in sediment is visually indistinguishable from clay formed from other sources, but it is possible to identify using geochemical modeling (e.g. Scudder et al., 2014).

We see the clear presence of a radiogenic source in the sediment since 35 Ma, especially at Site 1209 and in the 3 epsilon unit jump at Site 596, which is present in all three phases. The fact that Sites U1370, 596 and 464 have sequentially leached Fe-Mn oxides with Nd IC matching concurrent fish debris suggests that the Fe-Mn oxides are not biased by ash during the leaching process. We have the context of Nd IC of three phases of the sediment, which lends confidence in the first leach data. Therefore, we cannot generalize about the origin of the Nd IC in the fish teeth and leached phases. More detailed studies of the elemental composition of the leached phases could provide a clearer picture of the sources to each phase. The radiogenic signature from ash could also be moving into the ocean and overprinting water mass composition, resulting in a Nd IC driven by regional trace metal inputs into the ocean, and not circulation patterns. This could be occurring either via deposition on land and subsequent riverine transport, dissolution upon deposition in the water, or fluxing out of pore water after burial in the sediment (e.g Abbot et al., 2014; Du et al., 2015). As our understanding of the distribution of Nd in the modern Pacific improves we will be able to better disentangle the sources to the sediment, seawater and leached phases.

The presence of altered ash may also explain how analysis of leached residues used to constrain eolian inputs of Nd into the Pacific underestimated the influence of ash (Jones et al., 1994). The ash is likely removed during the aggressive leaching procedure performed by Jones et al., (1994) targeting the Fe-Mn oxides; thus, the zonation of Nd IC identified in Jones et al. (1994), with radiogenic material dominating the edges of the Pacific basin and unradiogenic material dominating the center, is based on the assumption that all of the aluminosilicate material in the sediment was preserved by their leaching procedure. The pattern identified instead likely reflects relative amounts of ash and not the presence or absence of ash. Low ash concentrations would be completely leached while high concentrations leave a radiogenic signature behind. This is very similar to what we see in the Site 1209 data presented here. It is important to note that over the course of the record all of the sites are moving north-west on the Pacific Plate, and so with time the sites move closer to the source of ash.

Radiogenic bottom water at Sites 1209, 464 and 883, has been previously identified and interpreted as North Pacific Deep-water formation in the North Pacific from 70 to ~35 Ma. However, the late Paleogene-early Neogene North Pacific's ε_{Nd} signature could also be dominated by volcanic ash inputs accumulating through the water column, in which case it is not possible to differentiate the signature of surface-ventilated deep-water from the modern North Pacific gradient created by sluggish circulation of deep-water accumulating a radiogenic signature and slowly upwelling in the eastern basin. Overprinting of bottom water signatures due to reversible scavenging could leave the same record in fish debris and oxide coatings as the signature of surface ventilated deep-water sinking from top to bottom in the water column. It is especially striking that the $\varepsilon_{Nd}(t)$ values at Sites 883, 464 and 1209 decrease with time from 70 Ma to 35 Ma as they move Northwest, and are not likely to be subsiding due to their crustal ages

(>110 Ma, see supplemental material for details). We would expect these ratios to become more radiogenic as they travel north if their signature was controlled by over printing from volcanic activity. The formation of NPDW has been corroborated previously with coupled climate model simulations that find surface ventilated deep-water formation in North and South Pacific. Given the location of the sites at 35Ma the more likely of the two explanations for the signature in the North Pacific before 35 Ma is the sinking of very radiogenic surface water in the North Pacific that subsequently travels south as North Pacific Deep-water (NPDW).

There is a 10 million year window between 35 and 25 Ma where the values in both North and South Pacific regions converge at ~-4 before the central sites begin to become more radiogenic (Figure 2.5). The Nd IC of the North Pacific sites increase to ~-4 by 35 Ma and the subsequent shift of the Equatorial Pacific sites to more radiogenic values after 25 Ma. We identify this 10 Ma window as the slow transition from the Paleogene mode of surface-ventilated deep-water convection in the North Pacific to the Modern mode with sluggish diffusive mixing.

The fact that the transition occurs so slowly over 10 million years, and after the EOT indicates that it is a response to either tectonic movement or climate changes, and it is not the cause of the initial transition to a cooler climate. Climate related factors like temperature gradients and evaporation / precipitation are not the only controls on of surface-ventilated deep-water formation. Increased tidal energy dissipation for instance, which can increase vertical diffusivity and MOC, is not controlled by long term changes in climate, but is instead controlled by the shape of the ocean basin (Mattias Green et al., 2009; Schmittner et al., 2015). Changes in the mechanical energy for mixing could allow for downwelling of deep-water in the North Pacific that is responsible for the deep radiogenic signature of Nd captured from ~70 to 40 Ma (Hague et al., 2012; Thomas et al., 2004). The timing of the transition between modes does occur

in conjunction with many other changes in climate state over 10 million years and we would expect the transition to sluggish circulation would exert influence on the ocean / atmosphere system.

2.6 Conclusion

The North and South Pacific $\varepsilon_{Nd}(t)$ records do not seem to reflect concurrent basin-wide changes in ocean circulation. Overall, the South Pacific gradient confirms deep-water formation in the Pacific sector of the Southern Ocean before the opening of the Drake Passage / Tasman Gateway and throughout the study period. There is a distinct negative 3 epsilon unit shift in the South Pacific Nd IC that indicates an event at 20 Ma during which there was a rapid increase in radiogenic Nd IC. This is followed by a gradual return to unradiogenic values (~-7 $\varepsilon_{Nd}(t)$ by ~10Ma. We conclude the influence of change in input source to the region is the most likely explanation for the shift and subsequent rebound. The slow trend towards unradiogenic values that bookmarks the sharp three unit jump in Nd IC at Site 596 could be caused by the decrease in influence of radiogenic water (i.e. weakening of sources of North Pacific water to the region) or increased influence of NADW in the Southern Ocean.

While our interpretations are complicated by sources with similar signatures in the region, deep-water formation in the North Pacific remains a durable explanation of radiogenic the values of North Pacific Bottom Water from 70 to 35 Ma. The sequential changes in the pattern of Nd IC in the Equatorial and North Pacific suggest a shift from surface ventilated deepwater to the sluggish modern mode that occurs between 35 and 25 Ma.

The sequential leaching results highlight the potential influence of readily reducible portions of sediment on oxide values, as well as on the composition of the bottom water itself. Therefore, there are likely short-term concurrent and related changes in sources of sediment

input and Nd IC of water. This is clear at Site 1209 in addition to Site 596. The influence of periodic volcanism, especially at sites dominated with carbonate, makes vital a careful evaluation of sediment lithology and leaching procedure before proceeding with sediment isotope analysis.

2.7 References

Abbott, April N, Brian A Haley, and James McManus. 2015. "Bottoms up: Sedimentary control of the deep North Pacific Ocean's εNd signature." *Geology* 43 (11):1035-1035.

Allen, Mark B., and Howard A. Armstrong. 2008. "Arabia–Eurasia collision and the forcing of mid-Cenozoic global cooling." *Palaeogeography, Palaeoclimatology, Palaeoecology* 265 (1):52-58. doi: https://doi.org/10.1016/j.palaeo.2008.04.021.

Basak, Chandranath, Katharina Pahnke, Martin Frank, Frank Lamy, and Rainer Gersonde. 2015. "Neodymium isotopic characterization of Ross Sea Bottom Water and its advection through the southern South Pacific." *Earth and Planetary Science Letters* 419:211-221.

Blanc, Paul-Louis, and Jean-Claude Duplessy. 1982. "The deep-water circulation during the Neogene and the impact of the Messinian salinity crisis." *Deep Sea Research Part A. Oceanographic Research Papers* 29 (12):1391-1414. doi: http://dx.doi.org/10.1016/0198-0149(82)90033-4.

Blaser, Patrick, Jörg Lippold, Marcus Gutjahr, Norbert Frank, Jasmin M. Link, and Martin Frank. 2016. "Extracting foraminiferal seawater Nd isotope signatures from bulk deep sea sediment by chemical leaching." *Chemical Geology* 439:189-204. doi: https://doi.org/10.1016/j.chemgeo.2016.06.024.

Bralower, T.J., Premoli Silva, I., Malone, M.J., et al.,. 2002. "Initial Reports " *Proceedings of the Ocean Drilling Program* 198. doi: doi:10.2973/odp.proc.ir.198.2002.

Broecker, WS, and TH Peng. 1982. "Tracers in the Sea, 690 pp." *Lamont-Doherty Geological Observatory, Palisades, NY*.

Cramer, B. S., J. R. Toggweiler, J. D. Wright, M. E. Katz, and K. G. Miller. 2009. "Ocean overturning since the Late Cretaceous: Inferences from a new benthic foraminiferal isotope compilation." *Paleoceanography* 24 (4):n/a-n/a. doi: 10.1029/2008PA001683.

Dalziel, Ian W.D., Lawrence A. Lawver, Ian O. Norton, and Lisa M. Gahagan. 2013. "The Scotia Arc: Genesis, Evolution, Global Significance." *Annual Review of Earth and Planetary Sciences* 41 (1):767-793. doi: 10.1146/annurev-earth-050212-124155.

Dunlea, Ann G, Richard W Murray, Justine Sauvage, Arthur J Spivack, Robert N Harris, and Steven D'Hondt. 2015. "Dust, volcanic ash, and the evolution of the South Pacific Gyre through the Cenozoic." *Paleoceanography* 30 (8):1078-1099.

Flower, Benjamin P., and James P. Kennett. 1995. "Middle Miocene deepwater paleoceanography in the southwest Pacific: Relations with East Antarctic Ice Sheet development." *Paleoceanography* 10 (6):1095-1112. doi: 10.1029/95PA02022.

Frank, Martin. 2002. "Radiogenic isotopes: tracers of past ocean circulation and erosional input." *Reviews of geophysics* 40 (1).

Hague, Ashley M, Deborah J Thomas, Matthew Huber, Robert Korty, Stella C Woodard, and L Blake Jones. 2012. "Convection of North Pacific deep water during the early Cenozoic." *Geology* 40 (6):527-530.

Horikawa, Keiji, Ellen E. Martin, Yoshihiro Asahara, and Takuya Sagawa. 2011. "Limits on conservative behavior of Nd isotopes in seawater assessed from analysis of fish teeth from Pacific core tops." *Earth and Planetary Science Letters* 310 (1):119-130. doi: https://doi.org/10.1016/j.epsl.2011.07.018.

Howe, Jacob N. W., Alexander M. Piotrowski, Taryn L. Noble, Stefan Mulitza, Cristiano M. Chiessi, and Germain Bayon. 2016. "North Atlantic Deep Water Production during the Last Glacial Maximum." *Nature Communications* 7:11765. doi: 10.1038/ncomms11765
https://www.nature.com/articles/ncomms11765#supplementary-information.

Huber, Matthew, Henk Brinkhuis, Catherine E. Stickley, Kristofer Döös, Appy Sluijs, Jeroen Warnaar, Stephen A. Schellenberg, and Graham L. Williams. 2004. "Eocene circulation of the Southern Ocean: Was Antarctica kept warm by subtropical waters?" *Paleoceanography* 19 (4):n/a-n/a. doi: 10.1029/2004PA001014.

Huck, Claire E., Tina van de Flierdt, Steven M. Bohaty, and Samantha J. Hammond. 2017. "Antarctic climate, Southern Ocean circulation patterns, and deep water formation during the Eocene." *Paleoceanography* 32 (7):674-691. doi: 10.1002/2017PA003135.

Jones, Charles E, Alex N Halliday, David K Rea, and Robert M Owen. 1994. "Neodymium isotopic variations in North Pacific modern silicate sediment and the insignificance of detrital REE contributions to seawater." *Earth and Planetary Science Letters* 127 (1-4):55-66.

Kawabe, Masaki, and Shinzou Fujio. 2010. "Pacific Ocean circulation based on observation." *Journal of oceanography* 66 (3):389.

Kryc, KA, RW Murray, and DW Murray. 2003. "Elemental fractionation of Si, Al, Ti, Fe, Ca, Mn, P, and Ba in five marine sedimentary reference materials: results from sequential extractions." *Analytica chimica acta* 487 (1):117-128.

Lacan, Francois, and Catherine Jeandel. 2005. "Neodymium isotopes as a new tool for quantifying exchange fluxes at the continent–ocean interface." *Earth and Planetary Science Letters* 232 (3):245-257.

Lambelet, Myriam, Tina van de Flierdt, Kirsty Crocket, Mark Rehkämper, Katharina Kreissig,

Barry Coles, Micha JA Rijkenberg, Loes JA Gerringa, Hein JW de Baar, and Reiner Steinfeldt. 2016. "Neodymium isotopic composition and concentration in the western North Atlantic Ocean: results from the GEOTRACES GA02 section." *Geochimica et Cosmochimica Acta* 177:1-29.

Le Houedec, Sandrine, Laure Meynadier, and Claude J. Allègre. 2016. "Seawater Nd isotope variation in the Western Pacific Ocean since 80 Ma (ODP 807, Ontong Java Plateau)." *Marine Geology* 380:138-147. doi: https://doi.org/10.1016/j.margeo.2016.07.005.

Ling, H. F., K. W. Burton, R. K. O'Nions, B. S. Kamber, F. von Blanckenburg, A. J. Gibb, and J. R. Hein. 1997. "Evolution of Nd and Pb isotopes in Central Pacific seawater from ferromanganese crusts." *Earth and Planetary Science Letters* 146 (1–2):1-12. doi: https://doi.org/10.1016/S0012-821X(96)00224-5.

Lyle, Mitchell, John Barron, Timothy J Bralower, Matthew Huber, Annette Olivarez Lyle, A Christina Ravelo, David K Rea, and Paul A Wilson. 2008. "Pacific Ocean and Cenozoic evolution of climate." *Reviews of Geophysics* 46 (2).

Martin, EE, and HD Scher. 2004. "Preservation of seawater Sr and Nd isotopes in fossil fish teeth: bad news and good news." *Earth and Planetary Science Letters* 220 (1):25-39.

Miller, Kenneth G, James D Wright, and Richard G Fairbanks. 1991. "Unlocking the ice house: Oligocene-Miocene oxygen isotopes, eustasy, and margin erosion." *Journal of Geophysical Research: Solid Earth* 96 (B4):6829-6848.

Molina-Kescher, Mario, Martin Frank, and Ed Hathorne. 2014. "South Pacific dissolved Nd isotope compositions and rare earth element distributions: Water mass mixing versus biogeochemical cycling." *Geochimica et Cosmochimica Acta* 127:171-189. doi: https://doi.org/10.1016/j.gca.2013.11.038.

Molina-Kescher, Mario, Martin Frank, and Ed C. Hathorne. 2014. "Nd and Sr isotope compositions of different phases of surface sediments in the South Pacific: Extraction of seawater signatures, boundary exchange, and detrital/dust provenance." *Geochemistry, Geophysics, Geosystems* 15 (9):3502-3520. doi: 10.1002/2014GC005443.

Mudelsee, Manfred, Torsten Bickert, Caroline H Lear, and Gerrit Lohmann. 2014. "Cenozoic climate changes: A review based on time series analysis of marine benthic δ18O records." *Reviews of Geophysics* 52 (3):333-374.

Pälike, Heiko, Mitchell W. Lyle, Hiroshi Nishi, Isabella Raffi, Andy Ridgwell, Kusali Gamage, Adam Klaus, Gary Acton, Louise Anderson, Jan Backman, Jack Baldauf, Catherine Beltran, Steven M. Bohaty, Paul Bown, William Busch, Jim E. T. Channell, Cecily O. J. Chun, Margaret Delaney, Pawan Dewangan, Tom Dunkley Jones, Kirsty M. Edgar, Helen Evans, Peter Fitch, Gavin L. Foster, Nikolaus Gussone, Hitoshi Hasegawa, Ed C. Hathorne, Hiroki Hayashi, Jens O. Herrle, Ann Holbourn, Steve Hovan, Kiseong Hyeong, Koichi Iijima, Takashi Ito, Shin-ichi Kamikuri, Katsunori Kimoto, Junichiro

Kuroda, Lizette Leon-Rodriguez, Alberto Malinverno, Ted C. Moore Jr, Brandon H. Murphy, Daniel P. Murphy, Hideto Nakamura, Kaoru Ogane, Christian Ohneiser, Carl Richter, Rebecca Robinson, Eelco J. Rohling, Oscar Romero, Ken Sawada, Howie Scher, Leah Schneider, Appy Sluijs, Hiroyuki Takata, Jun Tian, Akira Tsujimoto, Bridget S. Wade, Thomas Westerhold, Roy Wilkens, Trevor Williams, Paul A. Wilson, Yuhji Yamamoto, Shinya Yamamoto, Toshitsugu Yamazaki, and Richard E. Zeebe. 2012. "A Cenozoic record of the equatorial Pacific carbonate compensation depth." *Nature* 488:609. doi: 10.1038/nature11360 https://www.nature.com/articles/nature11360#supplementary-information.

Prothero, Donald R, Linda C Ivany, Elizabeth A Nesbitt, and Elizabeth R Nesbitt. 2003. *From greenhouse to icehouse: the marine Eocene-Oligocene transition*: Columbia University Press.

Reimi, Maria A, and Franco Marcantonio. 2016. "Constraints on the magnitude of the deglacial migration of the ITCZ in the Central Equatorial Pacific Ocean." *Earth and Planetary Science Letters* 453:1-8.

Scher, Howie, Joanne Whittaker, Simon William, Jennifer Latimer, Wendy Kordesch, and Margaret Delaney. 2015. "Onset of antarctic circumpolar current 30 million years ago as Tasmanian Gateway aligned with westerlies." *Nature* 523 (7562):580-583.

Scher, Howie D, and Ellen E Martin. 2006. "Timing and climatic consequences of the opening of Drake Passage." *Science* 312 (5772):428-430.

Scudder, Rachel P., Richard W. Murray, Julie C. Schindlbeck, Steffen Kutterolf, Folkmar Hauff, and Claire C. McKinley. 2014. "Regional-scale input of dispersed and discrete volcanic ash to the Izu-Bonin and Mariana subduction zones." *Geochemistry, Geophysics, Geosystems* 15 (11):4369-4379. doi: 10.1002/2014GC005561.

Scudder, Rachel P, Richard W Murray, Julie C Schindlbeck, Steffen Kutterolf, Folkmar Hauff, Michael B Underwood, Samantha Gwizd, Rebecca Lauzon, and Claire C McKinley. 2016. "Geochemical approaches to the quantification of dispersed volcanic ash in marine sediment." *Progress in Earth and Planetary Science* 3 (1):1.

Sijp, Willem P., and Matthew H. England. 2004. "Effect of the Drake Passage Throughflow on Global Climate." *Journal of Physical Oceanography* 34 (5):1254-1266. doi: 10.1175/1520-0485(2004)034<1254:EOTDPT>2.0.CO;2.

Tachikawa, Kazuyo, Thomas Arsouze, Germain Bayon, Aloys Bory, Christophe Colin, Jean-Claude Dutay, Norbert Frank, Xavier Giraud, Alexandra T. Gourlan, Catherine Jeandel, François Lacan, Laure Meynadier, Paolo Montagna, Alexander M. Piotrowski, Yves Plancherel, Emmanuelle Pucéat, Matthieu Roy-Barman, and Claire Waelbroeck. 2017. "The large-scale evolution of neodymium isotopic composition in the global modern and Holocene ocean revealed from seawater and archive data." *Chemical Geology* 457:131-148. doi: http://dx.doi.org/10.1016/j.chemgeo.2017.03.018.

Tachikawa, K., V. Athias, and C. Jeandel. 2003. "Neodymium budget in the modern ocean and paleo-oceanographic implications." *Journal of Geophysical Research: Oceans* 108 (C8):n/a-n/a. doi: 10.1029/1999JC000285.

Talley, L.D. 2013. "Closure of the Global Overturning Circulation Through the Indian, Pacific, and Southern Oceans: Schematics and Transports." *Oceanography* 26. doi: doi.org/10.5670/oceanog.2013.07.

Taylor, Stuart Ross, and Scott M. McLennan. 1995. "The geochemical evolution of the continental crust." *Reviews of Geophysics* 33 (2):241-265. doi: 10.1029/95RG00262.

Tessier, Andre, Pg GC Campbell, and M Bisson. 1979. "Sequential extraction procedure for the speciation of particulate trace metals." *Analytical chemistry* 51 (7):844-851.

Thomas, Deborah J. 2004. "Evidence for deep-water production in the North Pacific Ocean during the early Cenozoic warm interval." *Nature* 430 (6995):65.

Thomas, Deborah J, Robert Korty, Matthew Huber, Jessica A Schubert, and Brian Haines. 2014. "Nd isotopic structure of the Pacific Ocean 70–30 Ma and numerical evidence for vigorous ocean circulation and ocean heat transport in a greenhouse world." *Paleoceanography* 29 (5):454-469.

van de Flierdt, Tina, Martin Frank, Alex N. Halliday, James R. Hein, Bodo Hattendorf, Detlef Günther, and Peter W. Kubik. 2004. "Deep and bottom water export from the Southern Ocean to the Pacific over the past 38 million years." *Paleoceanography* 19 (1):n/a-n/a. doi: 10.1029/2003PA000923.

Via, Rachael K, and Deborah J Thomas. 2006. "Evolution of Atlantic thermohaline circulation: Early Oligocene onset of deep-water production in the North Atlantic." *Geology* 34 (6):441-444.

Wilson, David J, Alexander M Piotrowski, Albert Galy, and Josephine A Clegg. 2013. "Reactivity of neodymium carriers in deep sea sediments: Implications for boundary exchange and paleoceanography." *Geochimica et Cosmochimica Acta* 109:197-221.

Zhou, Lei, and Frank T. Kyte. 1992. "Sedimentation history of the South Pacific pelagic clay province over the last 85 million years Inferred from the geochemistry of Deep Sea Drilling Project Hole 596." *Paleoceanography* 7 (4):441-465. doi: 10.1029/92PA01063.

Ziegler, CL, RW Murray, SA Hovan, and DK Rea. 2007. "Resolving eolian, volcanogenic, and authigenic components in pelagic sediment from the Pacific Ocean." *Earth and Planetary Science Letters* 254 (3):416-432.

3. THE REPRODUCIBILITY AND FIDELITY OF ACID REDUTIVE LEACHING TARGETING FE-MN OXYHYDROXIDE COATINGS IN THE NORTH AND SOUTH PACIFIC OCEAN

3.1 Introduction

Fe-Mn oxyhydroxide crusts and coatings form by the scavenging of dissolved seawater components. Elements including Pb and Nd become incorporated into the coatings by adsorption, replacement, and / or co-precipitation with the major oxides (Koschinsky and Hein, 2003; Lee, 1981). Nd isotopes recorded in fossil fish debris, foraminifera and authigenic oxide coatings of marine sediment have been established as tracers of the ε_{Nd} of bottom water masses, enabling paleo-circulation reconstructions back in time. Pb isotopes have similar characteristics to Nd; however they also exhibit distinct differences. Pb is generally thought to be a proxy of weathering inputs when dissolved in seawater. When Pb and Nd are viewed concurrently both contribute context that aid in paleoceanographic interpretations and reconstructions.

While separating and dissolving fossil fish debris and foraminifera from the bulk sediment matrix is relatively simple, isolating the authigenic Fe-Mn oxide coatings of marine sediment requires an acid reductive leaching process. Separation of this component can provide valuable insight into paleo-circulation, particularly in regions that are devoid of calcium carbonate (forams), where fish debris are found at low resolution, or when analyzing Pb and Nd isotopes concurrently is advantageous.

In order to use sequential leaching to answer paleoceanographic questions we must understand the reproducibility and fidelity of our acid reductive leaching procedure. The purpose of any sequential extraction procedure is to isolate a specific portion of the sediment for analysis

(Tessier et al., 1979). The material that is extracted by each leaching step is defined operationally as a specific phase of sediment (Kryc et al., 2003). That is, leaching in buffered acetic acid dissolves the carbonate fraction, while leaching with a reducing agent dissolves the oxide fraction, etc. Several recent studies have indicated that the individual reagents in the leaching process may dissolve other phases of sediment in addition to the primary target, particularly such phases susceptible to dissolution such as glacial flour, dispersed or altered volcanic ash (e.g., Du et al., 2016; Molina-Kesher et al., 2014; Wilson et al., 2013;). These volcanic or detrital components are generally referred to as "contaminants" and alter the Rare Earth Element (REE) concentrations and isotopic composition of leached samples (e.g. Wilson et al., 2013). The ability to apply oceanographic interpretations to the data generated by acid reductive leaching is limited by the effectiveness of the extraction method and how inter-grown the oxides minerals are with each other and the particle to which they are attached (Koschinsky and Hein, 2003). While there is no physical or chemical process that can uniquely separate Fe-Mn Oxide coatings from the rest of the sediment (Kyrc et al., 2003) an acid reductive leaching procedure (such as the one used here) is designed to isolate the Fe-Mn oxide coatings and the associated sorbed and incorporated trace metals via reductive dissolution of the loosely bound fraction of Fe-Mn oxides.

In order to assess the potential "contamination" that results from dissolution of phases other than the authigenic oxide fraction, we must explore a broader suite of elemental compositions. One motivation to pursue a quantitatively reproducible procedure for accessing the loosely bound Fe-Mn oxides is to exploit the entire inventory of elements and isotopic tracers recorded by the oxide precipitation. Specifically, even though fossil fish debris are believed to more accurately record dissolved Nd at the seafloor (Martin et al., 2004) they only permit

analysis of Nd and Sr. Pb in fish debris is an unsuitable proxy because the Pb adsorbed and incorporated cannot be distinguished from Pb that has decayed from the U present in apatite and carbonate. The oxide fraction offers the ability to analyze several trace metals concomitantly, including Pb isotopes, which provides synergistic value to paleoceanographic interpretations. In the Pacific, where there are not many sources of Nd that have appreciably unique signatures (Tachakawa et al., 2017), this could be particularly valuable. Nd and Pb isotopes provide useful information about source provenance, trace metal processes in the ocean as well as water mass movement. However, it is difficult to evaluate the results of operationally defined acid reductive leaching procedure with only two isotopes The results of the Chapter II highlight the importance of being able to constrain where signatures originate. A unique challenge of applying acid reductive leaching to paleoceanographic questions is that the materials available for analysis span several lithologies, and varied ocean conditions (i.e., pH, oxygen, temperature, and CCD depth) throughout space and time. The chemical leaching procedures applied to these varied sediments may dissolve different components of the oxides when applied to different sediments deposited under different conditions, and therefore the leach may bias the resulting elements/isotopic compositions. Furthermore, application of this procedure to sediments with relatively labile components such as glacial flour, volcanic ash, or altered volcanic ash, may result in dissolution of more than just the oxide that precipitated from seawater (Wilson et al., 2013). Leaching is employed in many contexts for varied purposes and leaching can remove organic material and quantify contributions of a specific phase of sediment (Marsay et al., 2017; Reimi and Marcantonio, 2016).

To this end, we examine the major, trace, and REE elements of leached and residual fractions of marine sediment at two compositionally distinct sites: ODP Site 1149 in the Northwestern Pacific Ocean and IODP Site U1370 in the central South Pacific Ocean.

3.2 Scope of the work presented in this paper

There is a growing understanding of the complicated array of sources, sinks, and pathways of major, trace and REE elements within the water column and sedimentary pore fluids. One goal of paleoceanographic proxy investigations is to isolate the composition of elements/isotopic ratios that reflect a "quasi-conservative" trace of water mass composition. This means Nd would reflect simple fluvial and weathering input in a region of water convection or subduction and would reveal mixing with other signatures in seawater along the flow path. The observation that Nd isotopes are quasi-conservative, and function as described above formed the basis of a body growing literature using Nd isotopes as water mass tracers (Frank 2002; Goldstein and Hemming 2000). We now recognize that there are numerous additional pathways by which dissolved Nd can influence the isotopic composition of waters at the seafloor. One pathway is a "bottom-up" source of Nd: the oxides and oxyhydroxides onto which Nd and Pb are adsorbed are readily reduced as the sediment becomes anoxic. This can lead to porewater-derived fluxes of REE into bottom waters that can bias paleoceanographic interpretations (Abbott et al., 2015; Haley et al., 2017). A second is submarine ground water discharge (Johannesson and Burdige, 2007), which is another mechanism for bottom up control of Nd composition. A third is top down overprinting via inputs of eolian material like dust or ash and subsequent reversible scavenging (Jeandel et al., 2013, Molina-Kesher et al., 2018). In order to transport these signatures from the surface to the bottom water there has to be a relatively high flux of sinking material, that generally relegates this process to the margins. All three of these

possible pathways indicate or explain non-conservative behavior of modern Nd and complicate using Nd as a quasi-conservative tracer of water mass movement. While not a unique pathway, Lecan and Jeandel (2001, 2005) present evidence for another non-conservative processes impacting Nd: the exchange between particulate and dissolved fractions that they term "boundary exchange". Their data indicate that there are changes in the Nd Isotopic Composition (IC) along deep flow paths (Lecan and Jeandel (2016)).

Additionally, the original pH and dissolved oxygen in bottom water control the trace elements that become adsorbed, incorporated, or co-precipitated (e.g. Huck et al, 2016; and Koschinsky and Hein, 2003). Even with the most selective leach we cannot control the source of the trace metals. Idealy the Pb and Nd isotopic signatures reflect the signature of water mass mixing, but ss outlined above, in many cases the ideal model is not the only process controlling the IC distribution at the sediment water interface. Our understanding of how and where these processes interact, and their influence on the distribution of trace metals in at the sediment water interface is critical to how we interpret the isotopic composition of fossil fish debris, Fe-Mn crusts and sediment oxide coatings. Thus, here we aim to use our multi-element data on leach fractions to characterize their sources across sediment lithologies.

Additionally we hope to test reproducibility of acid reductive leaching results from leach to leach and lab to lab, which is currently poorly constrained. It is important to be constantly vigilant about the results of sequential leaching. Under stringent conditions Kryc et al. (2003) concluded sequential leaching can yield consistent (reproducible within approximately 15%) elemental results for the major elements.

By investigating which geochemical fractions are mobilized by the acid reductive leaching technique we aim to identify the fidelity of our acid reductive leaching process across

different lithologies. The leaching procedure we use is well established (Wilson et al., 2013) and widely used (e.g., Basak et al., 2010; Gutjahr et al., 2007; Kryc et al., 2003;Wilson et al., 2013) Thus, we seek to evaluate the performance of this established leaching procedure across large variations in sediment composition. It was not our goal to identify an optimal procedure or variations on this procedure. For those questions, we refer you to Wilson et al., (2013) and Blaser et al., (2016).

We focus on three main objectives: 1) major, trace and REE analysis of each step of the leaching process in order to establish a detailed understanding of how elements partition across phases (i.e. are aluminosilicate phases being leached into the operationally defined Fe-Mn Oxide coatings?); 2) Analysis of the reproducibility of the acid reductive leaching procedure by leaching and analyzing replicate splits of MAG-1, a USGS standard reference material (SRM) composed of clayey mud with low carbonate content and a homogenized internal lab standard of pelagic clay from the Central Atlantic, INTL-STD-A.

3.3 Methods

3.3.1 Sample Sites

We selected sites from the North and South Pacific with robust bulk sediment geochemical and statistical characterizations (Dunlea et al., 2015; Scudder et al., 2014). ODP Site 1149 is near the Izu-Bonin-Arc (Modern location: 31.33, 143.35, Paleo location at 50 Ma: 24.95, -178.07) and was drilled at a water depth of 5818m. Samples were collected at the IODP Gulf Coast Repository.

The sediment at Site 1149 is heterogeneous and divided into five units. Unit I (top to 118.2 mbsf) consists of clay that is free of carbonate, contains diatoms/ radiolarians, and both discrete and dispersed ash material. Discrete ash layers vary from a few millimeters to 5 cm. Unit

II (118.2 to 179.1mbsf) consists of ash-bearing clay and pelagic clay that also bears radiolarians and diatoms. Units III, IV, and V contain progressively more indurated siliceous lithologies like chert, progressing from zeolitic clay mixed with chert in Unit III to recrystallized calcareous marlstone in Unit V. The original bulk geochemistry focused on the top two units and because we are most interested on the behavior of the leach in the preasance of ash we focus here on Units I and II as well. Scudder et al., (2009 and 2014) investigated the composition of the sediment in depth. In order to avoid dilution effects from biogenic material they focused on the contributions to the aluminosilicate portions of the sediment. The aluminosilicate portions of Units I and II of Site 1149 are composed primarily of dispersed ash (~20-50%) and eolian dust from Asia (~50-80%; Scudder et al., 2014).

IODP Site U1370 is in the South Pacific Ocean (Modern Location: -41.85, -153.105, Paleo-location at 50 Ma: -55.97,-122.38) at a water depth of 5084.7 m. Unit I (from the sediment water interface to 62mbsf) and is dominantly zeolitic metalliferous clay and metalliferous clay, over all this is the dominant lithology of Site U1370. Unit II is a thin (61.9–64.6mbsf) layer of nannofossil ooze. Unit III (64.6–69.4mbsf) is also composed of metalliferous clay. A Co based age model, with a lower age constraint at the K-Pg boundary is used to model ages; there are no age constraints below the K-Pg (Dunlea et al., 2015). However, the site's crust is within Chron 33n, which means the crustal age ranges from 73.6 to 79.5 Ma (D'Hondt et al., 2011). Dunlea et al., (2015a and 2015b) investigated the composition of the sediment in depth. It is mainly (~60%) composed of Rhyolite (the models use a whole-rock average from GEOROC, which we refer to as Average Rhyolite) and a ~10% Fe-Mn oxyhydroxide component (Dunlea et al., 2015). Its slow accumulation rate makes it unique in that the pore water remains oxic to basement (D'Hondt et al., 2015). With such a high concentration of authigenic sediment and oxic

porewater, there is not likely to be a porewater flux at Site U1370, which makes it an advantageous location to evaluate the effects of leaching.

3.3.2 Sequential Acid Reductive Leaching Methods

The main phase of sediment targeted for our purposes was the Fe-Mn oxide coating fraction. Hydroxylamine hydrochloride (HH) is universally employed as the reductant in leaching procedures (e.g., Basak et al., 2010; Gutjahr et al., 2007; Kryc et al., 2003;Wilson et al., 2013). Our leaching procedure follows the recommendation of recent leaching studies (Du et al., 2016; Wilson et al., 2013) and discontinues use of an initial acetic acid leach to target metals bound to the carbonate fraction before performing the HH extraction. Therefore, we utilized a two-step leaching procedure. Leach 1: A short one-hour HH leach modified from Gutjar et al. (2007) with 0.02M hydroxylamine hydrochloride in 15% (v/v) acetic acid, chelated with Na-EDTA and buffered to a pH 4 with sodium acetate at room temperature. Followed by Leach 2: a longer 24 hours HH leach (same recipe) to remove any remaining oxides from the residual component (Table 3.1). Gutjahr et al. (2007) use the addition of Na-EDTA to help prevent readsorption of REE after leaching. Wilson et al., (2013) omitted the EDTA from their solution and suggest it the addition of EDTA in the future could improve their results. Before extraction each sediment sample was freeze dried, powdered by hand with an agate mortar and pestle, and weighed (0.75g +/- 0.03) for leaching. The sediment and 14mL of the HH-Acedic Acid-EDTA mixture were poured into an acid cleaned, pre-weighed 50ml centrifuge tube. The contents were shaken by hand, and then placed on a shaker table for one hour. Each sample was

Leach Step	Phases Targeted	Extractant	Time
Leach 1	Metals bound to Carbonate and Fe- and Mn- oxides fractions	0.02 M hydroxylamine hydrochloride win Na-EDTA in 20% acetic acid buffered to pH 4	1 Hour
Leach 2	Remaining Metals bound to Fe- and Mn-oxides	0.02 M hydroxylamine hydrochloride win Na-EDTA in 20% acetic acid buffered to pH 4	24 Hours
Residue	Ddetrital / Aluminosilicate residue	HF, HNO3 and HCL Acid Digestion	NA

Table 3.1 Description of the phases targeted by each leach, the extractant or digestion applied and the time of each leach

centrifuged for 20 minutes at 2000 rpm, and the supernatant was transferred into a second pre-weighed 50ml centrifuge tube. In-between extraction steps we followed the five step washing procedure outlined in Kryc et al., (2003) to ensure that we collected as much of each leached phase as possible. First, 2mL of the HH mixture was added to the remaining sediment "residual plug" in tube one and centrifuged again. The liquid was transferred via pipette into the second tube with the first leach supernatent and the same process was repeated with 2mL of Milli-Q water. The MQ rinse was repeated two more times. The second tube with the first leach in it was subsequently centrifuged for one hour to remove any persistent residual material, eluted into a third pre-weighed centrifuge tube, dried and weighed. Any remaining solids were gently rinsed back into the tube with the residual fraction. The "residual plug" was dried overnight at 60°C and then re-weighed. 14mL of the HH-Acetic Acid-EDTA mixture was again added to the dried plug, shaken by hand, and then vortex mixed to re-suspend the sediment. The mixture was placed on the shaker table for 24 hours. The sample was centrifuged for 20 minutes and rinsed via the same rinsing procedure described above. The second leach was dried and weighed. Leached samples were converted to a nitric matrix and diluted with MQ for analysis; a split from each leach was taken for ICP-MS and ICP-ES analysis. Following the second leach the residues were oven dried and powdered by hand with an agate mortar and pestle. Residue samples were

dissolved via flux fusion and REE elements were dissolved via acid digestion following the methods described in Dunlea et al. (2015).

3.3.3 Elemental and Isotopic Analysis

We analyzed all three resulting fractions (Leach 1, Leach 2 and the residue) for a large suite of major, trace and REE. A subset of the samples was also analyzed for Nd and Pb isotopic composition. A subset of leached samples was further split and reserved for Pb and Nd isotopic analysis. Each split of the leached sample was dried and dissolved in HBr for Pb column chemistry (Lugmair and Galer, 1992). The residues were weighed and dissolved via HCL-HNO3 and HF digestion, before being converted to the HBr matrix as well. The washes from the Pb chemistry contain the REE split and are collected for Nd column chemistry. We use Eichrom Tru Spec™ to separate the REEs fraction and volumetrically calibrated columns with Eichrom LN Spec™ to separate the Nd from the REEs. The Pb and Nd isotope samples were analyzed on the Thermo Triton Thermal Ionization Mass Spectrometer (TIMS) in the R. Ken Williams ’45 Radiogenic Isotope Geosciences Laboratory at Texas A&M.

ICP-MS and ICP-ES analyses were performed at the Analytical Geochemistry Laboratory at Boston University. Major element analyses of the residue were measured using ICP-ES. To calculate concentrations the leached extracts and residues were calibrated to standard reference materials designed to be matrix matched, and to bracket the concentration ranges of the samples: AGV-1, BCR-2, BIR-1, DNC-1, MAG-1, NIST-1C, PACS, W-2. A procedural blank was also included in the calibration.The standard reference materials and the residues were all corrected for variations in weight of original sample analyzed, however, because clear crystals precipitated after the solution was dried precipitate we were unable to perform a weight correction on the extracted solutions.

In order to track internal precision of our samples we created and analyzed an internal standard produced from homogenized Cariaco Basin sediment (to be referred to as CAR). CAR was digested with the standard reference materials following the same methods. Results of CAR and the reference materials are shown in Table 3.2 and described below in the "Results" section.

3.4 Results

3.4.1 Instrumental Precision and Detection Limits

To evaluate the precision and reproducibility of our results, we analyzed replicates of CAR, as an unknown. This is distinct from the reproducibility of the leach extractions, which is discussed below. The precision (RSD) of the major elements is less than 3% (n=8), except for Na (3.58%, Table 3.2). The overall average precision of all elements is 6.44% (n=10). Where the lowest RSD is for Mn (0.04%), and the highest is for Rb (15.36%). The RSD for Pb and Nd are 3.79% and 5.57% respectively. The internal RSDs of CAR for all of elements are reported in Table 3.2

We measured procedural blanks for the flux fusion and acid digestion processes applied to CAR and the residues. We also measured blanks for the entire leaching procedure and blanks of our HH reductive mixture. For CAR and the residues we use 3 times the standard deviation of the procedural digestion blanks (n = 10 for the ICP-ES and n= 8 for the ICP-MS) to determine the detection limits. The detection limits for the procedural digestion blanks for the elements analyzed on the ICP-MS range from 0.01ppm (Cd) to 75.45ppm (Ni) with an average of 6.49ppm. The detection limits for the digestion blanks for the elements analyzed on the ICP-ES range from 0.01wt% (Mn) to 2.97 wt%(Si) with an average of 0.79wt%. To be conservative with the leach analysis we screened for detection limit using 3 times the standard deviation of the procedural blank, or 3 times the standard deviation of the leach blank (n=8 for the ICP-ES and

Sample		SiO2 wt.%	Al2O3 wt.%	TiO2 wt.%	Fe2O3 wt.%	MnO wt.%	CaO wt.%	MgO wt.%	Na2O wt.%	K2O wt.%	P2O5 wt.%
CAR	Average Concentration	38.26	12.64	0.48	6.68	23.42	29.97	7.56	15.03	5.19	8.45
	Stdev	1.11	0.26	0.01	0.13	0.01	0.63	0.12	0.54	0.05	0.02
	RSD%	2.89	2.05	2.94	2.00	0.04	2.09	1.65	3.58	0.92	0.26
	Detection Limit 3X STD procedural blank	2.98	0.33	0.03	0.30	0.02	0.72	0.28	2.39	0.21	0.55
INTL-STD-A											
Leach 1	Average Concentration	<det	<det	<det	0.54	0.52	5.79	0.72	0.00	0.30	0.00
	Percent of total analyzed	0.00	0.00	0.00	6.36	85.84	0.00	22.13	0.00	0.00	0.00
	RSD%	<det	<det	<det	26.74	84.28	21.65	21.76	<det	4.14	<det
Leach 2	Average Concentration	<det	<det	0.60	0.54	0.04	<det	0.37	38.08	<det	<det
	Percent of total analyzed	0.00	0.00	0.25	6.37	7.33	0.00	11.19	91.90	0.00	0.00
	RSD%	<det	<det	42.33	29.56	11.92	<det	<det	<det	<det	<det
Residue	Average Concentration	50.30	19.39	0.80	7.46	0.04	0.00	2.17	3.35	2.93	17.40
	Percent of total analyzed	100.00	100.00	57.09	87.27	6.83	0.00	75.09	0.00	90.63	0.00
	RSD%	9.34	7.25	7.67	8.00	7.96	<det	7.03	5.65	7.34	<det
	Sum of total analyzed in all three phases	50.30	19.39	1.40	8.55	0.60	5.79	2.90	117.58	3.23	17.40
MAG-1											
Leach 1	Average Concentration	<det	<det	0.30	0.32	0.04	2.00	0.87	<det	0.49	<det
	Percent of total analyzed	0.00	0.00	28.20	3.99	28.24	100.00	22.42	46.32	12.26	0.00
	RSD%	<det	<det	N=1	N=1	15.81	N=1	11.36	<det	51.81	<det
Leach 2	Average Concentration	<det	<det	<det	0.47	0.02	<det	0.44	83.19	<det	<det
	Percent of total analyzed	0.00	0.00	0.00	5.92	17.94	0.00	11.26	52.02	0.00	0.00
	RSD%	<det	<det	<det	19.87	20.61	<det	5.20	12.45	<det	<det
Residue	Average Concentration	53.64	17.03	0.76	7.14	0.07	0.00	2.57	2.66	3.53	<det
	Percent of total analyzed	100.00	100.00	71.80	90.09	53.82	0.00	66.32	1.66	87.74	0.00
	RSD%	2.40	2.93	2.52	2.33	5.52	<det	6.06	1.39	3.72	<det
	Sum of total analyzed in all three phases	53.64	17.03	1.06	7.92	0.14	2.00	3.87	159.92	4.02	<det

Table 3.2 Compilation of the internal instrument precision (the detection limits established by multiplying 3x the standard deviation of the procedural blank) as average concentration and precision of the in-house standard and standard reference material used to evaluated the reproducibility of the leach. The sum of total analyzed in all three phases refers to the sum of the element analyzed

Sample		Li ppm	Be ppm	Sc ppm	V ppm	Cr ppm	Co ppm	Ni ppm	Cu ppm	Zn ppm	Rb ppm	Sr ppm	Y ppm	Zr ppm
CAR	Average Concentration	47.69	1.58	10.07	200.29	94.28	9.25	<det	28.18	<det	63.73	711.93	12.46	47.14
	Stdev	2.24	0.07	1.43	10.55	8.27	0.45	<det	0.98	<det	9.79	35.46	1.29	3.59
	RSD%	4.70	4.19	14.18	5.27	8.77	4.88	<det	3.48	<det	15.36	4.98	-	7.62
	Detection Limit 3X STD procedural blank	0.90	0.04	1.36	5.64	11.10	2.14	82.93	8.34	62.23	4.20	39.11	1.72	2.70
INTL-STD-A														
Leach 1	Average Concentration	4.48	0.43	3.41	46.60	<det	<det	<det	45.97	<det	<det	<det	27.07	15.54
	Percent of total analyzed	4.48	11.68	7.76	0.00	0.00	0.00	0.00	36.22	0.00	0.00	0.00	67.45	11.58
	RSD%	44.47	30.89	66.34	38.51	<det	<det	<det	65.69	<det	<det	<det	79.98	34.67
Leach 2	Average Concentration	3.82	0.36	1.30	<det	<det	3.75	<det	18.47	<det	4.99	<det	6.57	11.49
	Percent of total analyzed	3.83	9.68	2.96	0.00	0.00	22.57	0.00	14.56	0.00	4.00	0.00	16.37	8.56
	RSD%	5.71	20.44	<det	<det	<det	4.99	<det	4.31	<det	<det	<det	25.71	16.86
Residue	Average Concentration	91.68	2.91	39.26	155.74	97.84	12.86	0.00	62.48	113.33	119.89	71.71	6.49	107.16
	Percent of total analyzed	91.69	78.72	99.06	75.78	100.00	77.53	0.00	49.17	0.00	95.15	100.00	15.50	79.62
	RSD%	4.29	4.69	159.32	4.57	4.04	4.26	<det	7.28	<det	13.90	23.63	24.89	11.31
	Sum of total analyzed in all three phases	99.98	3.70	42.67	202.34	97.84	16.61	0.00	126.93	113.33	124.88	71.71	40.13	134.19
MAG-1														
Leach 1	Average Concentration	5.82	0.31	1.68	28.20	<det	3.80	<det	14.89	<det	4.60	126.10	14.06	11.13
	Percent of total analyzed	6.66	8.23	9.55	16.23	0.00	16.16	0.00	31.58	0.00	3.31	60.53	47.15	9.33
	RSD%	18.11	24.17	22.68	28.35	<det	18.47	<det	2.33	<det	9.73	13.33	13.23	28.78
Leach 2	Average Concentration	7.93	0.43	<det	26.51	<det	4.30	<det	<det	<det	5.23	<det	4.99	12.47
	Percent of total analyzed	9.07	11.44	0.00	15.26	0.00	18.32	0.00	0.00	0.00	3.75	0.00	16.73	10.46
	RSD%	22.84	24.81	<det	N=1	<det	36.82	<det	<det	<det	28.36	<det	17.44	2.96
Residue	Average Concentration	73.68	3.01	15.92	119.04	87.45	15.39	<det	32.25	85.15	129.39	82.23	10.77	95.62
	Percent of total analyzed	84.27	80.33	90.45	68.51	100.00	65.52	0.00	68.42	100.00	92.94	39.47	36.12	80.21
	RSD%	34.96	34.99	6.73	34.25	38.79	37.30	<det	78.98	30.14	38.01	28.27	27.76	33.89
	Sum of total analyzed in all three phases	87.43	3.75	17.60	173.74	87.45	23.49	<det	47.14	85.15	139.22	208.33	29.82	119.21

Table 3.2 Continued

Sample		Gd ppm	Tb ppm	Dy ppm	Ho ppm	Er ppm	Tm ppm	Yb ppm	Lu ppm	Hf ppm	Ta ppm	Pb ppm	Th ppm	U ppm
CAR	Average Concentration	2.8571	0.43	2.37	0.47	1.36	<det	1.32	0.20	1.38	0.59	12.22	7.588	11.845
	Stdev	0.2501	0.04	0.21	0.04	0.12	<det	0.13	0.02	0.12	0.04	0.46	0.4619	0.646
	RSD%	8.7524	9.39	9.00	9.32	9.00	<det	10.16	10.99	8.36	6.04	3.79	6.0879	5.45
	Detection Limit 3X STD procedural blank	0.17	0.03	0.23	0.05	0.12	0.73	0.12	0.02	0.16	0.05	0.49	0.27	0.02
INTL-STD-A														
Leach 1	Average Concentration	6.89	1.10	5.70	1.02	2.74	<det	2.13	0.32	0.36	0.00	30.59	9.20	0.64
	Percent of total analyzed	66.45	67.65	67.22	65.31	64.95	0.00	61.00	60.69	9.81	0.00	63.06	57.01	21.70
	RSD%	77.63	79.93	77.47	74.63	78.54	<det	75.63	75.84	33.81	<det	80.68	92.42	62.56
Leach 2	Average Concentration	1.67	0.25	1.25	0.23	0.57	<det	0.41	0.06	0.35	<det	5.22	2.04	0.28
	Percent of total analyzed	16.09	15.36	14.71	14.43	13.40	0.00	11.85	11.61	9.55	0.00	10.75	12.66	9.61
	RSD%	22.04	22.91	26.12	25.45	26.06	<det	25.68	23.41	4.96	<det	20.15	24.97	9.99
Residue	Average Concentration	1.81	0.28	1.53	0.32	0.91	0.00	0.95	0.15	2.97	1.15	12.70	4.89	2.0307
	Percent of total analyzed	16.73	16.29	17.35	19.53	20.81	0.00	26.14	26.72	80.50	100.00	26.51	28.62	68.60
	RSD%	22.30	22.05	22.49	23.61	23.38	<det	27.93	27.31	9.31	8.62	2.14	27.45	7.90
	Sum of three phases	10.37	1.63	8.47	1.57	4.22	0.00	3.48	0.53	3.69	1.15	48.51	16.14	2.9563
MAG-1														
Leach 1	Average Concentration	4.27	0.64	3.24	0.57	1.43	<det	1.10	0.16	0.30	<det	36.79	5.12	0.61
	Percent of total analyzed	51.33	51.02	49.95	47.40	45.40	0.00	40.58	39.10	8.97	0.00	72.46	38.37	20.39
	RSD%	13.54	9.82	8.27	8.46	9.16	<det	9.96	10.75	23.68	<det	11.62	25.94	18.49
Leach 2	Average Concentration	1.69	0.25	1.18	0.21	0.51	<det	0.37	0.06	0.26	0.00	5.01	2.67	0.20
	Percent of total analyzed	20.31	19.65	18.21	17.30	16.35	0.00	13.78	13.57	7.92	0.00	9.87	19.97	6.77
	RSD%	22.86	24.47	21.65	19.93	21.42	<det	21.25	20.74	30.41	<det	24.48	50.90	26.59
Residue	Average Concentration	2.36	0.37	2.06	0.42	1.20	<det	1.24	0.19	2.74	1.09	8.97	5.56	2.19
	Percent of total analyzed	28.36	29.33	31.84	35.30	38.25	0.00	45.64	47.33	83.11	100.00	17.67	41.65	72.83
	RSD%	43.71	43.35	43.48	42.30	43.68	<det	44.25	43.00	33.48	37.21	34.47	46.87	36.92
	Sum of three phases	8.32	1.26	6.48	1.20	3.15	0.00	2.72	0.41	3.30	1.09	50.77	13.35	3.01

Table 3.2 Continued

Sample		Nb ppm	Mo ppm	Cd ppm	Sn ppm	Sb ppm	Cs ppm	Ba ppm	La ppm	Ce ppm	Pr ppm	Nd ppm	Sm ppm	Eu ppm
CAR	Average Concentration	9.46	99.18	5.37	1.63	2.03	4.27	283.85	21.84	45.10	5.09	19.21	3.60	0.72
	Stdev	0.46	9.10	0.41	0.12	0.16	0.42	31.72	1.84	2.27	0.21	1.08	0.27	0.07
	RSD%	4.82	9.18	7.65	7.21	8.03	9.88	11.17	8.45	5.03	4.15	5.64	7.44	9.11
	Detection Limit 3X STD procedural blank	0.04	2.98	0.01	0.67	0.17	0.15	20.87	1.23	3.10	0.16	0.31	0.17	0.03
INTL-STD-A														
Leach 1	Average Concentration	0.44	36.66	0.16	<det	<det	<det	53.59	20.22	77.35	7.36	30.19	7.20	1.54
	Percent of total analyzed	1.21	0.00	16.38	0.00	0.00	0.00	11.66	45.68	54.34	56.05	58.38	63.09	64.64
	RSD%	77.48	41.22	19.94	<det	<det	<det	26.34	89.76	86.90	83.02	76.34	76.85	73.92
Leach 2	Average Concentration	16.36	<det	0.78	7.36	11.52	59.21	43.54	6.02	27.19	1.96	8.12	1.84	0.38
	Percent of total analyzed	45.24	0.00	80.97	69.05	90.38	89.12	9.47	13.60	19.10	14.93	15.69	16.10	15.80
	RSD%	143.51	<det	140.61	64.68	129.58	<det	1.80	17.83	18.84	19.39	20.72	22.54	24.99
Residue	Average Concentration	19.37	0.00	0.03	3.30	1.23	7.23	362.41	18.03	37.79	3.81	13.41	2.37	0.47
	Percent of total analyzed	53.52	0.00	2.89	30.55	9.29	10.79	78.77	39.71	26.07	27.81	24.88	19.92	18.76
	RSD%	6.62	<det	5.52	10.82	16.45	20.78	10.77	31.48	21.96	29.31	28.75	25.42	24.38
	Sum of total analyzed in all three phases	36.17	36.66	0.96	10.65	12.75	66.44	459.55	44.28	142.33	13.12	51.72	11.41	2.39
MAG-1														
Leach 1	Average Concentration	1.55	<det	16.70	8.03	0.81	<det	38.33	19.26	41.84	5.36	21.64	4.85	0.94
	Percent of total analyzed	8.49	0.00	99.73	67.77	36.58	0.00	7.59	42.43	42.60	45.38	47.16	50.02	49.88
	RSD%	201.99	<det	195.25	<det	143.81	<det	12.32	33.74	23.20	24.67	20.00	16.00	12.03
Leach 2	Average Concentration	0.13	<det	0.02	<det	0.39	<det	52.56	8.19	17.30	2.20	8.68	1.90	0.36
	Percent of total analyzed	0.74	0.00	0.13	0.00	17.89	0.00	10.40	18.05	17.62	18.63	18.93	19.63	19.01
	RSD%	N=1	<det	N=1	<det	74.79	<det	20.22	36.13	32.55	31.26	26.95	25.81	20.04
Residue	Average Concentration	16.55	<det	0.02	3.82	1.00	7.12	414.31	17.94	39.07	4.25	15.56	2.94	0.58
	Percent of total analyzed	90.77	0.00	0.15	32.23	45.54	100.00	82.01	39.52	39.78	35.99	33.91	30.35	31.11
	RSD%	35.06	<det	36.47	13.22	47.20	41.73	35.90	45.73	42.89	46.14	44.82	44.56	45.18
	Sum of total analyzed in all three phases	18.23	0.00	16.75	11.84	2.20	7.12	505.20	45.38	98.20	11.80	45.88	9.69	1.88

Table 3.2 Continued

between the three leaches. The percent of total analyzed refers to the concentration measured in an individual leach phase divided by sum of the total analyzed n=7 for the ICP-MS), whichever was higher (Table 3.2). The detection limits for the HH blanks analyzed on the ICP-MS range from 0.01ppm (Cd) to 87.26ppm (Zn) with an average of 6.78ppm. The detection limits for the HH blanks analyzed on the ICP-ES range from 0.01wt% (Mn) to 72.21 wt% (Na) with an average of 7.91. The higher blanks of the acid reductive leaching mixture highlight the challenges of analyzing the major, trace and REE elements from an acid reductive procedure focused on targeting elements for isotopic measurements. There is a large increase in the blanks, and therefore the detection limit, of the majors when the HH leaching solution is used. It is likely that this is due to the sodium acetate that we use to buffer the pH of the leaching solution, or the Na-EDTA used to prevent chelation. In both the first and second leach, clear crystals precipitated after the solution was dried, and we attribute this to the use of sodium acetate as a buffer. The precipitate that formed added mass to the leached fractions and the resulting samples weighed more than the original mass of bulk sediment. The inability to accurately assess the mass remaining in each fraction propagates throughout the study, precluding our ability to quantify the elemental concentration in each step.

3.4.2 Major, Trace and Rare Earth Elements

To examine the reproducibility of the procedure we performed replicate leaches and analyses on splits of MAG-1 and the Central Atlantic pelagic in-house internal standard INTL-STD-A. We selected MAG-1 because Kyrc et al., (2003) evaluated the reproducibility of several SRMs and found that when leached MAG-1 came closest to complete recovery between their total leaching procedure and the established bulk concentration. We also measured repeat analyses of MAG-1 and INTL-STD-A for Pb and Nd isotopes.

Standard		Overall Average %RSD	Element	%RSD	Concentration	Units
MAG-1						
Residue	Element with Minimum RSD%	32.08	Cu	2.33	14.89	ppm
	Element with Maximum RSD%		Nb	201.99	1.55	ppm
Leach 1	Element with Minimum RSD%	25.65	Zr	2.96	12.47	ppm
	Element with Maximum RSD%		Sb	74.78	0.39	ppm
Leach 2	Element with Minimum RSD%	32.33	Na	1.39	2.66	ppm
	Element with Maximum RSD%		Cu	78.98	32.25	ppm
INTL-STD-A						
Leach 1	Element with Minimum RSD%	60	K2O	4.14	0.30	wt%
	Element with Maximum RSD%		Th	92.41	9.20	ppm
Leach 2	Element with Minimum RSD%	32.3	Ba	1.80	43.54	ppm
	Element with Maximum RSD%		Nb	143.51	16.36	ppm
Residue	Element with Minimum RSD%	18.12	Pb	2.14	12.70	ppm
	Element with Maximum RSD%		Sc	159.32	39.26	ppm

Table 3.3 Summary of the concentrations and precisions of the elements with the highest and lowest relative standard deviations of both standards including their concentrations of each element the overall average RSD of each phase.

We present a summary of the concentrations and precisions of the elements with the highest and lowest relative standard deviations of both standards in Table 3.3. Table 3.3 tabulates the overall average RSD of each phase for MAG-1 and INTL-STD-A, and the element (and concentration) with the minimum and maximum RSD. For INTL-STD-A the major aluminosilicate associated elements (measured as oxides by the ICP-ES) SiO_2, Al_2O_3 and TiO_2 were all below detection limit in Leach 1. The concentrations and RSD of Leach 1 of the INTL-STD-A the target Fe_2O_3 and MnO phases are 0.54wt% (26.74%, RSD) and 0.52wt% (84.28% RSD) respectively. In Leach 2 SiO_2 and Al_2O_3 are below detection limit, and TiO_2 has a RSD of 43.33% with an average concentration of 0.60 wt%. The RSD and concentrations for target Fe_2O_3 and MnO phases in Leach 2 are 29.56%, 0.54 wt% and 11.92%, 0.04 wt% respectively. The Fe_2O_3 concentration and RSD are the same in Leach 1 and 2, however more MnO is captured in Leach 1 than in Leach 2.The average RSD for the aluminosilicate residues are SiO_2

(50.30 wt%), Al_2O_3 (19.39 wt%), TiO_2 (0.80wt%). Fe_2O_3 (8.00wt%) and MnO (0.04wt%) have an average RSD of 8.00% and 7.96%, respectively.

For MAG-1 the SiO_2, and Al_2O_3 are below detection limit in Leach 1. TiO_2 and Fe_2O_3 both have one sample that has concentration above detection limit, 0.30wt% and 0.32wt%, respectively; however, this is not enough information to report a RSD. The RSD and concentration for MnO are 15.81% and 0.04wt%. SiO_2, Al_2O_3 and TiO_2 are below detection limit in Leach 2. The RSD and concentrations for Fe_2O_3 and MnO in Leach 2 of MAG-1 are 19.87% 0.47wt% and 20.61% and 0.02wt%, respectively, so Fe increased and Mn decreased in comparison to Leach 1. The average RSD for the aluminosilicate residues are SiO_2 (50.30 wt%), Al_2O_3 (19.39 wt%), TiO_2 (0.80wt%) Fe_2O_3 (8.00wt%) and MnO (0.04wt%) have an average a RSD of 8.04%.

The lowest RSD for Si, Al, Ti are in the residual portions in both MAG-1 and the INTL-STD-A. The behavior of the patterns between elements leached from INTL-STD-A and MAG-1 diverge from there. In Leach 1 of INTL-STD-A the RSD of the elements between La and U are very high, above 70%, except for Hf (33.981%). In MAG-1 the Leach 1 RSD average is 16.13%. for elements between La and U . INTL-STD-A, on the other hand, has much lower RSD for the elements between La and U for Leach 2 (mean RSD= 20.94%). Nb, Cd and Sb all have very high, RSD greater that 120%, RSD in Leach 2 in INTL-STD-A; whereas the same elements in Leach 2 of MAG-1 are much lower. They are, however, greater than 150% in Leach 1. If we remove Nb, Cd and Sb from the RSD average the Leach 2 overall average in INTL-STD-A decreases from 32.20% to 20.87%. If we remove Nb, Cd and Sb from the RSD average the Leach 1 overall average in MAG-1 decreases from 32.08% to 17.74%.

3.4.3 Nd and Pb Isotopic Ratios and Concentrations

We also measured repeat analyses of the MAG-1 and INTL-STD-A Pb and Nd isotopes. We present them here within the context of the averaged concentrations and RSD for Nd and Pb. We interpret what is "acceptable" error for Nd and Pb isotopes based on what we would typically interpret as a significant difference for paleoceanographic interpretations. For Nd that is one epsilon unit and for Pb that is changes that are greater than the applied fractionation factor (0.1%), or variations in the second decimal place.

We present a summary of the average Nd and Pb concentrations, isotopic compositions, and precisions for each phase of INTL-STD-A and MAG-1 in Table 3.4. The standard and phase with the lowest RSD for ε_{Nd} is the first leach of INTL-STD-A (Table 3.4) with an ε_{Nd} of -11.58 and RSD of 1.38%. The first leach of MAG-1 has a similarly low RSD (1.84%) (Table 3.4), with an ε_{Nd} of -12.95. The average concentration of the Nd in the MAG-1 leach is 21.64ppm with an RSD of 20.0%. Leach 1 of MAG-1 has the lowest RSD for both the concentration and isotopic composition of Nd. The standard and phase with the highest percent RSD is the MAG-1 residue with an average ε_{Nd} of -30.18, and an RSD of 112.18%. The average concentration of Nd in the residue of MAG-1 is 15.56ppm with an RSD of 44.82%. This high variability is also reflected in the Pb isotopes of the residue where the three Pb ratios also have the highest RSDs of any other standard or phase. The average $^{206}Pb/^{204}Pb$ =18.93, with an RSD of 0.68%, the average $^{207}Pb/^{204}Pb$ =15.66, with an RSD of 0.36%, the average $^{208}Pb/^{204}Pb$ =38.97, with an RSD of 0.52%. The RSD of the residue is the second highest in INTL-STD-A; the ε_{Nd}, -15.66, with an RSD of 20.72%, where the average Nd concentration is 13.41ppm and the RSD is 38.25%. The Pb isotopic RSDs of INTL STD-A are not correspondingly high. The poor reproducibility of the residues may be due to the difficulty in dissolving the residues for isotopic analysis. We dissolve

MAG-1	Element	ppm	RSD	Isotopic Ratio	Average	N	STDDEV	RSD
Leach 1	Nd	21.64	20	εNd	-12.95	5	0.239	1.84
	Pb	36.79	11.62	$^{206}Pb/^{204}Pb$	18.85	3	0.037	0.19
				$^{207}Pb/^{204}Pb$	15.66	3	0.038	0.25
				$^{208}Pb/^{204}Pb$	38.69	3	0.169	0.44
Leach 2	Nd	8.68	26.59	εNd	-9.39	3	1.08	11.52
	Pb	5.01	24.48	$^{206}Pb/^{204}Pb$	18.78	5	0.05	0.26
				$^{207}Pb/^{204}Pb$	15.63	5	0.01	0.08
				$^{208}Pb/^{204}Pb$	38.56	5	0.17	0.45
Residue	Nd	15.56	44.82	εNd	-30.18	5	33.85	112.18
	Pb	8.97	34.4	$^{206}Pb/^{204}Pb$	18.93	3	0.13	0.68
				$^{207}Pb/^{204}Pb$	15.66	3	0.06	0.36
				$^{208}Pb/^{204}Pb$	38.97	3	0.20	0.52
INTLSTD-A								
Leach 1	Nd	30.19	76.34	εNd	-11.58	4	0.16	1.38
	Pb	30.59	80.68	$^{206}Pb/^{204}Pb$	18.98	6	0.01	0.07
				$^{207}Pb/^{204}Pb$	15.67	6	0.01	0.07
				$^{208}Pb/^{204}Pb$	38.96	6	0.10	0.26
Leach 2	Nd	5.22	20.15	εNd	-10.61	4	1.13	10.63
	Pb	8.12	20.72	$^{206}Pb/^{204}Pb$	18.94	4	0.11	0.59
				$^{207}Pb/^{204}Pb$	15.69	4	0.02	0.13
				$^{208}Pb/^{204}Pb$	39.01	4	0.15	0.38
Residue	Nd	13.41	38.25	εNd	-15.66	3	3.24	20.72
	Pb	12.7	2.14	$^{206}Pb/^{204}Pb$	18.95	3	0.05	0.24
				$^{207}Pb/^{204}Pb$	15.69	3	0.05	0.32
				$^{208}Pb/^{204}Pb$	39.07	3	0.08	0.22

Table 3.4 Summary of the concentrations and precisions of the Nd and Pb leached from the standards as well the Nd and Pb isotopes analyzed for paleoceanographic reconstructions.

between 0.25 and 0.50g in order to ensure high enough concentrations of Nd and Pb for isotopic analysis.

Overall, there is not a clear relationship between the precision of the concentration from extraction of Nd or Pb and the precision of the isotopic compositions. The low RSD in the extraction corresponds to the low RSD of the ε_{Nd} for the first leach of MAG-1. But this is not true of the first leach of INTL-STD-A, which has the highest concentration of Nd in any of the phases (30.19ppm) but also has the highest RSD, 76.34%. However, this does not translate to a high RSD for the $\varepsilon_{Nd,}$ which is 1.38%, and the lowest RSD overall. The highest RSD of Pb concentration is also in the INTL-STD-A where the average concentration is 30.59ppm and the RSD is 80.68%. This also does not translate into a high RSD of the Pb isotopes; in fact they are on average the lowest: Average $^{206}Pb/^{204}Pb$ =18.98, RSD 0.07%, average $^{207}Pb/^{204}Pb$ =15.67, RSD 0.07%, average $^{208}Pb/^{204}Pb$ =38.96, RSD 0.26% (Table 3.4).

The isotopic analyses with the lowest reproducibility were the residues of both MAG-1 and INTL-STD-A. The best reproducibility of the Nd isotopic composition from the phases of both INTL-STD-A and MAG-1 are of Leach 1, which has the highest concentrations. The best reproducibility of the Pb isotopic composition from the phases extracted from INTL-STD-A are also of Leach 1. However, the best reproducibility of the Pb isotopic composition from the phases extracted from and MAG-1 are of Leach 2. There is a general pattern of highest Nd and Pb concentrations having the best isotope RSD.

3.5 Discussion

3.5.1 Is the Leaching Procedure Reproducible?

Kyrc et al., (2003) found that their best operational precision for a leached and analyzed natural sample occurred as a function of the targeted elemental distribution (i.e., Al, Ti and Si

had the lowest RSD in the residual, Fe and Mn had the lowest RSD in the oxide fraction), and our findings agree with theirs. We have also improved on the reproducibility of the major elements reported by Kyrc et al (2003) and attribute this to the fact that we have limited the number of extractions we perform to two, and that Si, Al and Ti are below detection limit in two phases.

The reproducibility of the leach seems to depend on the behavior of the elements when exposed to reductive acid, and the element's concentration in the different phases of the sediment. There seems to be no pattern between concentration and RSD with Nb, Cd and Sb. For INTL-STD-A and MAG-1 the leach with the best average reproducibility is the second leach. Overall the, trace, REE and isotopic results from MAG-1 are more reproducible. This is to be expected because it is a standard reference material, as opposed to a sample homogenized in the lab, and INTL-STD-A is likely more heterogeneous. The differences begin to provide representation of the potential range and reproducibility of our acid reductive leaching procedure.

3.5.2 What is the Fidelity of the Acid Reductive Leaching Procedure?

To monitor the fidelity of our acid reductive leaching procedure, we examine elements that we expect to be strongly associated with a specific target phase. We forgo a separate leach step targeting carbonate but the HH and acetic acid mixture of our acid reductive mixture should dissolve carbonate. We use Ca to monitor the carbonate extracted during each step. In their analysis of a full sequential leaching procedure Kyrc et al., (2003) selected a natural sample from the Equatorial Pacific to be able to evaluate the leaching procedure in a depositional setting with relatively low terrigenous inputs. At Sites 1149 and U1370 the average amount of CaO in the bulk sediment is very low, at 1.96 and 1.82 wt%, respectively. At Site 1149 an average of 19%

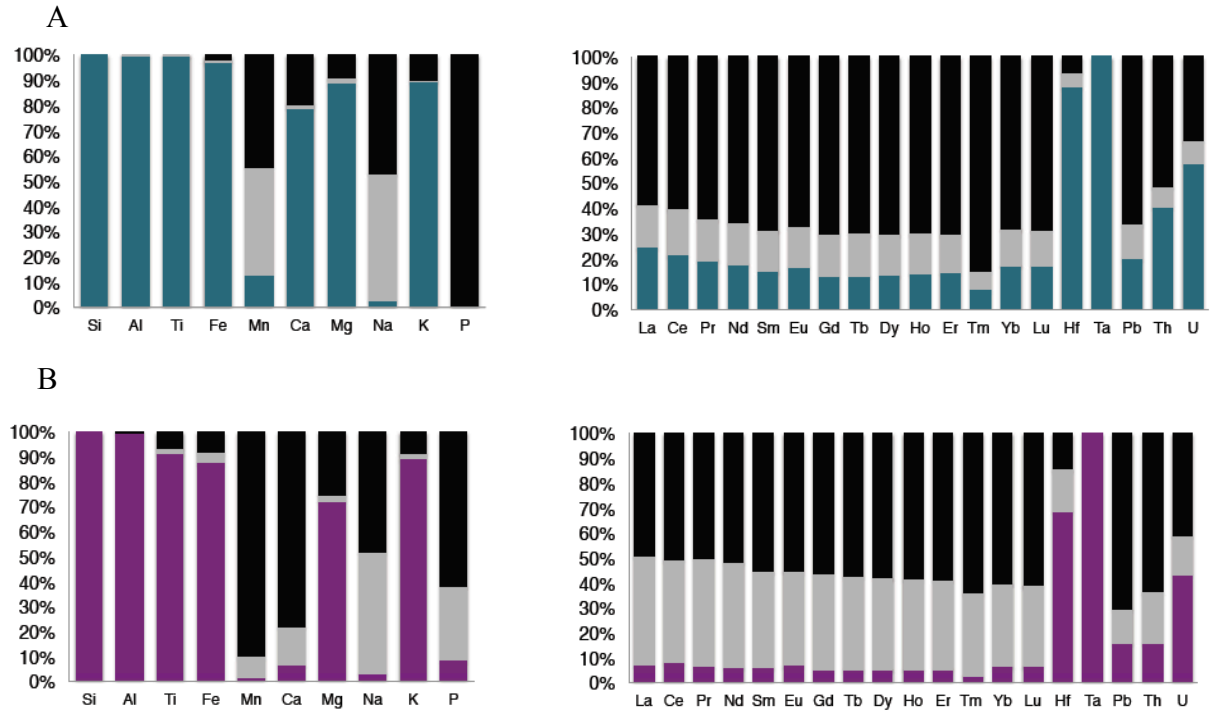

Figure 3.1 Average proportions of each element in the three leach phases at Sites U1370 (A) and 1149 (B). Black bars are Leach 1, light grey are Leach 2 and the blue (1149) and purple (U1370) are the residues.

of the Ca is removed by the first leach, 1.64% is removed by the second leach and 79.14% remains in the residue (Figure 3.1A). At Site U1370 an average of 78% of the Ca is removed by the first leach, 15% is removed by the second leach and 7% remains in the residue (Figure 3.1). The percentages reported here are the amounts leached from each phase from every sample averaged. The Ca at U1370 reflects the portion of the sediment made of apatite (~ 40 wt% CaO; Takebe, 2005; Li and Schoonmaker 2003) in the sediment (Dunlea et al., 2015a), which explains why the Ca is dominant in the leach. Whereas. at Site 1149 the sources to the sediment with high CaO concentrations are terrigenious components like Chinese Loess (9.62 wt%) and Izu-Bonin Front Arc Basalt (10.27 wt%) The bulk composition of both sites and our results highlight the unsuitability of a separate carbonate leach at locations that are dominantly composed of clay. At

U1370 and 1149, where there is so little calcium carbonate that the first leach extracts what is present, a separate leach intended for carbonate would likely over-leach the clay components.

At Site U1370, 62% of the P is extracted in the first leach and 30% is extracted in the second and 8% remains in the residue (3.1A), these percentages agree well with the leaches performed by Kyrc et al. (2003) who identify 60% of the P in their natural sample extracted by the HH leach targeting authigenic material. It is important to note that there is only an average of 385ppm P at Site U1370. Dunlea et al., (2015) identify a discernable, likely biogenic apatite portion of the sediment at Site U1370, and we attribute the high P in Leach 1 to the extraction of that portion of apatite the sediment. At Site 1149, where the average concentration of P in the bulk sediment is 0.26 wt%,the P is below detection limit (0.55wt%) in all three phases except for Leach 1 samples .at 164.64mbsf (0.62wt%) and 170.73mbsf(1.14wt%).

An average of 100% of the Si at both sites remains in the residue (Figure 3.1A&B and 2A&B). 100% of the Al at Site 1149 remains in the residue, whereas a slightly lower average of 99% of Al remains in the residue at Site U1370 (Figure 3.1). This confirms overall that the aluminosilicate portion of the sediment is not extracted by the leach. At Site 1149, 99% of the Ti also remains in the residue, and ~1% is extracted in Leach 2. At Site U1370, 6% of Ti is extracted by Leach 1, 2% by Leach 2 and 91% remains in the residue. We tentatively attribute this to the hydrothermal portion of the sediment at the bottom of Site U1370, where Ti can replace Fe in oxyhydroxides. The major, trace and REE concntrations in each phase are summarized in Table 3.5.

To monitor the extraction Fe oxyhydroxides and Mn oxides we monitor the concentration of Fe and Mn. At Site 1149 an average of 2% of the Fe is extracted by Leach 1, and average of 1% by Leach 2 and an average of 97% of the Fe remains in the residue (Figure 3.1B). In contrast

Site	Hole	Core	Core Type	Sect.	Interval Top (cm)	Interval Bot (cm)	Depth (mbsf)	Phase	SiO2 wt.%	Al2O3 wt.%	TiO2 wt.%	Fe2O3 wt.%	MnO wt.%	CaO wt.%	MgO wt.%	Na2O wt.%	K2O wt.%	P2O5 wt.%	Li ppm	Be ppm	Sc ppm	V ppm	Cr ppm	Co ppm	Ni ppm	Cu ppm	Zn ppm	Rb ppm	Sr ppm
U1370	E	1	H	1	5	15	0.1	R	57.58	15.73	3.12	6.20	0.05	0.87	2.51	2.78	2.69	<det	272.95	10.25	16.18	511.86	246.20	40.93	112.90	464.58	467.47	468.67	786.53
U1370	E	1	H	1	140	150	1.45	R	53.73	16.51	0.72	6.51	0.06	<det	2.32	2.68	2.71	<det	66.42	2.70	20.41	115.68	48.94	10.79	<det	103.61	65.88	93.72	176.82
U1370	E	1	H	2	90	100	2.45	R	54.67	16.76	0.70	6.63	0.05	<det	2.39	3.05	2.79	<det	55.49	2.06	18.97	103.45	75.41	10.20	<det	68.81	81.37	89.17	134.04
U1370	E	2	H	2	140	150	9.15	R	54.43	16.86	<det	6.65	0.05	<det	2.71	3.04	2.76	<det	84.69	2.80	21.49	100.05	44.73	10.47	<det	160.44	135.82	116.44	136.96
U1370	E	2	H	4	140	150	12.15	R	56.78	17.17	0.70	6.77	0.04	<det	2.31	3.49	3.06	<det	61.47	2.40	20.37	96.65	35.11	4.40	<det	195.32	<det	98.42	67.15
U1370	E	2	H	5	140	150	13.65	R	55.95	17.22	0.71	6.80	0.04	<det	2.17	3.38	3.11	<det	45.26	1.70	17.73	117.07	62.06	7.79	<det	219.62	166.90	72.15	195.67
U1370	E	3	H	3	140	150	20.15	R	55.03	16.79	0.86	7.46	0.04	<det	2.38	3.01	3.21	<det	67.27	2.48	17.81	102.52	52.11	6.69	<det	190.14	98.52	92.67	67.28
U1370	E	3	H	4	140	150	21.65	R	54.28	17.22	1.04	8.72	0.04	1.04	2.61	3.30	3.09	<det	70.00	2.64	17.73	106.12	60.83	7.27	<det	188.34	72.97	84.49	64.58
U1370	E	3	H	5	140	150	23.15	R	54.94	16.64	0.93	7.61	0.04	<det	2.54	3.32	3.01	<det	75.30	2.66	19.73	102.00	50.01	7.35	<det	180.91	78.91	90.21	49.49
U1370	E	4	H	1	140	150	26.65	R	56.00	16.90	0.85	8.01	0.05	<det	2.48	3.88	3.16	<det	67.06	2.56	17.98	101.47	53.55	6.56	<det	153.91	86.17	100.28	47.93
U1370	E	4	H	3	140	150	29.65	R	56.22	17.13	0.89	7.54	0.05	<det	2.41	3.52	3.26	<det	38.51	2.48	18.05	111.65	35.35	11.44	<det	100.89	91.58	93.56	347.19
U1370	E	5	H	1	140	150	36.15	R	53.65	17.29	0.73	7.55	0.04	<det	2.34	3.37	3.37	<det	68.20	2.59	16.86	106.33	49.65	6.97	<det	136.61	73.47	106.30	<det
U1370	F	5	H	3	140	150	39.65	R	51.47	16.92	0.77	7.57	0.04	<det	2.32	3.24	3.32	<det	69.58	2.55	17.26	106.12	48.83	7.61	<det	149.07	84.82	116.59	72.79
U1370	E	5	H	6	60	70	42.79	R	54.14	15.96	0.76	6.89	0.04	<det	2.23	2.86	3.35	<det	67.60	2.64	14.50	103.03	50.41	7.30	<det	133.00	86.98	113.44	65.47
U1370	E	6	H	2	134	144	47.09	R	54.37	17.97	0.68	8.22	0.04	<det	2.39	3.08	3.48	<det	58.59	2.05	18.22	96.80	74.03	9.06	<det	70.31	92.16	87.10	60.79
U1370	E	6	H	5	100	110	51.18	R	52.32	17.60	0.68	7.75	0.03	<det	2.32	3.64	3.16	<det	75.93	2.69	20.37	91.45	46.55	7.87	<det	221.21	66.32	100.64	<det
U1370	F	7	H	3	140	150	58.65	R	50.90	14.89	<det	5.76	0.02	<det	1.93	2.97	3.65	0.77	69.54	2.60	21.96	104.37	73.50	9.63	<det	195.01	142.86	100.93	97.29
U1370	F	7	H	4	140	150	60.15	R	53.47	16.02	0.17	4.34	0.03	1.00	1.08	4.65	5.02	0.96	21.78	1.02	20.64	25.98	<det	<det	<det	72.12	<det	68.90	46.50
U1370	F	7	H	6	140	150	63.15	R	54.15	15.03	<det	8.53	0.04	<det	1.72	3.42	5.59	<det	34.74	1.64	25.45	54.21	19.65	5.97	<det	310.29	167.16	70.96	<det
U1370	E	9	H	2	140	150	65.05	R	50.86	14.85	0.38	8.61	0.04	<det	1.93	3.59	5.51	<det	34.86	1.54	39.94	59.54	19.96	3.64	<det	296.87	98.26	59.94	<det
U1370	E	1	H	1	5	15	0.1	L2	<det	<det	<det	0.51	0.09	<det	<det	<det	<det	<det	5.40	0.39	2.02	<det	<det	3.90	<det	39.10	<det	<det	<det
U1370	E	1	H	1	140	150	1.45	L2	-	-	0.03	-	-	-	-	-	-	-	6.75	0.46	2.16	19.46	<det	4.47	<det	25.66	<det	<det	<det
U1370	E	1	H	2	90	100	2.45	L2	<det	<det	0.03	0.35	0.03	<det	<det	<det	<det	<det	7.87	0.46	2.31	22.61	<det	3.24	<det	35.90	<det	<det	<det
U1370	E	2	H	2	140	150	9.15	L2	<det	<det	<det	<det	0.03	<det	<det	<det	<det	<det	4.71	0.38	1.85	<det	<det	3.50	<det	15.57	<det	<det	<det
U1370	E	2	H	4	140	150	12.15	L2	<det	<det	<det	0.38	0.10	<det	<det	<det	<det	<det	4.10	0.41	1.67	<det	<det	2.77	<det	18.95	<det	<det	<det
U1370	E	2	H	5	140	150	13.65	L2	<det	<det	<det	0.34	0.11	<det	<det	<det	<det	<det	4.26	0.39	1.90	<det	<det	5.07	<det	21.92	<det	<det	<det
U1370	E	3	H	3	134	150	20.15	L2	<det	<det	<det	0.40	0.04	<det	<det	<det	<det	<det	4.16	0.48	2.28	22.71	<det	3.27	<det	20.24	<det	<det	45.21
U1370	E	3	H	4	140	150	21.65	L2	<det	<det	<det	<det	0.03	<det	<det	<det	<det	<det	3.98	0.48	2.31	24.05	<det	3.28	<det	16.54	<det	<det	<det
U1370	E	3	H	5	140	150	23.15	L2	<det	<det	<det	0.54	1.59	<det	1.31	<det	0.29	0.65	5.73	0.66	2.55	21.23	<det	4.57	<det	17.03	<det	<det	<det
U1370	E	4	H	1	140	150	26.65	L2	<det	<det	<det	0.45	0.03	<det	<det	<det	<det	<det	4.44	0.46	<det	<det	<det	<det	<det	12.05	<det	<det	<det
U1370	E	4	H	3	140	150	29.65	L2	<det	<det	<det	0.409	0.1	<det	<det	<det	<det	<det	5.9529	0.585	2.444	29.584	<det	4.142	<det	16.29	<det	<det	<det
U1370	E	5	H	1	140	150	36.15	L2	<det	<det	0.03	0.545	0.05	<det	<det	<det	<det	<det	7.6059	0.661	3.586	36.405	<det	3.532	<det	25.839	<det	4.0577	40.252
U1370	F	5	H	3	140	150	39.65	L2	<det	0.64	<det	0.794	0.11	<det	<det	<det	<det	<det	5.1182	0.497	1.628	24.828	<det	3.286	<det	15.044	<det	<det	<det
U1370	E	5	H	6	60	70	42.79	L2	<det	<det	<det	0.367	0.1	<det	<det	<det	<det	<det	4.3947	0.47	2.217	29.897	<det	4.421	<det	18.345	<det	<det	<det
U1370	E	6	H	2	134	144	47.09	L2	-	-	0.03	-	-	-	-	-	-	-	7.1065	0.569	3.783	41.366	<det	9.28	<det	22.31	<det	4.1012	310.73
U1370	E	6	H	5	100	110	51.18	L2	<det	<det	0.07	0.345	0.08	<det	<det	<det	0.23	<det	15.13	1.021	23.14	126.63	<det	488.3	972.52	177.41	<det	3.7841	308.32
U1370	F	7	H	3	140	150	58.65	L2	<det	<det	<det	0.509	0.17	2.64	<det	<det	0.36	2.02	5.8906	0.638	3.477	36.37	<det	28.58	<det	29.292	<det	<det	164.73
U1370	F	7	H	4	140	150	60.15	L2	<det	<det	0.05	0.317	0.12	1.86	<det	<det	0.62	1.71	2.8278	0.567	21.71	29.599	<det	18.88	<det	15.469	<det	4.4074	139.87
U1370	F	7	H	6	140	150	63.15	L2	<det	<det	<det	<det	0.15	<det	<det	<det	<det	0.55	2.1064	1.87	3.624	279.05	<det	32.35	268.63	182.09	<det	<det	260.87
U1370	E	9	H	2	140	150	65.05	L2	<det	<det	0.1	0.764	0.33	2.18	<det	<det	0.34	1.32	5.738	1.231	23.74	95.132	<det	37.37	<det	65.665	<det	4.0752	179.6
U1370	E	1	H	1	5	15	0.1	L1	-	-	-	-	-	-	-	-	-	-	-	-	-	-	-	-	-	-	-	-	-
U1370	E	1	H	1	140	150	1.45	L1	<det	<det	0.06	0.742	1.05	<det	0.77	<det	0.24	<det	4.7232	0.398	2.312	23.333	<det	174.7	230.9	193.76	<det	<det	119.21
U1370	E	1	H	2	90	100	2.45	L1	<det	<det	0.08	0.386	2.13	<det	1.22	86.5	0.46	<det	7.3347	0.452	2.498	32.949	<det	207.6	261.94	177.26	<det	<det	117.14
U1370	E	2	H	2	140	150	9.15	L1	<det	<det		<det	0.6	<det	0.78	<det	0.23	<det	3.1381	0.21	1.516	<det	<det	82.44	183.48	46.937	<det	<det	55.669

Table 3.5 Major, trace, REE concentrations of three leached phases Leach 1 (L1), Leach 2 (L2) and Residue (R) of sediment samples from Site U1370 and Site 1149

Y ppm	Zr ppm	Nb ppm	Mo ppm	Cd ppm	Sn ppm	Sb ppm	Cs ppm	Ba ppm	La ppm	Ce ppm	Pr ppm	Nd ppm	Sm ppm	Eu ppm	Gd ppm	Tb ppm	Dy ppm	Ho ppm	Er ppm	Tm ppm	Yb ppm	Lu ppm	Hf ppm	Ta ppm	Pb ppm	Th ppm	U ppm
45.66	427.28	56.36	<det	0.09	13.28	5.30	27.80	7481.57	52.83	122.42	13.67	49.40	10.40	2.96	8.88	1.46	8.49	1.72	5.09	0.80	5.19	0.77	12.02	3.75	35.81	29.0	7.72
6.85	100.11	13.19	<det	0.03	2.64	1.10	5.86	2289.37	11.71	26.00	2.70	10.32	2.14	0.72	1.73	0.29	1.64	0.34	0.94	<det	0.93	0.14	2.98	0.87	8.50	4.83	1.50
13.12	114.81	12.75	<det	0.08	2.31	1.35	4.73	1277.28	20.96	39.98	4.80	18.98	3.81	0.91	3.13	0.47	2.62	0.52	1.46	<det	1.43	0.22	3.30	0.79	17.15	6.01	1.97
6.49	116.60	12.38	<det	<det	2.52	<det	7.85	1532.44	8.00	17.78	1.98	7.52	1.65	0.49	1.50	0.26	1.57	0.37	1.00	<det	1.16	0.18	3.02	0.91	4.56	4.56	1.67
3.68	99.34	12.40	<det	0.03	2.29	1.06	5.42	1096.36	5.13	11.58	1.08	4.22	0.93	0.31	0.85	0.15	0.96	0.21	0.62	<det	0.65	0.10	2.88	0.71	4.45	2.38	1.51
10.97	80.23	11.11	4.83	0.44	11.17	6.16	3.99	758.19	12.58	25.91	2.82	11.57	2.46	0.68	2.25	0.35	2.01	0.41	1.15	<det	1.15	0.18	2.41	0.66	107.39	3.44	1.99
3.67	117.20	19.56	<det	0.03	2.76	1.12	5.61	918.21	7.43	12.32	1.41	5.45	1.06	0.32	0.89	0.14	0.81	0.18	0.50	<det	0.56	0.09	3.18	1.18	6.82	1.99	1.28
2.60	124.14	20.95	3.73	0.03	2.67	1.09	4.73	943.67	5.95	13.73	1.25	4.72	0.91	0.31	0.78	0.12	0.75	0.16	0.46	<det	0.51	0.09	3.37	1.27	6.22	1.86	1.27
2.34	121.66	20.74	<det	0.03	2.66	0.96	4.75	846.03	5.31	13.31	1.15	4.37	0.85	0.28	0.70	0.12	0.69	0.15	0.43	<det	0.49	0.08	3.23	1.24	6.48	1.82	1.23
3.14	110.76	17.92	<det	0.03	2.58	0.96	5.86	488.69	6.12	14.15	1.28	4.86	0.93	0.26	0.79	0.13	0.77	0.18	0.49	<det	0.57	0.09	3.02	1.09	6.50	2.05	1.20
12.30	174.40	16.39	<det	0.05	8.04	15.27	4.26	828.53	26.78	44.25	5.02	19.36	3.60	1.00	2.96	0.43	2.29	0.45	1.26	<det	1.21	0.19	4.28	0.96	109.43	4.46	1.65
3.08	105.65	16.87	<det	0.03	2.79	1.00	6.32	544.67	7.14	13.49	1.37	5.22	0.99	0.25	0.83	0.14	0.80	0.18	0.52	<det	0.61	0.10	3.01	1.02	7.23	1.93	1.31
4.79	122.07	16.65	<det	0.02	3.38	1.41	7.03	611.19	6.85	15.46	1.63	6.09	1.21	0.30	1.11	0.19	1.15	0.25	0.76	<det	0.89	0.15	3.33	1.06	6.93	3.21	1.39
5.83	117.75	16.64	<det	0.02	3.24	1.34	6.75	457.54	8.99	20.03	1.89	6.86	1.34	0.30	1.18	0.20	1.17	0.26	0.76	<det	0.84	0.13	3.10	0.99	6.97	2.94	1.41
10.87	117.07	14.22	3.35	0.08	2.34	0.88	4.70	294.95	18.40	36.85	4.09	16.07	3.17	0.66	2.61	0.39	2.14	0.44	1.21	<det	1.23	0.20	3.32	0.82	16.75	4.39	1.77
3.24	115.96	15.85	<det	0.03	2.64	1.19	7.25	285.35	7.48	18.02	1.55	5.85	1.03	0.24	0.81	0.13	0.80	0.20	0.51	<det	0.56	0.10	3.45	0.98	5.55	2.47	1.12
3.88	137.44	23.77	<det	<det	2.93	<det	6.42	958.01	7.33	16.89	1.69	6.03	1.18	0.38	1.02	0.16	0.99	0.25	0.62	<det	0.80	0.13	3.40	1.40	5.97	2.67	1.33
38.25	93.07	6.30	<det	0.03	1.07	1.14	1.50	1364.52	46.32	60.98	12.57	53.17	11.53	2.45	9.75	1.45	7.92	1.53	3.97	1.01	2.97	0.42	3.39	0.18	2.19	3.74	0.52
3.37	146.62	12.46	5.03	<det	3.06	<det	2.41	642.29	5.83	15.64	1.35	5.09	1.05	0.28	1.04	0.16	0.94	0.23	0.52	<det	0.61	0.10	4.81	0.80	3.03	1.87	0.42
19.85	144.90	12.60	11.13	0.03	3.23	3.68	1.71	539.35	15.82	25.08	4.61	18.72	4.39	1.03	4.30	0.66	3.74	0.73	1.96	<det	1.64	0.24	4.89	0.72	3.33	2.33	0.43
3.72	19.55	0.69	<det	0.02	<det	<det	<det	178.01	5.13	107.45	1.39	5.03	1.05	0.22	1.01	0.16	0.83	0.16	0.44	<det	0.39	0.06	0.55	<det	10.76	2.27	0.18
3.10	30.71	0.70	<det	0.02	<det	<det	<det	166.25	6.07	102.84	1.49	5.45	1.09	0.23	1.02	0.17	0.85	0.17	0.45	<det	0.43	0.07	0.98	<det	8.37	3.64	0.20
2.78	33.91	0.70	<det	0.02	<det	<det	<det	187.70	7.19	165.29	1.64	5.71	1.13	0.23	1.01	0.17	0.86	0.17	0.46	<det	0.44	0.07	1.10	<det	8.75	4.01	0.27
3.08	18.99	0.15	<det	<det	<det	<det	<det	158.74	4.08	106.90	0.89	3.23	0.66	0.14	0.73	0.12	0.67	0.14	0.37	<det	0.35	0.05	0.52	<det	4.83	0.61	0.41
3.97	24.13	0.27	<det	0.03	<det	0.68	<det	101.41	4.55	90.33	1.02	4.11	0.95	0.20	1.00	0.16	0.93	0.19	0.50	<det	0.44	0.07	0.69	<det	5.10	0.52	0.44
4.50	18.13	0.30	4.50	0.02	<det	<det	<det	53.06	4.51	83.66	1.05	4.13	0.88	0.18	0.98	0.16	0.86	0.18	0.48	<det	0.45	0.07	0.46	<det	5.43	0.71	0.43
16.33	27.00	0.32	<det	<det	<det	<det	<det	119.94	11.15	30.28	3.17	13.40	3.04	0.63	2.85	0.45	2.56	0.51	1.49	<det	1.25	0.20	0.88	<det	3.62	1.63	0.47
13.56	26.17	0.35	<det	0.02	<det	<det	<det	122.33	10.10	26.48	2.86	12.09	2.67	0.57	2.61	0.40	2.26	0.45	1.22	<det	1.00	0.15	0.79	<det	4.01	2.06	0.43
7.74	27.27	0.41	<det	0.02	<det	<det	<det	169.24	6.35	23.41	1.76	7.50	1.67	0.34	1.68	0.26	1.46	0.29	0.77	<det	0.62	0.10	0.80	<det	4.58	1.06	0.40
3.50	21.04	0.25	<det	0.02	<det	<det	<det	166.27	3.91	16.48	0.94	3.98	0.88	0.18	0.90	0.14	0.80	0.16	0.42	<det	0.33	0.05	0.57	<det	2.65	<det	0.30
6.4398	26.046	0.539	<det	<det	<det	<det	<det	147.926	5.874	20.026	1.335	5.482	1.213	0.25	1.308	0.21	1.141	0.24	0.65	<det	0.57	0.09	0.771	<det	3.8976	1.9	0.4
6.8275	27.101	0.772	<det	0.016	<det	<det	0.144	126.913	6.677	23.654	1.488	6.162	1.367	0.26	1.447	0.23	1.255	0.26	0.69	<det	0.61	0.09	1.002	<det	4.5855	2.2	0.6
2.6445	11.369	<det	<det	<det	<det	<det	<det	144.131	3.441	17.41	0.732	3.157	0.655	0.12	0.704	0.11	0.607	0.13	0.34	<det	0.31	0.05	0.224	<det	2.5021	0.6	0.3
5.5377	11.945	<det	<det	<det	<det	<det	<det	140.436	5.211	22.706	1.263	5.238	1.157	0.22	1.22	0.19	1.059	0.22	0.58	<det	0.49	0.08	0.247	<det	4.617	1.3	0.3
6.8735	35.837	1.039	4.999	0.021	<det	<det	<det	168.195	7.579	56.776	1.962	7.466	1.606	0.3	1.651	0.29	1.456	0.28	0.81	<det	0.64	0.1	1.225	<det	6.2868	2.3	0.4
473.61	80.465	4.581	110.2	0.379	<det	1.003	<det	65.4999	250.8	392.42	80.25	308.2	61.69	14.2	61.72	9.59	55.75	11.4	31.3	4.44	26	3.88	1.792	<det	112.87	45	2.2
461.82	14.142	<det	3.93	0.076	<det	<det	<det	42.0986	395.3	657.48	83.92	334.1	64.53	14.3	64.27	9.18	51.42	10.4	28.5	3.9	21.5	3.29	0.478	<det	2.5684	6.5	0.8
544.97	46.456	2.146	3.015	0.099	<det	0.349	<det	37.4162	436.2	419.14	90.44	333.6	69.41	15.7	70.1	10.5	59.71	11.7	32	4.39	25.1	3.7	1.622	<det	9.828	17	1
111.47	35.977	0.206	12.92	0.214	<det	0.865	<det	1009.53	128.6	33.31	24.81	104.9	19.78	4.65	20.71	3.1	17.86	3.53	9.68	1.37	8.02	1.16	0.396	<det	83.16	1.3	1.3
687.4	116.72	4.29	32.58	0.166	<det	0.75	<det	53.5972	498.6	533.85	147.9	638.8	114.7	26	111.6	17	94.39	18	48.2	6.55	36.5	5.27	3.38	<det	36.647	18	1
-	-	-	-	-	-	-	-	-	-	-	-	-	-	-	-	-	-	-	-	-	-	-	-	-	-	-	-
28.64	32.96	0.931	13.4	0.345	<det	<det	<det	41.971	18	104.51	6.701	27.89	7.222	1.57	6.809	1.1	6.058	1.16	3.16	<det	2.91	0.46	0.663	<det	68.472	12	0.6
28.917	39.054	1.007	48.33	0.278	<det	0.244	<det	37.7828	15.69	112.97	5.465	22.96	6.101	1.35	6.222	1.01	5.821	1.13	3.14	<det	2.96	0.48	0.754	<det	77.602	13	0.6
45.174	11.838	0.403	30.33		<det		<det	<det	19.26	68.568	7.437	32.56	8.32	1.92	8.131	1.34	7.732	1.48	3.97		3.67	0.57	0.396	<det	34.286	7.8	0.3

Table 3.5 continued

Site	Hole	Core	Core Type	Sect.	Interval Top (cm)	Interval Bot (cm)	Depth (mbsf)	Phase	SiO2 wt.%	Al2O3 wt.%	TiO2 wt.%	Fe2O3 wt.%	MnO wt.%	CaO wt.%	MgO wt.%	Na2O wt.%	K2O wt.%	P2O5 wt.%	Li ppm	Be ppm	Sc ppm	V ppm	Cr ppm	Co ppm	Ni ppm	Cu ppm	Zn ppm	Rb ppm	Sr ppm
U1370	E	2	H	4	140	150	12.15	L1	-	-	-	-	-	-	-	-	-	-	-	-	-	-	-	-	-	-	-	-	-
U1370	E	2	H	5	140	150	13.65	L1	<det	<det	0.03	0.993	1.12	<det	0.88	<det	0.22	<det	5.5548	0.581	5.906	62.379	<det	206.9	246.95	86.729	<det	<det	132.86
U1370	E	3	H	3	140	150	20.15	L1	<det	<det	0.05	0.568	1.28	<det	0.95	<det	0.22	0.71	5.0742	0.836	11.38	78.358	<det	200.1	215.79	95.718	<det	<det	185.41
U1370	E	3	H	4	140	150	21.65	L1	<det	<det		<det	0.03	<det	<det	<det	<det	<det	2.1041	0.357	5.035	36.817	<det	71.8	91.343	31.853	<det	<det	79.725
U1370	E	3	H	5	140	150	23.15	L1	<det	<det	<det	0.312	0.19	<det	<det	95.2	<det	<det	5.5573	0.96	4.468	85.42	<det	213.9	283.41	80.38	<det	<det	192.28
U1370	E	4	H	1	140	150	26.65	L1	<det	<det	0.06	0.638	1.47	<det	1.31	<det	0.24	0.73	6.6863	0.799	9.008	96.085	<det	200.1	218.3	77.494	<det	<det	187.75
U1370	E	4	H	3	140	150	29.65	L1	<det	<det	<det	0.598	1.41	4.09	1.07	<det	1.22	0.84	6.8275	0.727	9.786	83.063	<det	210	232.31	80.331	<det	<det	166.85
U1370	E	5	H	1	140	150	36.15	L1	<det	<det	0.13	1.203	2.05	2.12	1.25	<det	0.32	1.21	4.2486	0.712	5.058	127.21	<det	314.6	83.289	57.735	<det	4.37	188.33
U1370	F	5	H	3	140	150	39.65	L1	-	-	0.08	-	-	-	-	-	-	-	11.401	1.007	18.04	115.28	<det	310.2	455.88	180.78	<det	4.2888	235.52
U1370	E	5	H	6	60	70	42.79	L1	<det	<det	-	1.147	2.1	<det	1.04	<det	<det	0.91	-	-	-	-	-	-	-	-	-	-	-
U1370	E	6	H	2	134	144	47.09	L1	<det	<det	0.08	1.015	2.57	<det	1.23	<det	0.25	0.67	10.525	0.996	12.55	130.79	<det	394.4	539.41	150.44	<det	3.9502	238.74
U1370	E	6	H	5	100	110	51.18	L1	-	-	<det	-	-	-	-	-	-	-	5.1196	0.549	2.429	27.628	<det	7.244	<det	9.1981	<det	<det	36.274
U1370	F	7	H	3	140	150	58.65	L1	<det	<det	-	1.029	4.68	3.81	1.61	<det	0.48	2.32	-	-	-	-	-	-	-	-	-	-	-
U1370	F	7	H	4	140	150	60.15	L1	<det	<det	-	0.839	2.99	2.96	0.81	<det	0.7	2.12	-	-	-	-	-	-	-	-	-	-	-
U1370	F	7	H	6	140	150	63.15	L1	<det	<det	<det	<det	2.31	2.56	0.72	<det	0.29	<det	4.246	2.338	6.677	135.72	<det	86.98	513.09	412.6	153.45	<det	637.88
U1370	E	9	H	2	140	150	65.05	L1	<det	<det	0.11	1.219	4.26	4.81	1.14	<det	0.42	0.79	9.8423	0.967	30.11	212.87	<det	638.2	1670.3	525.3	169.08	4.0351	401.45
1149	A	1	H	1	75	77	0.75	R	62.07	13.83	0.64	5.368	0.08	<det	2.19	3.27	2.18	<det	40.066	1.686	13.22	98.909	54.293	11.15	<det	44.426	93.111	85.576	119.99
1149	A	2	H	4	33	35	9.03	R	59.06	10.45	0.54	3.979	2.58	2.86	1.97	2.61	1.7	<det	43.969	1.728	11.18	146.89	54.605	16.4	<det	61.238	93.209	87.747	113.54
1149	A	3	H	6	46	48	21.66	R	64.33	13.06	0.63	4.38	0.1	1.87	2.09	2.91	2.21	<det	46.326	1.917	12.1	114.09	53.871	14.36	<det	25.407	85.355	96.885	140.41
1149	A	4	H	6	49	51	31.19	R	58.92	13.56	0.69	4.832	0.06	0.77	2.43	<det	2.51	<det	55.952	2.311	12.76	158.39	70.618	16.93	<det	33.038	93.825	112.7	127.42
1149	A	5	H	6	84	86	41.04	R	55.41	13.58	0.62	4.956	0.1	<det	2.25	2.61	2.37	<det	58.831	2.299	13.14	135.09	53.684	14.22	<det	89.283	<det	93.329	137.22
1149	A	6	H	3	44	46	45.64	R	59.83	14.62	0.59	5.518	0.14	<det	2.15	3.5	2.32	<det	42.382	1.756	15.24	121.83	45.472	17.19	<det	51.417	<det	70.826	100.5
1149	A	7	H	5	12	14	57.82	R	56.68	14.06	0.55	5.436	0.11	<det	2.04	3.31	2.51	<det	-	-	15.18	-	-	-	-	-	-	-	-
1149	A	8	H	6	38	40	69.08	R	56.84	14.99	0.69	6.634	0.1	<det	2.59	3.36	2.5	<det	47.87	2.037	17.24	170.28	60.445	25.68	<det	68.962	<det	86.376	93.484
1149	A	9	H	2	71	73	72.91	R	59.38	14.81	0.68	6.342	0.14	2.06	2.25	2.74	2.02	<det	44.647	1.661	18.13	120.1	47.493	18.25	<det	94.18	<det	62.179	124.22
1149	A	10	H	6	15	18	87.85	R	61.08	13.8	0.65	5.645	0.11	1.68	2.19	2.56	2.08	<det	48.175	1.996	14.5	139.13	55.575	24.3	<det	113.97	<det	67.619	89.886
1149	A	11	H	5	65	67	96.35	R	49.56	12.76	0.55	6.505	0.17	2.3	2.03	2.53	1.66	<det	31.007	1.293	19.71	155.66	29.573	25.12	<det	127.76	<det	56.654	96.057
1149	A	12	H	2	44	46	101.14	R	-	-	-	-	-	-	-	-	-	-	60.875	2.057		89.789	45.848	8.81	<det	187.41	67.496	84.878	51.239
1149	A	13	H	1	94	96	109.64	R	57.16	14.75	0.72	6.446	0.17	<det	2.62	2.96	2.37	<det	57.106	2.274	15.01	139.99	60.831	36.06	<det	154.45	<det	98.677	64.263
1149	A	14	H	6	66	68	126.36	R	54.63	16.37	0.69	7.118	0.11	<det	2.8	3.88	2.72	<det	66.871	2.408	16.6	102.15	51.939	14.99	<det	200.77	<det	99.525	60.112
1149	A	15	H	5	37	39	134.07	R	50.82	14.21	0.66	6.032	0.08	<det	2.59	3	2.46	<det	20.347	2.641	14.89	285.51	<det	3.036	<det	619.78	173.41	30.049	305.68
1149	A	16	H	4	62	64	142.32	R	55.87	14.21	0.65	5.86	0.08	<det	2.67	3.23	2.44	<det	82.042	3.54	13.64	126.16	85.588	15.72	<det	138.58	<det	138.53	54.655
1149	A	17	H	6	20	22	153.45	R	47.17	16.3	0.64	6.46	0.06	<det	2.24	4.15	2.85	<det	62.192	1.973	15.73	91.294	47.586	8.13	<det	177.95	<det	106.28	64.491
1149	A	18	H	1	36	38	156.56	R	47.56	16.19	0.71	7.347	0.05	<det	2.57	3.46	2.99	<det	58.537	2.135	21.19	84.874	46.415	11.11	<det	166.96	122.97	97.205	72.806
1149	A	19	X	1	24	26	164.64	R	54.84	15.43	0.64	5.802	0.04	<det	2.46	3.04	3.34	<det	63.085	2.819	12.87	92.698	98.285	10.33	<det	92.505	120.1	142.42	145.27
1149	A	20	X	1	93	95	170.73	R	60.11	13.78	0.72	5.418	0.04	<det	3.06	2.78	3.14	<det	43.367	2.023	17.02	85.63	50.943	7.895	<det	74.717	<det	114.06	59.567
1149	A	1	H	1	75	77	0.75	L2	<det	<det	<det	<det	0.03	<det	<det	<det	<det	<det	1.1524	0.118	<det	<det	<det	2.023	<det	19.21	<det	<det	<det
1149	A	2	H	4	33	35	9.03	L2	<det	<det	<det	<det	10.8	<det	0.67	<det	<det	<det	6.5882	0.54	<det	<det	<det	24.19	<det	116.51	<det	<det	48.448
1149	A	3	H	6	46	48	21.66	L2	<det	<det	<det	<det	0.74	<det	<det	<det	<det	<det	4.4263	0.095	<det	<det	<det	8.217	<det	38.241	<det	<det	<det
1149	A	4	H	6	49	51	31.19	L2	<det	<det	<det	<det	0.07	<det	<det	<det	<det	<det	4.2072	0.178	1.577	<det	<det	4.444	<det	33.464	<det	<det	<det
1149	A	5	H	6	84	86	41.04	L2	<det	<det	<det	<det	0.34	<det	<det	<det	<det	<det	3.2082	0.19	<det	<det	<det	3.81	<det	38.599	<det	<det	<det
1149	A	6	H	3	44	46	45.64	L2	<det	<det	<det	<det	0.56	<det	<det	89.5	<det	<det	3.2708	0.202	<det	23.461	<det	4.106	<det	12.055	<det	<det	<det
1149	A	7	H	5	12	14	57.82	L2	<det	<det	<det	<det	0.17	<det	<det	97.9	<det	<det	2.3045	0.132	<det	<det	<det	4.311	<det	8.8356	<det	<det	<det
1149	A	8	H	6	38	40	69.08	L2	<det	<det	<det	<det	0.3	<det	<det	89	<det	<det	<det	<det	<det	<det	<det	<det	89.016	<det	<det	<det	<det
1149	A	9	H	2	71	73	72.91	L2	<det	<det	<det	<det	0.1	<det	<det	<det	<det	<det	3.0661	0.155	<det	<det	<det	5.194	<det	9.568	<det	<det	<det
1149	A	10	H	6	15	18	87.85	L2	<det	<det	<det	<det	0.2	<det	<det	<det	<det	<det	3.1602	0.231	<det	20.768	<det	6.842	<det	10.991	<det	<det	<det
1149	A	11	H	5	65	67	96.35	L2	-	-	-	-	-	-	-	-	-	-	-	-	-	-	-	-	-	-	-	-	-
1149	A	12	H	2	44	46	101.14	L2	<det	<det	<det	<det	0.16	<det	<det	<det	<det	<det	3.3349	0.238	<det	<det	<det	5.336	<det	12.167	<det	<det	<det

Table 3.5 continued

Y ppm	Zr ppm	Nb ppm	Mo ppm	Cd ppm	Sn ppm	Sb ppm	Cs ppm	Ba ppm	La ppm	Ce ppm	Pr ppm	Nd ppm	Sm ppm	Eu ppm	Gd ppm	Tb ppm	Dy ppm	Ho ppm	Er ppm	Tm ppm	Yb ppm	Lu ppm	Hf ppm	Ta ppm	Pb ppm	Th ppm	U ppm
-	-	-	-	-	-	-	-	-	-	-	-	-	-	-	-	-	-	-	-	-	-	-	-	-	-	-	-
148.6	16.521	<det	68.8	0.155	<det	0.158	<det	<det	85.36	174.7	26.61	110.7	27.48	5.98	25.99	4.12	23.37	4.53	12.3	1.82	11.1	1.71	0.299	<det	70.279	19	1
235.2	41.799	1.761	95.25	0.209	<det	0.555	<det	57.4928	128.7	181.96	28.3	120.5	26.63	6.18	28.2	4.49	26.34	5.48	15.7	2.29	13.8	2.15	0.985	<det	75.876	23	2
81.077	19.677	0.947	31.4		<det		<det	39.0172	42.81	83.537	10.78	47.91	11.47	2.66	11.62	1.88	11.03	2.24	6.14		5.52	0.86	0.534	<det	28.811	9.1	0.7
213.57	13.717	0.389	49.91	0.163	<det	0.176	<det	85.5121	127.1	195.77	31.96	132.5	31.38	6.82	31.09	4.86	28.3	5.65	15.7	2.35	13.9	2.14	0.414	<det	60.078	6.7	1.6
245.67	43.17	2.034	58.07	0.175	<det	0.876	<det	91.2213	142.1	197.58	31.05	131.3	29.15	6.72	29.78	4.67	27.54	5.55	16	2.29	13.7	2.13	1.012	<det	84.567	30	1.8
234.56	17.526	<det	42.09	0.166	<det	<det	<det	91.4869	137.5	205.75	34.49	144.2	33.85	7.38	33.83	5.27	31.26	6.26	17.6	2.57	15.2	2.35	0.299	<det	82.214	26	1.8
244.42	46.509	3.92	42.91	0.177	<det	1.879	<det	868.392	118.4	248.32	23.56	101.1	23.48	5.67	25.84	4.23	24.8	5.5	15.3	2.33	14.2	2.3	0.779	<det	104.66	23	2.6
384.84	68.79	3.008	75.91	0.261	<det	0.72	<det	112.751	209.6	318.27	50.65	215.9	48.03	10.9	49.73	7.79	45.71	9.31	26	3.8	22.1	3.42	1.387	<det	144.9	41	2.4
-	-	-	-	-	-	-	-	-	-	-	-	-	-	-	-	-	-	-	-	-	-	-	-	-	-	-	-
276.37	67.795	4.856	107.3	0.333	<det	0.964	<det	270.129	162.7	321.73	39.8	172	39.09	8.76	38.19	5.98	34.3	6.74	19.1	2.68	15.6	2.36	1.474	<det	149.81	36	1.6
16.171	11.323	<det	<det	<det	<det	<det	<det	40.0151	14.37	124.94	3.215	12.67	2.864	0.62	2.976	0.46	2.643	0.55	1.51	<det	1.29	0.19	0.207	<det	4.5413	2.4	0.4
-	-	-	-	-	-	-	-	-	-	-	-	-	-	-	-	-	-	-	-	-	-	-	-	-	-	-	-
-	-	-	-	-	-	-	-	-	-	-	-	-	-	-	-	-	-	-	-	-	-	-	-	-	-	-	-
187.95	81.733	0.126	9.057	0.527	<det	0.785	<det	599.836	74.13	21.837	19.4	98	23.45	5.96	28.01	4.31	26.38	5.39	14.9	2.11	12.3	1.79	0.555	<det	42.793	2.2	3.8
364.48	107.16	7.853	70.99	0.722	<det	1.187	<det	101.332	222.6	320.98	69.46	294.2	59.58	13.4	57.22	8.94	50.07	9.8	26.5	3.76	22	3.35	2.327	<det	208.9	12	1.9
21.619	105.26	8.944	<det	<det	2.105	<det	7.243	486.254	16.13	31.908	3.746	14.5	3.142	0.76	3.199	0.54	3.408	0.74	2.19	-	2.36	0.37	2.764	0.642	8.3779	5.4	1.4
13.523	83.308	9.481	<det	<det	2.031	<det	7.449	605.749	18.3	37.095	4.084	15.2	3.032	0.68	2.77	0.44	2.671	0.58	1.65	-	1.78	0.28	2.205	0.668	7.017	5.8	2
18.834	115.62	10.23	<det	<det	2.25	<det	7.585	584.15	19.23	37.733	4.386	16.5	3.375	0.78	3.065	0.5	3.082	0.65	1.91	-	2.11	0.33	3.024	0.73	7.4786	6.1	1.5
11.698	101.23	12.22	<det	<det	2.603	<det	9.544	598.43	20.86	40.903	4.52	16.28	3.049	0.66	2.55	0.41	2.431	0.53	1.55	-	1.73	0.27	2.637	0.892	8.1961	7.3	1.8
7.8364	94.176	12.19	<det	0.032	2.459	1.711	6.068	1647.75	12.35	24.859	2.84	11.13	2.255	0.63	1.866	0.3	1.744	0.36	1.04	<det	1.05	0.16	2.804	0.772	11.192	4.8	1.5
13.241	85.544	9.036	<det	0.041	2.003	0.852	5.448	518.967	12.46	24.945	2.927	11.77	2.565	0.6	2.393	0.4	2.459	0.53	1.59	<det	1.69	0.27	2.545	0.54	12.546	4.1	1.3
-	-	-	-	-	-	-	-	-	-	-	-	-	-	-	-	-	-	-	-	-	-	-	-	-	-	-	-
7.127	81.417	10.59	<det	0.033	2.215	1.215	6.028	645.31	13.73	28.365	3.163	12.21	2.35	0.52	1.866	0.3	1.72	0.36	1.04	<det	1.06	0.16	2.316	0.639	15.179	4.1	1.5
14.941	102.91	9.221	<det	0.031	2.247	1.251	4.408	517.771	11.99	27.188	3.252	12.6	2.782	0.7	2.706	0.46	2.881	0.61	1.84	<det	1.92	0.3	2.895	0.576	12.408	4.4	1.4
9.7042	103.23	10.94	<det	0.027	2.531	1.497	4.563	520.226	12.58	30.182	3.206	11.85	2.36	0.54	2.128	0.35	2.158	0.46	1.36	<det	1.4	0.21	2.82	0.68	14.833	5	1.7
14.916	94.237	7.116	<det	0.032	1.782	1.247	3.471	347.244	10.16	22.908	2.693	10.57	2.426	0.56	2.541	0.43	2.741	0.58	1.76	<det	1.83	0.29	2.713	0.782	10.84	4.1	1.2
5.7618	157.47	20.12	6.341	0.03	3.847	3.078	6.341	189.978	10.8	25.27	2.054	7.319	1.343	0.28	1.202	0.19	1.195	0.26	0.77	<det	0.84	0.13	4.548	1.106	5.8409	2.8	1.4
6.0497	76.188	10.69	<det	0.03	2.242	1.146	7.267	403.214	14.15	32.156	3.044	11.56	2.135	0.46	1.641	0.26	1.46	0.3	0.86	<det	0.92	0.14	2.195	0.639	18.547	5.2	1.5
4.7476	87.814	11.5	<det	0.025	2.411	1.232	8.529	285.657	13.64	32.147	2.674	9.999	1.797	0.37	1.339	0.21	1.148	0.25	0.71	<det	0.79	0.12	2.492	0.68	7.022	4.3	1.4
27.15	165.51	6.908	173.1	0.186	1.752	11.36	1.595	8915.17	61.58	34.053	13.43	52.37	9.67	4.18	9.094	1.4	7.461	1.44	3.9	1.18	3.55	0.52	3.063	0.238	43.617	1.6	0.7
7.6073	101.37	15.59	<det	0.033	3.054	1.027	8.71	386.458	17.33	33.908	3.708	14.31	2.611	0.51	1.889	0.3	1.635	0.37	0.97	<det	0.97	0.16	3.025	0.959	9.731	4.7	2
6.305	126.47	14.32	<det	0.025	3.206	2.043	9.326	307.338	13.29	30.576	2.48	8.595	1.513	0.3	1.251	0.2	1.237	0.27	0.82	<det	0.86	0.14	3.517	0.816	6.8541	4	1.6
11.213	155.73	19.6	10.46	<det	3.597	<det	7.971	254.676	21.99	38.535	4.06	14.47	2.699	0.58	2.359	0.36	2.179	0.47	1.33	-	1.46	0.23	4.501	1.243	6.2966	4.9	1.4
6.9082	129.79	13.5	<det	<det	3.199	<det	12.61	420.637	19.34	37.174	3.238	10.74	1.709	0.37	1.367	0.22	1.411	0.35	1.01	-	1.27	0.2	3.473	0.937	9.3736	5.6	1.6
8.4202	121.36	14.38	<det	0.027	3.53	1.763	9.168	191.116	13.16	29.009	2.722	9.806	1.802	0.36	1.539	0.25	1.511	0.32	0.98	<det	1.07	0.18	3.377	0.981	7.6233	3.5	1.5
<det	<det	<det	<det	<det	<det	<det	<det	138.635	1.729	6.1967	0.569	2.036	0.437	0.1	0.49	0.07	0.321	0.06	0.15	-	<det	0.02	<det	<det	3.6671	0.6	0.1
24.453	<det	<det	3.114	<det	<det	<det	<det	102.129	5.757	13.937	1.443	6.416	1.731	0.49	2.658	0.47	3.235	0.76	2.35	-	2.48	0.42	<det	<det	1.9355	<det	0.4
2.239	<det	<det	<det	<det	<det	<det	<det	50.6259	2.177	6.4122	0.719	2.788	0.643	0.13	0.723	0.1	0.53	0.1	0.26	-	0.19	0.03	<det	<det	4.9875	<det	0.2
2.7071	<det	<det	<det	<det	<det	<det	<det	132.308	3.995	10.626	0.845	3.34	0.724	0.15	0.769	0.11	0.569	0.11	0.27	<det	0.21	0.03	0.17	<det	5.0755	0.7	0.2
3.0106	<det	<det	<det	0.023	<det	<det	<det	73.6632	4.705	17.899	1.135	4.767	1.061	0.22	1.029	0.15	0.793	0.15	0.37	<det	0.28	0.04	0.19	<det	7.5011	1.1	0.4
3.6493	11.013	<det	<det	0.026	<det	<det	<det	79.1995	5.166	14.578	1.193	4.896	1.092	0.22	1.081	0.17	0.885	0.17	0.45	<det	0.4	0.06	0.247	<det	6.8247	2	0.1
2.1945	10.557	<det	<det	<det	<det	<det	<det	88.216	4.072	13.56	0.983	3.981	0.821	0.15	0.813	0.14	0.652	0.12	0.33	<det	0.25	0.04	0.224	<det	6.4314	1.3	0.1
32.675	<det	1.501	<det	<det	6.619	<det	38.79	108.841	8.402	24.76	2.246	9.088	2.085	0.45	2.038	0.31	1.661	0.3	0.78	<det	0.69	0.1	0.224	<det	8.5725	3	0.2
2.3292	10.231	<det	<det	<det	<det	<det	<det	181.973	3.015	10.388	0.947	3.83	0.857	0.15	0.871	0.15	0.698	0.13	0.35	<det	0.26	0.04	0.203	<det	5.4587	1	0.1
3.3434	10.932	<det	<det	<det	<det	<det	<det	91.2917	3.034	9.4425	0.871	3.824	0.877	0.18	0.948	0.15	0.793	0.16	0.41	<det	0.37	0.06	0.218	<det	8.0365	1	0.1
-	-	-	-	-	-	-	-	-	-	-	-	-	-	-	-	-	-	-	-	-	-	-	-	-	-	-	-
4.1481	12.253	<det	<det	<det	<det	<det	<det	76.6933	2.32	8.9374	0.749	3.563	0.871	0.18	1.011	0.16	0.859	0.18	0.45	<det	0.41	0.06	0.265	<det	8.2696	0.6	0.2

Table 3.5 continued

Site	Hole	Core	Core Type	Sect.	Interval Top (cm)	Interval Bot (cm)	Depth (mbsf)	Phase	SiO2 wt.%	Al2O3 wt.%	TiO2 wt.%	Fe2O3 wt.%	MnO wt.%	CaO wt.%	MgO wt.%	Na2O wt.%	K2O wt.%	P2O5 wt.%	Li ppm	Be ppm	Sc ppm	V ppm	Cr ppm	Co ppm	Ni ppm	Cu ppm	Zn ppm	Rb ppm	Sr ppm
1149	A	13	H	1	94	96	109.64	L2	<det	<det	<det	<det	0.18	<det	<det	<det	<det	<det	2.4045	0.249	<det	<det	<det	4.775	<det	8.2835	<det	<det	<det
1149	A	14	H	6	66	68	126.36	L2	-	-	-	-	-	-	-	-	-	-	2.6647	0.289	1.63	<det	<det	9.176	<det	15.749	<det	<det	<det
1149	A	15	H	5	37	39	134.07	L2	<det	<det	<det	0.409	0.16	<det	<det	73	<det	<det	3.0569	0.327	1.417	<det	<det	7.791	<det	17.17	<det	3.8653	<det
1149	A	16	H	4	62	64	142.32	L2	<det	<det	<det	0.415	0.09	<det	<det	76.4	<det	<det	3.7452	0.532	1.759	<det	<det	6.622	<det	23.49	<det	3.8867	<det
1149	A	17	H	6	20	22	153.45	L2	<det	<det	0.04	0.333	0.53	<det	<det	92.2	0.27	<det	2.4738	0.309	2.092	32.308	<det	35.35	90.181	46.576	<det	<det	44.073
1149	A	18	H	1	36	38	156.56	L2	<det	<det	<det	<det	0.96	<det	<det	<det	<det	<det	8.1756	0.307	1.507	35.63	<det	111.5	306.25	77.27	<det	<det	109.14
1149	A	19	X	1	24	26	164.64	L2	<det	<det	<det	<det	0.18	<det	<det	<det	<det	<det	2.8827	0.32	1.958	<det	<det	9.644	<det	22.306	<det	<det	45.152
1149	A	20	X	1	93	95	170.73	L2	<det	<det	<det	<det	0.08	<det	<det	<det	<det	<det	1.1785	0.204	1.744	19.484	<det	9.973	<det	13.211	<det	<det	146.46
1149	A	1	H	1	75	77	0.75	L1	<det	<det	0.03	<det	0.13	<det	0.43	<det	<det	<det	2.0937	0.198	1.742	<det	<det	63.8	<det	99.157	<det	<det	105.97
1149	A	2	H	4	33	35	9.03	L1	<det	<det	<det	<det	1.52	<det	0.78	<det	0.34	<det	2.5869	0.217	1.632	<det	<det	12.89	<det	216.03	<det	<det	67.007
1149	A	3	H	6	46	48	21.66	L1	<det	<det	<det	<det	0.21	<det	0.61	<det	0.37	<det	2.1534	0.044	<det	<det	<det	6.635	<det	93.147	<det	<det	40.171
1149	A	4	H	6	49	51	31.19	L1	<det	<det	<det	<det	0.03	<det	0.53	<det	0.3	<det	3.1585	0.142	<det	<det	<det	4.165	<det	127.56	<det	<det	49.107
1149	A	5	H	6	84	86	41.04	L1	<det	<det	<det	<det	0.04	<det	0.43	<det	0.31	<det	1.5778	0.166	<det	<det	<det	<det	<det	52.019	<det	<det	38.416
1149	A	6	H	3	44	46	45.64	L1	<det	<det	<det	<det	0.08	<det	0.57	83.8	0.36	<det	1.9884	0.121	<det	34.589	<det	<det	<det	16.215	<det	<det	56.195
1149	A	7	H	5	12	14	57.82	L1	<det	<det	<det	<det	0.03	<det	0.49	88.6	0.39	<det	1.4462	0.129	<det	19.866	<det	<det	<det	<det	<det	<det	54.193
1149	A	8	H	6	38	40	69.08	L1	<det	<det	<det	<det	0.04	<det	0.6	82.2	0.39	<det	1.761	0.131	<det	26.603	<det	<det	<det	13.051	<det	<det	53.834
1149	A	9	H	2	71	73	72.91	L1	-	-	-	-	-	-	-	-	-	-	1.7277	0.134	<det	<det	<det	<det	<det	<det	<det	<det	49.183
1149	A	10	H	6	15	18	87.85	L1	<det	<det	<det	<det	0.05	<det	0.65	<det	0.36	<det	1.6136	0.141	<det	22.542	<det	<det	<det	<det	<det	<det	50.106
1149	A	11	H	5	65	67	96.35	L1	<det	<det	<det	<det	0.02	<det	0.44	<det	<det	<det	1.5014	0.106	<det	<det	<det	<det	<det	<det	<det	<det	44.093
1149	A	12	H	2	44	46	101.14	L1	<det	<det	<det	<det	0.04	<det	0.6	<det	0.27	<det	2.4684	0.248	<det	<det	<det	<det	<det	<det	<det	<det	71.111
1149	A	13	H	1	94	96	109.64	L1	<det	<det	<det	<det	0.03	<det	0.7	<det	0.37	<det	2.2509	0.151	<det	<det	<det	<det	<det	<det	<det	<det	49.498
1149	A	14	H	6	66	68	126.36	L1	<det	<det	0.08	0.338	1.41	<det	0.76	<det	0.22	<det	2.5347	0.51	2.246	108.77	<det	143.9	<det	38.091	<det	<det	123.46
1149	A	15	H	5	37	39	134.07	L1	<det	<det	<det	0.366	1.68	<det	1.25	82.6	0.37	<det	-	-	-	-	-	-	-	-	-	-	-
1149	A	16	H	4	62	64	142.32	L1	-	-	-	-	-	-	-	-	-	-	-	-	-	-	-	-	-	-	-	-	-
1149	A	17	H	6	20	22	153.45	L1	<det	<det	<det	0.591	3.07	<det	0.69	<det	0.4	<det	7.0623	0.687	6.321	67.141	<det	660.4	427.72	297.76	<det	<det	318.43
1149	A	18	H	1	36	38	156.56	L1	<det	<det	<det	<det	2.98	<det	0.83	<det	0.27	<det	18.472	0.823	18.88	97.087	<det	951.2	1233.4	468.51	<det	<det	394.46
1149	A	19	X	1	24	26	164.64	L1	<det	<det	<det	0.67	2.5	<det	0.71	78	0.29	0.63	10.958	0.91	6.159	85.208	<det	409.2	564.82	226.64	<det	4.3516	824.61
1149	A	20	X	1	93	95	170.73	L1	<det	<det	<det	0.453	2.1	2.13	0.5	<det	0.55	1.14	3.285	0.435	15.21	66.605	<det	274.7	549.23	212.78	<det	<det	262.9

Table 3.5 continued

Y ppm	Zr ppm	Nb ppm	Mo ppm	Cd ppm	Sn ppm	Sb ppm	Cs ppm	Ba ppm	La ppm	Ce ppm	Pr ppm	Nd ppm	Sm ppm	Eu ppm	Gd ppm	Tb ppm	Dy ppm	Ho ppm	Er ppm	Tm ppm	Yb ppm	Lu ppm	Hf ppm	Ta ppm	Pb ppm	Th ppm	U ppm
3.0567	8.7926	<det	<det	0.031	<det	<det	<det	117.227	2.419	7.3893	0.491	2.092	0.494	0.11	0.65	0.1	0.565	0.12	0.33	<det	0.33	0.05	0.225	<det	7.2904	<det	0.1
4.2846	<det	<det	<det	<det	<det	<det	<det	70.529	2.834	14.864	0.611	2.598	0.631	0.15	0.803	0.13	0.73	0.16	0.42	<det	0.38	0.06	<det	<det	3.4333	<det	0.4
3.1293	17.91	0.11	<det	0.022	<det	<det	<det	57.7489	2.244	15.998	0.557	2.575	0.721	0.16	0.823	0.13	0.764	0.16	0.41	<det	0.37	0.06	0.428	<det	3.3618	0.5	0.4
3.4929	27.904	0.283	<det	0.024	<det	0.209	<det	77.1204	2.717	10.778	0.588	2.67	0.706	0.15	0.802	0.12	0.728	0.15	0.42	<det	0.37	0.06	0.65	<det	3.0164	0.6	0.4
19.671	24.65	0.8	16.16	0.038	<det	0.202	<det	36.5474	14.52	47.434	3.478	14.04	3.342	0.79	3.703	0.56	3.148	0.63	1.71	<det	1.4	0.22	0.661	<det	19.701	3.3	0.3
128.58	<det	<det	29.72	<det	<det	<det	<det	197.837	91.29	142.24	20.69	91.62	19.88	4.64	19.93	3.06	17.38	3.42	9.18	-	7.43	1.11	<det	<det	35.247	<det	0.4
9.9306	<det	0.109	3.252	<det	<det	<det	<det	65.3008	8.144	60.21	2.433	10.13	2.315	0.54	2.282	0.36	1.942	0.38	1.01	-	0.84	0.13	<det	<det	11.032	0.6	0.3
126.26	9.1856	<det	<det	<det	<det	<det	<det	50.8861	70.62	82.826	19.3	74.56	17.94	3.87	18.81	3.08	16.43	3.08	9.14	1.21	6.93	1.03	0.253	<det	4.9984	1.2	0.3
18.276	12.011	0.282	4.937	0.058	<det	0.456	<det	57.8549	10.01	32.265	3.34	14.22	3.616	0.8	3.643	0.58	3.262	0.65	1.78	<det	1.56	0.24	0.23	<det	28.515	2.4	0.3
7.5757	<det	<det	6.775	<det	<det	<det	<det	<det	5.218	17.487	1.574	6.696	1.598	0.38	1.661	0.26	1.424	0.28	0.77	-	0.67	0.11	<det	<det	17.933	2	2.9
9.0485	<det	0.368	13.59	<det	<det	<det	<det	<det	6.777	25.639	2.152	9.19	2.271	0.54	2.262	0.36	1.919	0.36	0.92	-	0.77	0.12	<det	<det	23.477	3	0.5
15.884	<det	<det	3.671	<det	<det	<det	<det	<det	9.443	45.991	3.347	14.87	3.855	0.93	4.02	0.65	3.688	0.71	1.87	-	1.67	0.26	0.159	<det	38.544	5.2	0.6
16.567	<det	<det	<det	<det	<det	0.165	<det	<det	6.537	14.917	2.134	9.529	2.558	0.62	2.823	0.47	2.769	0.56	1.56	<det	1.39	0.22	<det	<det	14.314	1.8	1
15.486	9.9339	<det	<det	<det	<det	<det	<det	31.7328	9.507	19.859	2.556	10.79	2.823	0.68	3.155	0.49	2.782	0.55	1.49	<det	1.27	0.2	0.22	<det	15.553	3.8	0.2
21.103	9.7158	<det	<det	<det	<det	<det	<det	32.302	12.31	23.679	3.547	15.03	3.924	0.93	4.297	0.67	3.773	0.74	1.99	<det	1.73	0.27	0.216	<det	11.664	4.1	0.2
12.036	9.8506	<det	<det	<det	<det	<det	<det	29.9226	6.057	12.454	1.707	7.503	2.015	0.48	2.29	0.37	2.141	0.44	1.18	<det	0.99	0.16	0.217	<det	12.281	2.3	0.2
18.451	9.6218	<det	<det	<det	<det	<det	<det	30.6931	9.429	18.985	2.944	12.54	3.28	0.79	3.702	0.59	3.367	0.66	1.81	<det	1.58	0.25	0.206	<det	8.9751	3.1	0.2
24.287	10.073	<det	<det	<det	<det	<det	<det	30.1392	10.65	23.874	3.36	14.66	3.939	0.97	4.593	0.72	4.251	0.85	2.36	<det	2.07	0.33	0.222	<det	12.194	2.4	0.2
18.286	9.3251	<det	<det	<det	<det	<det	<det	29.9203	6.719	12.021	2.201	9.82	2.686	0.68	3.296	0.53	3.178	0.64	1.77	<det	1.6	0.25	0.205	<det	5.6813	1.9	0.1
60.554	10.607	<det	<det	<det	<det	<det	<det	<det	17	64.194	6.853	30.41	8.099	1.9	9.059	1.47	8.967	1.85	5.3	0.78	4.9	0.78	0.263	<det	18.573	5	0.5
25.606	<det	<det	<det	0.024	<det	<det	<det	<det	7.915	21.226	2.993	13.63	3.67	0.88	4.076	0.68	4.082	0.85	2.39	<det	2.11	0.34	0.17	<det	10.728	2.6	0.2
89.647	24.822	1.482	24.34	0.123	<det	1.512	<det	527.12	30.39	120.26	10.47	46.99	11.58	2.86	12.91	2.11	12.57	2.61	7.58	1.11	6.97	1.1	0.451	<det	73.968	11	1.8
-	-	-	-	-	-	-	-	-	-	-	-	-	-	-	-	-	-	-	-	-	-	-	-	-	-	-	-
-	-	-	-	-	-	-	-	-	-	-	-	-	-	-	-	-	-	-	-	-	-	-	-	-	-	-	-
220.8	17.966	<det	77.59	0.434	<det	0.306	<det	92.2021	111.1	241.26	23.83	97.25	24.46	5.88	27.61	4.27	25.65	5.22	14.9	2.19	13.2	2.13	0.276	<det	77.833	13	2.1
365.33	10.845	<det	56.09	0.598	<det	0.25	<det	152.232	151.9	279.19	48.79	207.6	50.02	11.4	50.69	8.01	48.04	9.67	29.2	4.02	24.5	3.98	0.292	<det	86.821	9.4	1.8
290.79	13.581	0.15	63.99	0.283	<det	0.186	<det	210.858	192.4	372.94	47.98	181.2	43.53	9.4	44.98	7.44	39.19	7.27	21.5	2.93	16.2	2.44	0.344	<det	110.85	15	0.8
335.21	7.5682	<det	62.76	0.362	<det	0.161	<det	274.571	149.4	242.12	54.73	228.8	52.47	11.8	51.61	7.95	47.2	9.55	26.3	3.79	22.4	3.46	0.252	<det	137.48	18	1.8

Table 3.5 continued

an average of 44% of Mn is extracted in the first leach at Site 1149. An average of 43% of Mn is extracted from the second leach, and 13% remains in the residue at Site 1149. The distribution of Fe and Mn across the leached phases at Site U1370 are similar (Figure 3.1A). An average of 8% of the Fe is extracted in the first leach, 4% is extracted in the second and 88% remains in the residue. Whereas 90% of the Mn is extracted in the first leach, 8% is extracted in the second leach and 2% remains in the residue. Leach 1 is generally more sensitive to MnO_2 than Leach 2.

Kyrc et al. (2003) also found less Fe in the natural leach samples but only 38% less Fe than Mn. There are two potential explanations for the lack of congruence between Fe and Mn during the first leach step. One is that Fe oxides are not as readily reducible as Mn oxides, and our leaching procedure is not dissolving them. The second is that is that the concentration of Fe in the oxyhydroxides may be low relative to that of in the aluminosilicates. Below we examine each potential explanation.

One way to evaluate the contributions of Fe and Mn is to view them within the context of other elements by normalizing them to Al. The concentration of Al is high in continental materials and very low in seawater, especially where there is little to no dust input (Bruland and Lohan, 2003). Therefore, Al should represent contributions from the lithogenic fraction. As detailed above Al is below detection limit in both the first and second leach, so we examine the Fe/Al and Mn/Al ratios of the bulk and residue (Figure 3.2).

The Fe/Al ratios of the bulk sediment and residue at Site 1149 co-vary and their concentration falls between Chinese Loess and basalt likely sourced from the Izu-Bonin Arc (Scudder et al., 2014; Figure 3.2A). This indicates that the bulk sediment is not enriched in Fe oxides adsorbed onto the particulates and that Fe is not extracted into leach, as the Fe/Al of the residue is not altered after the leaching procedure. This pattern is also evident in the analyses

from Site U1370. In spite of the increased authigenic content and slow accumulation at Site U1370 the Fe/Al ratio of the bulk sediment and residue correlate with a ratio that is the same as PAAS (Fe/Al =0.50) to a depth of 18.65 mbsf (Figure 3.2A). Before that the residue and bulk ratios increase below this depth (Fe/Al ~0.58), but stay the same in the bulk and residue

In contrast at Site 1149 the Mn/Al ratio of the residue is lower than the bulk throughout and does not follow the increase in ratio at the bottom of the core. In general, the Mn/Al ratio of the residue at Site 1149 is lower than the bulk (figure 3.2B). This suggests that the Mn in the bulk was extracted by the leaches. The difference between the ratio in the bulk and the residue increases with depth.

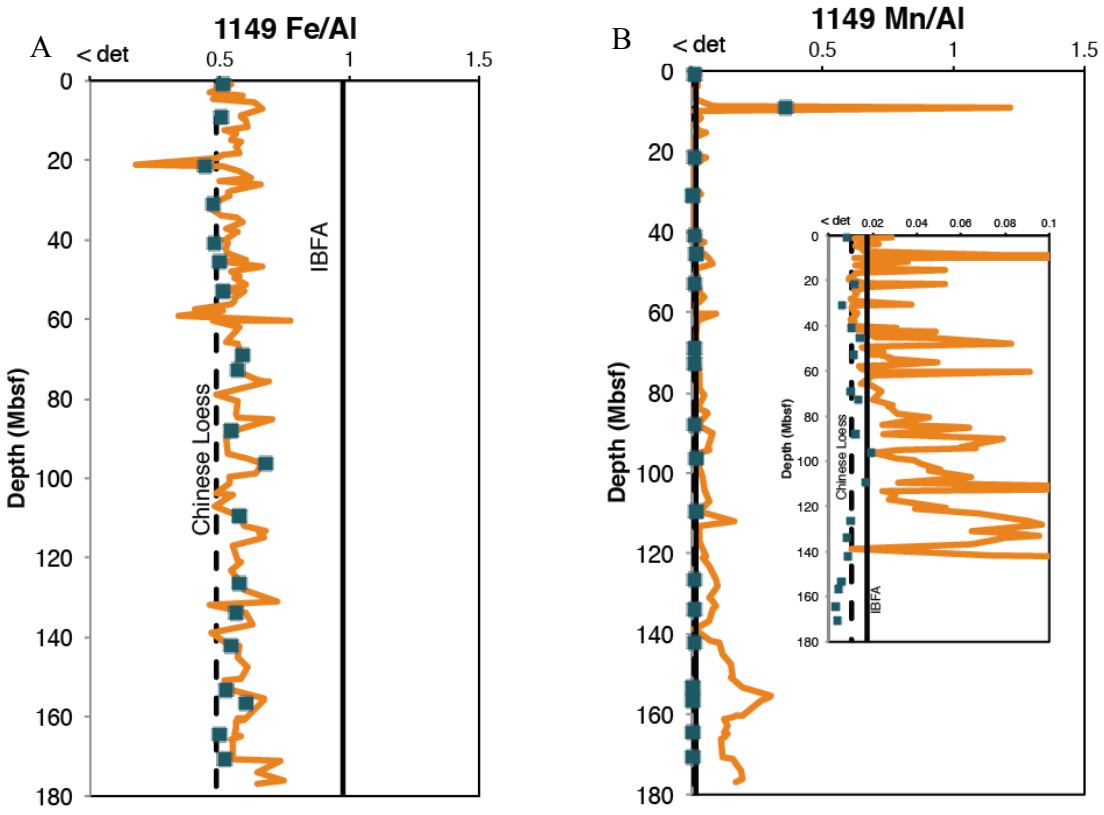

Figure 3.2 The Fe/Al (A) and Fe/Mn (B) ratios of the bulk (orange line) and residue (blue squares) at Site 1149, with representative Fe/Mn compositions for context. Note that samples plotting as zero on the x-axis reflect measurements that are below detection limit.

We have determined above that the Fe and Mn are not extracted in the same proportions as each other with respect to the total Fe and Mn. Examining how the leaching procedure extracts Fe will enable us to better evaluate the procedure. There is little to no Mn in the expected sources of aluminosilicates and in the residue, whereas the largest portion of the Fe in most samples remains in the residue. The range of Fe within the aluminosilicate fraction makes it difficult to determine if we are accessing the targeted proportion of Fe in our leach, or if we did extract FeOOH or an aluminosilicate phase. Because Si and Al are below detection limit we can rule out having outright extracted an aluminosilicate phase like ash as Wilson et al., (2013) and Molina-Kescher et al., (2014) observed with their leaching. Instead, we test the possibility that the procedure we have developed does not effectively extract FeOOH.

There are several methods that approach leaching Fe oxides with a different tactic. Koschinsky and Hein (2000) use two separate leachates to extract Mn oxides, which they term "easily reducible", and Fe oxyhydroxides that are "moderately reducible" from Fe-Mn nodules and crusts. They use oxalic acid/ammonia oxalate buffer to extract FeOOH phases after a HH leach targeted at Mn oxides. Revels et al., (2015) heat their Oxalate-EDTA leach solution to a temperature of 90°C in order to access the labile Fe from particles suspended in seawater, and it is possible that the increased temperature facilitates the extraction on Fe.

Leach phases 1 and 2 at Site 1149 both contain a portion of the trace and REE. Leach phases 1 and 2 at Site 1149 both contain a portion of the trace and REE, leading to the fundamental question "what is being leached at Site 1149 if not Fe oxyhydroxides?" Wilson et al., (2013) report that two thirds of the Nd they leach is extracted in association with Ca or Mn rich phases, and that all of the extractable Mn is removed from the sediment within a half hour of the start of the leach, whereas it takes 8 more hours to completely extract the Fe. They argue that

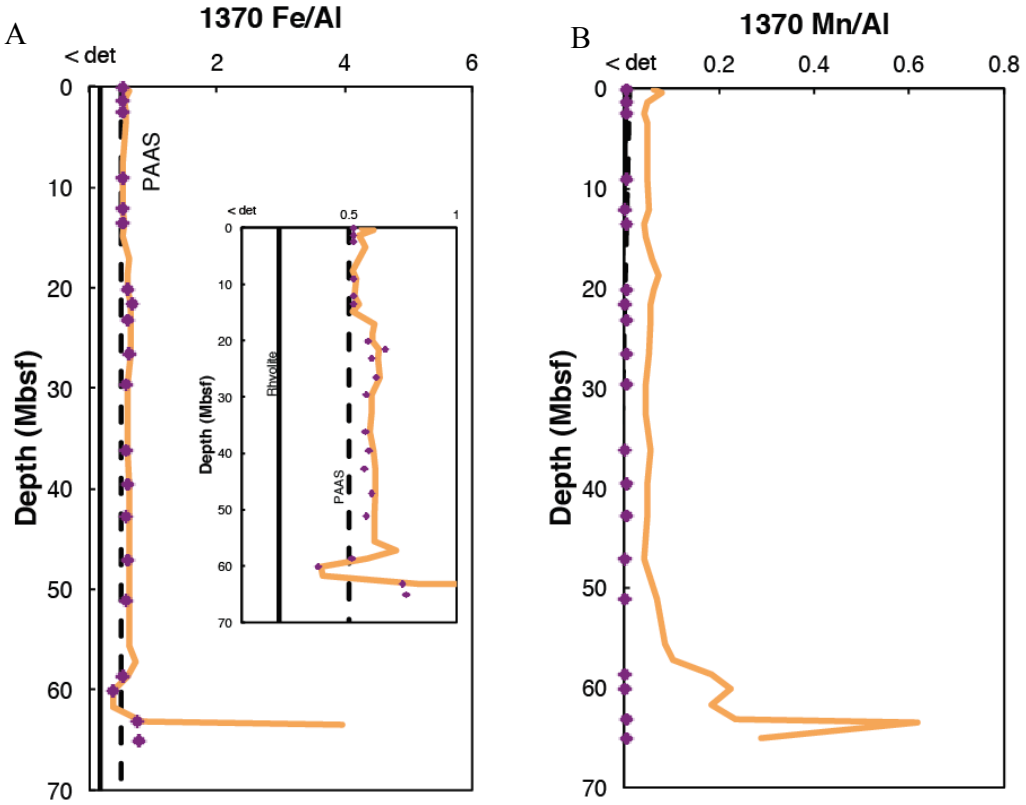

Figure 3.3 The Fe/Al (A) and Fe/Mn (B) ratios of the bulk (orange line) and residue (purple diamonds) at Site U1370, with representative Fe/Mn compositions for context. Note that samples plotting as zero on the x-axis reflect measurements that are below detection limit.

the two phases are extracted at different rates because of their different redox labilities. If the trace metals and REEs we seek to analyze are sorbed onto the Fe oxyhydroxide coatings and not incorporated into the mineral lattice it may be possible to extract one and not the other.

To look at the presence of Fe and Mn (oxyhydr)oxides on the sediment more quantitatively we use the ratio of Fe/Al and Mn/Al to calculate the range of excess Fe (Fe_{Ex}) and Mn (Mn_{Ex}) in the sediment. Lam et al., (2017) use the ratios upper continental crust of Fe/Al=0.39 and Mn/Al=0.0077 (CITE) to calculate excess Fe and Mn in particles in seawater (Figure 3.4). This allows for the identification of Fe & Mn (oxyhydr)oxides.

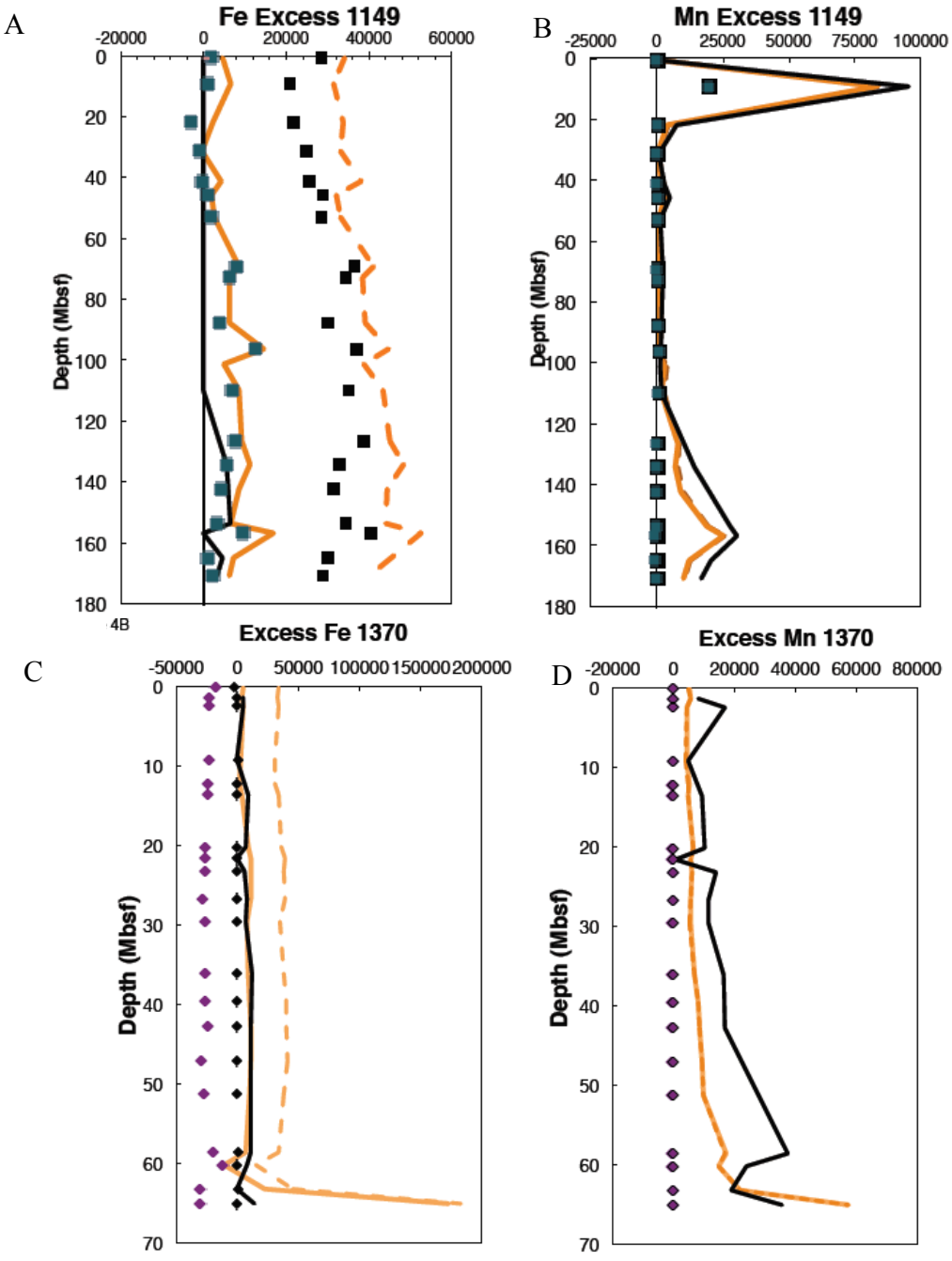

Figure 3.4 The excess Fe and Mn calculated with the Fe/Al and Mn/Al ratios of the known aluminosilicate portions of the sediment with Fe_{Ex}= [Fe]-([Al] x Fe/Al_{UCC}) Mn_{Ex}= [Mn]-([Al] x Mn/Al_{UCC}). The Site 1149 (4A) excess Fe and Mn in the bulk sediment and leached residue are calculated with the Fe/Al and Mn/Al ratios of Chinese Loess (Bulk: Solid orange line, Residue: closed blue squares) and Honshu Rhyolite (Bulk: dash orange line, Residue: open squares). The Site U1370 (4B) excess Fe and Mn in the bulk sediment and leached residue are calculated with the Fe/Al and Mn/Al ratios of PAAS (Bulk: Solid orange line, Residue: closed purple diamonds) and a Rhyolite average (Bulk: dash orange line, Residue: open diamonds). The black solid line on each plot is the sum of the Fe or Mn leached from Leach 1 and Leach 2.

The equation modified from Lam et al., (2017) is:

$$Fe_{Ex} = [Fe] - ([Al] \times Fe/Al_{UCC}) \quad Mn_{Ex} = [Mn] - ([Al] \times Mn/Al_{UCC})$$

The assumption that the lithogenic component of falling particles is Upper Continental Crust (UCC) may be a reasonable one; however, we know there are a large range of aluminosilicate sources to the sediment at both sites. The aluminosilicate portion of Site 1149 is dominated by Chinese Loess (Fe/Al=0.48, Mn/Al=0.01) and Honshu Rhyolite (Fe/Al=0.13, Mn/Al= 0.0023), in addition to small amounts of other geochemically distinguishable dust and ash sources (Scudder et al., 2014). The aluminosilicate portion of Site U1370 is dominated by a dust component with a composition similar to Post-Archean Australian Shale (PAAS, Fe/Al=0.50 , Mn/Al=0.0085) and the Average Rhyolite end member. Dunlea et al., (2015) used in their models of Site U1370, (average of n=1700, Fe/Al=0.17, Mn/Al=0.006). Therefore, we calculated the Fe and Mn excess with the ratios of each dominant component including an average of PAAS and Average Rhyolite (Fe/Al=0.34, Mn/Al= 0.0075), for Site U1370 (figure 3.4C&D) and an average of Chinese Loess and Honshu Rhyolite (Fe/Al=0.31, Mn/Al= 0.0063), for Site 1149 (figure 3.4A&B). While the range of ratios are relatively limited using different compositions to determine the aluminosilicate portion does change how the results of the calculation and potential interpretations.

At Site 1149 the differences between excess Fe calculated using the ratios of Chinese Loess (average excess Fe=6831 ppm) and Honshu Rhyolite (average excess Fe=-40068 ppm) are much larger. The differences in the Fe/Al ratios of Honshu Rhyolite and Chinese Loess span a range that results in the difference between the presence of little to no excess Fe (if we use the Chinese Loess ratio for the calculation), and significant excess Fe (if we use the Honshu Rhyolite ratio for the calculation). The sum of the total Fe leached is below detection limit above 109

mbsf, and then increases to 2362 ppm at 126.36 mbsf and stays around an average of 3570 ppm to the bottom of the core. It is important to note that the detection limit of FeO_3 on the ICP-ES is 0.3wt%, which converts to 2100ppm of Fe. So, it is possible that some quantity of Fe is extracted in the upper portion of the core, but it is still below detection limit.

At Site 1149 the excess Mn calculated with the Chinese Loess Mn/Al ratio (average excess Mn=9717 ppm) matches relatively well with the sum of the total Mn removed from the sediment via leaching, 6188ppm. Whereas, the calculation with the IBFA ratio suggests we extracted more Fe and Mn than there was excess to extract. Given the Fe/Al ratio of the residue is so similar to the ratio of Chinese Loess, and data with the Chinese Loess ratios best fit the Mn leach it seems reasonable to use the Chinese Loess value to calculate excess Fe. If we follow this logic further and use that ratio to calculate excess Fe and Mn the result of the calculation is that there is a small excess of both Mn (average, 9717ppm) and Fe (average 6811ppm). The excess increases with depth but still calculates an excess of Fe above 109mbsf that is on average greater than the detection limit of Fe (5175ppm). This indicates that our excess Fe calculation may not be not conservative enough and overestimates excess Fe, or that a small portion of the excess Fe is not extracted. We have established that there are only very small amounts of excess Fe to leach at Site 1149 and so while we may still be "under leaching" the Fe this result is favorable to "over leaching" and extracting contaminated phases.

At Site U1370 there is a large difference in the calculated excess Fe for the bulk sediment at Site U1370 depending on if we use PAAS (average excess Fe=42702 ppm) or Average Rhyolite (average excess Fe=15577 ppm) in the equation. However, both calculations yield an indication of excess Fe in the bulk. The corresponding calculations of the residue also indicate the removal of excess Fe by the extraction. When compared with the sum of the total Fe leached

from the sediment (sum of Leach 1 and Leach 2) of Site U1370 the excess Fe concentration calculated with the Fe/Al ratio of PAAS compares most closely. The results of the calculated excess Mn for the bulk sediment at Site U1370 using PAAS (average Mn excess=10617ppm) and average hyolite (average excess Mn=10585 ppm) are very similar. The difference between the excess Fe and Mn at Site U1370 is consistent with our understanding of the relative amounts of Mn oxides and Fe oxyhydroxides we would expect given the different labilities to oxygenentation of MnO and FeOOH.

3.5.3 Results from REE patterns

The evaluation of the leaching with the main elements targeted by each extraction is limited and so we next examine the REE patterns in order to look more closely at the results of each leach and the fidelity of the process. The REE concentrations normalized to PAAS have distinct patterns based on the reactivity and mass of each element (i.e., what becomes sorbed or enriched). The residue should have a similar REE composition as PAAS (which is a representation of all other lithogenic components) and be near to or less than one. Seawater has a negative, depleted, Ce anomaly, because once Ce^{3+} is oxidized to Ce^{4+} it becomes insoluble and becomes concentrated in precipitates, especially Mn nodules and Mn-oxide coatings on the seafloor. The concentrations of the REE elements in Seawater also increase from light to heavy, because they light elements are preferentially scavenged (Elderfiled, 1988). Another potential feature of sediment is a MREE bulge, which is typical of samples identified as hydrogenous Fe-Mn (oxyhydr)oxides (Hayes et al., 2004).

The REE patterns of the Site U1370 leached phases are distinct from those of the residues (Figure 3.5A). The majority of the samples in Leach 1 (N=11; Figure 3.5B) have a negative Ce anomaly and a MREE bulge, as would be expected for a phase sorbed from seawater

composition. One sample at 47.09mbsf is depleted with respect to PAAS and has a positive Ce anomaly, and the top three samples (from 0.1 to 1.45 mbsf) have positive Ce anomalies.

The REE patterns of Leach 2 of Site U1370 display the same two patterns. Four samples from the bottom of the core between 51.80 to 63.15mbsf have MREE bulges and negative Ce anomalies. All of the other samples (N=15) are depleted with respect to PASS and have positive Ce anomalies. We interpret the divergence of the behavior of the four bottom samples to the greater presence of hydrothermal contributions in the bottom of the core.

Unlike the leach phases every sample in the residue displays the same pattern: flat except for a positive Eu anomaly. Only one sample, from the very top of the core, 0.05mbsf, is enriched with respect to PAAS. Overall the REE patterns at Site U1370 confirm that the first leach effectively extracts the adsorbed target phase for paleoceanographic reconstructions and the second leach effectively removes the majority of the Fe-Mn (oxyhydr)oxides from the residue, leaving aluminosilicates behind.

The REE pattern differences between the three leach phases at Site 1149 are similar to those at Site U1370. However, there are differences in the distribution of the samples that increase our understanding of what components are being extracted in Site 1149. The Leach 1 pattern at Site 1149 is dominated by two distinct trends. Six samples at the bottom of the core (every sample, under 101.14 mbsf except 109.64 mbsf) are enriched with respect to PAAS, have the MREE bulge and a negative Ce anomaly, as would be expected from a phase sorbed from seawater composition. The rest of the samples (N=12) are depleted with respect to PAAS, and have a slightly positive Ce anomaly, if any. All of the Leach 1 samples have a MREE bulge (Figure 3.5A). Perhaps each sample has a component of hydrogenous sediment in it, even though it is depleted with respect to PAAS. Two Leach 1 samples from the bottom of the core (156.56

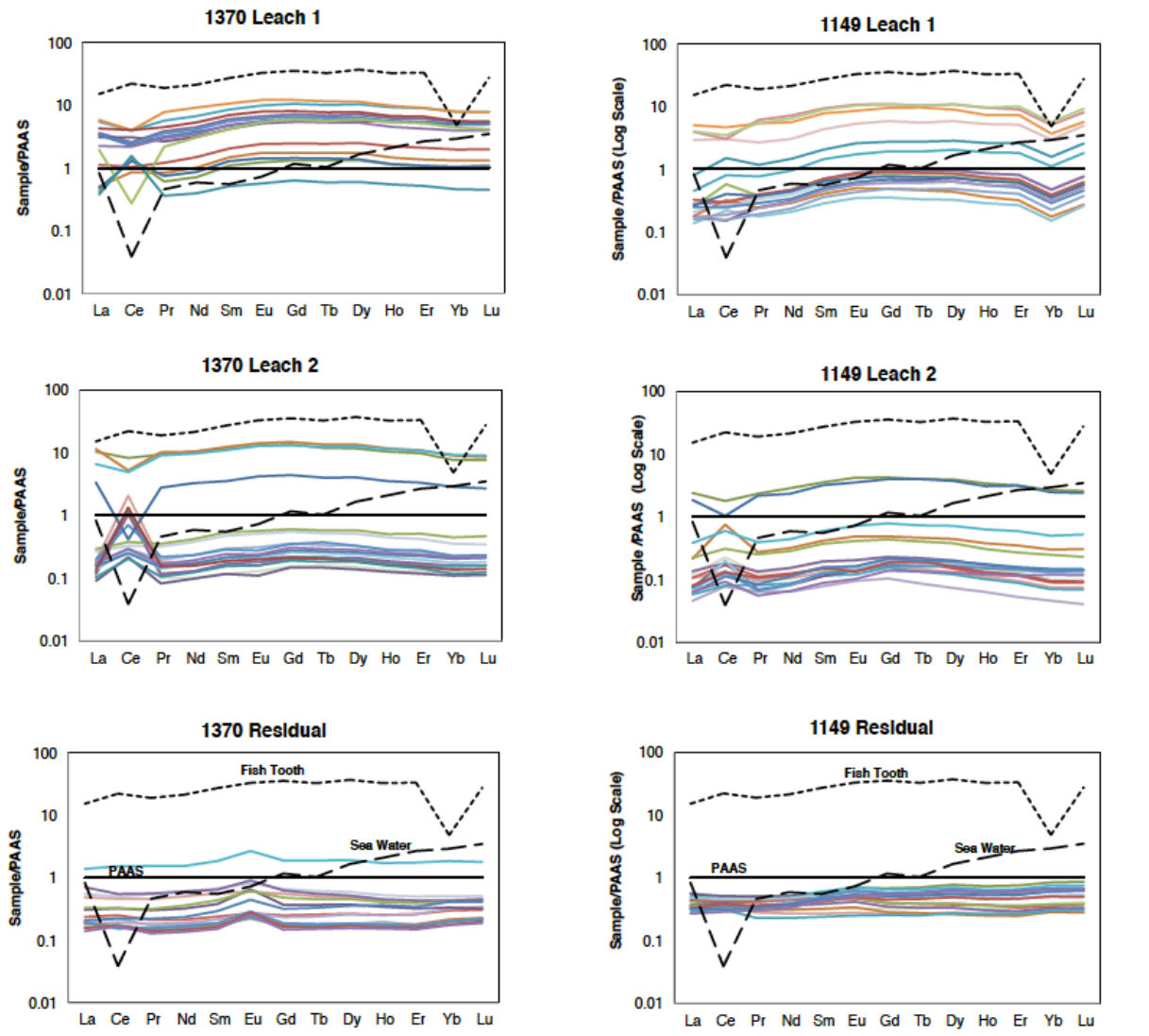

.

Figure 3.5 Post-Archean Average Australian shale (Taylor & McLennan, 1985) normalized Rare Earth Element plots for each the two phases and its respective detrital fraction (Sites U1370, A and 1149, B).

and 170.73mbsf) also have MREE bulges, negative Ce anomalies and are enriched with respect to PAAS. The remainder of the Leach 2 samples are depleted with respect to PAAS and have positive Ce anomalies. The residues from Site 1149 are also depleted with respect to PAAS and have positive Ce anomalies (Figure 3.5A). The REE element patterns at Site 1149 indicate that

above 101.14mbsf the leach is not selectively extracting elements with a "seawater pattern". This trend in the top and bottom of the core agrees well with the calculations that there is little to no excess Fe or Mn above 109.64 mbsf at Site 1149. In the top section of Site 1149 composition of the material leached is not controlled by an exclusively seawater-derived signal.

The sample at 9.03 mbsf at Site 1149 recorded unique values. We examine its bulk composition here in more detail because it is possible that this sample is an extreme example of the controls on elements extracted from the top portion of Site 1149. The bulk Mn concentration of the sample and the one below it at 10.10mbsf (measured by Scudder et al., 2014, but not leached) are an order of magnitude greater than the surrounding samples. The excess Mn calculated with the Mn/Al ratio of Chinese Loess for the sample is 83468ppm, and the total Mn leached from the same sample is 95565ppm. In addition to striking Mn concentrations, the first leach of the sample at 9.03mbsf has a distinct REE composition from the surrounding samples. It is the most depleted with respect to PAAS of all of the Leach 1 samples from Site 1149. We compared the Mn concentration of the sample to the concentration of Mn in the ash layer components analyzed from the Site 1149 and the Mn in the 9.03mbsf sample is greater than all but one measured ash layer (Average Mn concentration of ashes= 0.07ppm, max=3.73ppm at 64.85mbsf min=0.02 at 141.36mbsf). The interval between 4.73 -18.75mbsf contains the ash layers that make up the felsic end member Scudder et al., (2014) use in their geochemical models. Scudder et al., (2014) also report ~30 discrete ash layers in the region of 9.03mbsf, and the accumulation rate of dispersed ash in the interval is ~0.8 g/cm/ky (Scudder et al., 2014). There is every indication that this sample is in an area that has been influenced by an aluminosilicate component, likely volcanic ash. However, Al, Si and Ti are all below detection limits in this sample in both the first and second leach.

3.5.4 Relative Merits of the Leaching Procedure

We have established here that our leaching procedure does not extract the elements that make up the majority of aluminosilicates. This is true across sites, standards and Leach 1 & Leach 2. Therefore, for our purposes the procedure targets the appropriate phase. Depending on the composition of the residues (and the amount of Fe expected in the lithogenic portion of the sediment) our result may point towards the possibility that in some cases there are Fe oxyhydroxides left in the residual which would need to be addressed to enable the successful use of the residue as a proxy for dust (e.g. Reimi and Marcantonio (2016). We also have identified that while there is Fe present in the bulk material the majority of it is associated with the residue, and there is a larger portion of MnO extracted into the leach than FeOOH. This finding highlights a divergence from the common conceptual blueprint of how sorption and subsequent extraction via leaching occurs.

3.6 Conclusions

Our evaluation provides context for the range and reproducibility of element concentrations extracted by our acid reductive leaching procedure. The reproducibility of the major elements in the residue phases is improved from the evaluations done by Kyrc et al., (2003). There is better reproducibility of ε_{Nd} in samples with highest concentrations, however there is not a clear relationship between the concentration of the Pb or the reproducibility of the Pb and Nd concentration extracted and the reproducibility of the isotopic ratios. Overall, the ε_{Nd} values of Leach 1 are reproducible within 10% our in-house standard and 2% for MAG-1, the standard reference material. The Pb ratios are reproducible within an average of 0.13% our in-house standard and 0.29% for MAG-1.

The evaluation of major element portioning and REE patterns indicates that each leach targets and extracts the target phase of the sediments in Site U1370. There is less consistent portioning, especially of the REE patterns at Site 1149.

There is no evidence from the major elements that the aluminosilicate portion of the sediment is leached into Leach 1 or 2. However, a relatively low amount of Fe is extracted from the sediment into the leach at both sites. We determined that while it is possible that the procedure is slightly under leaching Fe oxyhydroxides, the low Fe in Leach 1 and Leach 2 are controlled by the low amounts of excess Fe available for extraction, compared to the amount of Fe in the lithogenic portion of the sediment at both sites. Specifically, there is very low excess Fe where the Fe in the extractions is below detection limit in the top 100 meters of Site 1149. What is encouraging here is that excess Fe could be a good indicator of where extractable Fe-Mn (oxyhyd)roxides record seawater derived signatures. The REE patterns of the samples that correspond to low Fe also indicate a PAAS-like composition of the REE in the leaches. Overall, we have proven that this leaching procedure can be selective and reproducible enough to allow for paleoceanographic studies, especially for Nd and Pb isotopes. Most importantly the leach does not appear to be accessing elements associated with the aluminosilicate portion of the sediment. However, we have also highlighted where the REE patterns of the first leach that indicate a lithogenic source has been extracted from the sediments at Site 1149. The pattern in the top 100 meters of Site 1149 confirms concerns about leaching in the Northwestern Pacific where there are high volcanic inputs. This discord between the major element and the REE pattern reaffirms the questions permeating the community about the sources of trace metals to the sediment water interface.

3.7 References

Abbott, April N, Brian A Haley, and James McManus. 2016. "The impact of sedimentary coatings on the diagenetic Nd flux." *Earth and Planetary Science Letters* 449:217-227.

Blaser, Patrick, Jörg Lippold, Marcus Gutjahr, Norbert Frank, Jasmin M. Link, and Martin Frank. 2016. "Extracting foraminiferal seawater Nd isotope signatures from bulk deep sea sediment by chemical leaching." *Chemical Geology* 439:189-204. doi: https://doi.org/10.1016/j.chemgeo.2016.06.024.

Bruland, K. W., R. Middag, and M. C. Lohan. 2014. "8.2 - Controls of Trace Metals in Seawater A2 - Holland, Heinrich D." In *Treatise on Geochemistry (Second Edition)*, edited by Karl K. Turekian, 19-51. Oxford: Elsevier.

Du, Jianghui, Brian A Haley, and Alan C Mix. 2016. "Neodymium isotopes in authigenic phases, bottom waters and detrital sediments in the Gulf of Alaska and their implications for paleo-circulation reconstruction." *Geochimica et Cosmochimica Acta* 193:14-35.

Dunlea, Ann G, Richard W Murray, Justine Sauvage, Arthur J Spivack, Robert N Harris, and Steven D'Hondt. 2015. "Dust, volcanic ash, and the evolution of the South Pacific Gyre through the Cenozoic." *Paleoceanography* 30 (8):1078-1099.

Gutjahr, Marcus, Martin Frank, Claudine H. Stirling, Veronika Klemm, Tina van de Flierdt, and Alex N. Halliday. 2007. "Reliable extraction of a deepwater trace metal isotope signal from Fe–Mn oxyhydroxide coatings of marine sediments." *Chemical Geology* 242 (3):351-370. doi: https://doi.org/10.1016/j.chemgeo.2007.03.021.

Haley, Brian A., Jianghui Du, April N. Abbott, and James McManus. 2017. "The Impact of Benthic Processes on Rare Earth Element and Neodymium Isotope Distributions in the Oceans." *Frontiers in Marine Science* 4 (426). doi: 10.3389/fmars.2017.00426.

Haley, Brian A., Gary P. Klinkhammer, and James McManus. 2004. "Rare earth elements in pore waters of marine sediments." *Geochimica et Cosmochimica Acta* 68 (6):1265-1279. doi: https://doi.org/10.1016/j.gca.2003.09.012.

Huck, Claire E, Tina van de Flierdt, Francisco J Jiménez-Espejo, Steven M Bohaty, Ursula Röhl, and Samantha J Hammond. 2016. "Robustness of fossil fish teeth for seawater neodymium isotope reconstructions under variable redox conditions in an ancient shallow marine setting." *Geochemistry, Geophysics, Geosystems*.

Jeandel, Catherine. 2016. "Overview of the mechanisms that could explain the 'Boundary Exchange' at the land–ocean contact." *Philosophical Transactions of the Royal Society A: Mathematical, Physical and Engineering Sciences* 374 (2081). doi: 10.1098/rsta.2015.0287.

Jeandel, C., H. Delattre, M. Grenier, C. Pradoux, and F. Lacan. 2013. "Rare earth element concentrations and Nd isotopes in the Southeast Pacific Ocean." *Geochemistry, Geophysics,*

Geosystems 14 (2):328-341. doi: 10.1029/2012GC004309.

Koschinsky, Andrea, and James Hein. 2003. *Uptake of elements from seawater by ferromanganese crusts: Solid-phase associations and seawater speciation*. Vol. 198.

Kryc, KA, RW Murray, and DW Murray. 2003. "Elemental fractionation of Si, Al, Ti, Fe, Ca, Mn, P, and Ba in five marine sedimentary reference materials: results from sequential extractions." *Analytica Chimica Acta* 487 (1):117-128.

Lam, Phoebe J., Jong-Mi Lee, Maija I. Heller, Sanjin Mehic, Yang Xiang, and Nicholas R. Bates. 2017. "Size-fractionated distributions of suspended particle concentration and major phase composition from the U.S. GEOTRACES Eastern Pacific Zonal Transect (GP16)." *Marine Chemistry*. doi: https://doi.org/10.1016/j.marchem.2017.08.013.

Lugmair, GW, and SJG Galer. 1992. "Age and isotopic relationships among the angrites Lewis Cliff 86010 and Angra dos Reis." *Geochimica et Cosmochimica Acta* 56 (4):1673-1694.

Marsay, Chris M., Phoebe J. Lam, Maija I. Heller, Jong-Mi Lee, and Seth G. John. 2017. "Distribution and isotopic signature of ligand-leachable particulate iron along the GEOTRACES GP16 East Pacific Zonal Transect." *Marine Chemistry*. doi: https://doi.org/10.1016/j.marchem.2017.07.003.

Martin, EE, and HD Scher. 2004. "Preservation of seawater Sr and Nd isotopes in fossil fish teeth: bad news and good news." *Earth and Planetary Science Letters* 220 (1):25-39.

Molina-Kescher, Mario, Martin Frank, and Ed C. Hathorne. 2014. "Nd and Sr isotope compositions of different phases of surface sediments in the South Pacific: Extraction of seawater signatures, boundary exchange, and detrital/dust provenance." *Geochemistry, Geophysics, Geosystems* 15 (9):3502-3520. doi: 10.1002/2014GC005443.

Murray, Natalie A., James McManus, Martin R. Palmer, Brian Haley, and Hayley Manners. "Diagenesis in tephra-rich sediments from the Lesser Antilles Volcanic Arc: Pore fluid constraints." *Geochimica et Cosmochimica Acta*. doi: https://doi.org/10.1016/j.gca.2018.02.039.

Reimi, Maria A, and Franco Marcantonio. 2016. "Constraints on the magnitude of the deglacial migration of the ITCZ in the Central Equatorial Pacific Ocean." *Earth and Planetary Science Letters* 453:1-8.

Scudder, Rachel P., Richard W. Murray, Julie C. Schindlbeck, Steffen Kutterolf, Folkmar Hauff, and Claire C. McKinley. 2014. "Regional-scale input of dispersed and discrete volcanic ash to the Izu-Bonin and Mariana subduction zones." *Geochemistry, Geophysics, Geosystems* 15 (11):4369-4379. doi: 10.1002/2014GC005561.

Tachikawa, Kazuyo, Thomas Arsouze, Germain Bayon, Aloys Bory, Christophe Colin, Jean-Claude Dutay, Norbert Frank, Xavier Giraud, Alexandra T. Gourlan, Catherine Jeandel, François Lacan, Laure Meynadier, Paolo Montagna, Alexander M. Piotrowski, Yves Plancherel, Emmanuelle Pucéat, Matthieu Roy-Barman, and Claire Waelbroeck. 2017. "The large-scale evolution of

neodymium isotopic composition in the global modern and Holocene ocean revealed from seawater and archive data." *Chemical Geology* 457:131-148. doi: http://dx.doi.org/10.1016/j.chemgeo.2017.03.018.

Tessier, Andre, Pg GC Campbell, and M Bisson. 1979. "Sequential extraction procedure for the speciation of particulate trace metals." *Analytical chemistry* 51 (7):844-851.

Wilson, David J, Alexander M Piotrowski, Albert Galy, and Josephine A Clegg. 2013. "Reactivity of neodymium carriers in deep sea sediments: Implications for boundary exchange and paleoceanography." *Geochimica et Cosmochimica Acta* 109:197-221.

Yuan-Hui, Li. 1982. "Interelement relationship in abyssal Pacific ferromanganese nodules and associated pelagic sediments." *Geochimica et Cosmochimica Acta* 46 (6):1053-1060. doi: https://doi.org/10.1016/0016-7037(82)90058-8.

4. MAJOR, TRACE AND RARE EARTH ELEMENTS IN THREE PHASES OF LEACHED SEDIMENTS, EXAMINING THE SOURCES AND SINKS OF NEODYMIUM AND LEAD CONCENTRATIONS AND ISOTOPIC COMPOSITIONS

4.1 Introduction

The distribution of Rare Earth Elements (REE) and their relationships to major and trace elements have been used as tracers of chemical properties in order to examine pore water chemistry (Haley et al., 2004), redox conditions (Huck et al., 2016), and deep ocean mineral deposits (Hein et al., 2013). Nd specifically is of interest because the isotopic composition of Nd, incorporated into fish debris, is an established tracer of paleo-circulation (Huck et al., 2017; Scher and Martin, 2006; Thomas et al., 2014). Additionally, Nd and Pb associated with and Fe-Mn (oxyhydr)oxide coatings on sediment have been applied in similar systems for paleo-circulation reconstructions (Nd) and/or as a tracer of weathering inputs (Pb, Basak & Martin, 2011; Wilson et al., 2017;). In order to isolate a specific phase of the sediment, in this case the Fe-Mn (oxyhydr)oxide coatings and the REE plus the trace metals that are sorbed onto them, they must be chemically separated from the sediment. The material that is extracted by the leaching procedure is the operationally defined Fe-Mn (oxyhydr)oxide coatings on the sediment. The interpretation of these data as a paleoproxy requires that the leaching procedure successfully separates the Fe-Mn (oxyhydr)oxides from the other phases of the sediment and that the REE and trace metals incorporated or sorbed reflect the composition of seawater.

In Chapter II we addressed the paleoceanographic history of the Pacific Basin from 40 to 15Ma and found the indication of a radiogenic overprinting of the Nd isotopic composition

between 35 and 25Ma, while there was little change in the isotopic composition in the South Pacific. Following with Chapter III, we focused on the subsequent question of "what are the reproducibility and fidelity of the leaching method?" We evaluated the leaching procedure and determined that with some exceptions it targets the desired portion of the sediment.

A critical step in using acid-reductive leaching to extract Fe-Mn (oxyhydr)oxides and answer paleoceanographic questions is to gain an understanding of the sources of trace metals and REE to the Fe-Mn (oxyhydr)oxides. As our understanding of what controls the REE distribution and Nd isotopic composition of the ocean, (especially bottom water) evolves, our use of Nd and Pb in reconstructions of past-ocean circulation has become more complex (Haley et al., 2017). Many mechanisms for the source of Nd and REE have been suggested and evaluated. Most recently they have been summarized in Haley et al. (2017) as submarine groundwater discharge, a benthic flux, boundary exchange and/or reversible scavenging. However, the sorption of these elements also is controlled by physiochemical processes that depend on the characteristics of each element and the constituents in the water column (Hein et al., 2014). If speciation is the main control on the REE distribution of the leach, the sediment compositions we leach and analyze are the result of the complicated relationship between bottom water's composition, characteristics (pH, temperature) and authigenic phases.

The leaching procedure, which is a reasonable representation of the leaching procedures widely used within the community (Gutjahr et al., 2007; Wilson et al., 2013), broadly consists of a short one-hour HH leach modified from Gutjahr et al. (2007). We use a leaching solution with hydroxylamine hydrochloride in 15% acetic acid, chelated with Na- EDTA and buffered to a pH 4 with sodium acetate. The first leach is followed by a longer 24 hours HH leach (same recipe) to remove any remaining oxides from the residual component (Leach 2). We also rinsed and

analyzed the residual solids (residue) in order to constrain the lithogenic or terrigenious contribution to the sediment. In chapter III we set out to answer the questions: “how reproducible is the leaching procedure we use?” and “does it faithfully separate the portions of the sediment that we intended to target?”. In the process of evaluating the fidelity and reproducibility in the leach we identified that although the aluminosilicate elements (Ti, Si, Al) were below detection limit in the first and second leach, the REE patterns of select samples in the leaches appear to have lithogenic REE distributions or a pattern similar to that of Post-Archean Australian Average Shale. The goal of this work is to use the large data that set we have generated to focus on the controls of the major, rrace, and REE in the leached phases and identify their relationship with the Pb and Nd isotopic compositions in the disparate components of the sediment.

4.2 Rare Earth Element Terminology

We use REE concentrations normalized to PAAS to assess characteristics of each leach because the normalized REE patterns are distinct in seawater and porewater (Haley et al., 2004). Although they behave coherently there are subtle differences between the REEs that are controlled by the reactivity and mass of each element. The elements are divided into three groups: Light (LREE: La, Ce, Pr, and Nd), (note that Sm is a light REE, but it is not included in the calculations where LREE= La_N+Ce_N+Pr_N+Nd_N, and $Nd_N = Nd_{sample} / Nd_{PAAS.}$ Middle (MREE: Eu, Gd, Tb, and Dy), and Heavy (HREE: Er, Tm, Yb, and Lu). The properties of the REE help to inform their sources and reactivity (Elderfield, 1988). Murray et al., (1991) outlines three major controls on the REE abundances and characteristics such as Ce/Ce* and HREE/LREE 1) the amount of metalliferous material present in the phase, 2) the amount of direct terrigenous input and 3) the overall rate of burial of the sediment. This framework allows

us to examine the behavior of the REE elements in the context of two distinct locations with unique metalliferous inputs, accumulation rates and terrigenous inputs. We examine three specific characteristics here in order to identify if the distinct patterns both down core and between leached phases. The first is Ce/Ce* which is a measure of the Ce anomaly.

$Ce/Ce^* = 2 \times Ce_N / (La_N + Pr_N)$

Cerium (Ce) is unique in having a second oxidation state of Ce(IV) which is relatively insoluble in seawater. Seawater has a negative, depleted, Ce anomaly, because once Ce^{3+} is oxidized to Ce^{4+} it becomes insoluble and becomes concentrated in precipitates, especially Mn nodules and Mn-oxide coatings on the seafloor. Therefore, the Ce anomaly is used to evaluate the oxic state in the water or porewater. When Ce/Ce* = > 1 the Ce anomaly is positive, when Ce/Ce* = 1 there is no Ce anomaly and when Ce/Ce* = < 1 the Ce anomaly is negative. While there is a lot we do not understand about the controls of Ce in seawater and its incorporation into oxide coatings in sediment, crust or nodules, we use it here to evaluate changes or difference in redox or adsorption behavior. We are not attempting to ascribe one pattern to representing "true adsorption from seawater" or any other specific state.

The second characteristic is MREE/MREE* which is a measure of the MREE's deviation from a linear pattern (i.e. is there a MREE bulge in the sample?). The MREE bulge is associated with REE adsorption to Fe and indicates that Fe has influences the REE pattern (Haley et al., 2004).

$MREE/MREE^* = (Eu_N+Gd_N+Tb_N+Dy_N)/((HREE+LREE)/2))$, where $LREE= La_N+Ce_N+Pr_N+Nd_N$ and $HREE=Er_N+Tm_N+Yb_N+Lu_N$.

The HREE/LREE ratio is the third characteristic we will evaluate:

$HREE/LREE= (Er_N+Tm_N+Yb_N+Lu_N)/ (La_N+Ce_N+Pr_N+Nd_N)$,

HREE/LREE evaluates how enriched the heavy REE are in comparison to the light REE, where the larger the ratio the more enriched the HREE are. The concentration of REE increases from light to heavy (La to Lu) in seawater (Haley et al., 2004), seawater is enriched in progressively heavier REEs because the light elements are preferentially removed.

4.3 Speciation and Residence Times

Nd and Pb are both trace metals in the ocean (<10 μmol/kg). Nd and Pb are not necessarily thought to come from the same sources (Grousset and Biscaye, 2005; Jones et al., 1994, 2000), nor do they have the same speciation, so they are not adsorbed or incorporated at or by the same processes (Byrne, 2002). Therefore, with a better understanding of their sources and scavenging controls, we hope to leverage their differences and similarities for better paleo-interpretations in order to make more robust interpretations of past circulation patterns and the possible influences of changing input sources or pathways.

The charges of elemental species in seawater are dependent on speciation. We are concerned with the speciation of Nd and Pb because speciation controls chemical behavior in seawater specifically, solubility, ocean residence times, absorptive processes and oxidation/reduction behaviors (Hein, 2013). In seawater, speciation is dominantly controlled by pH; however, temperature and the presence of oxygen are also factors that can alter speciation (Bryne et al., 2002). The speciation of Pb and Nd influences their charge and whether they become adsorbed onto Fe oxyhydroxides or Mn oxides. Pb exists as Pb^{+2} in the ocean and should be complexed dominantly as $PbCO_3^0$ at a pH of 8.0 (Bryne et al., 2002). The species of Nd, like most lanthanides, besides Ce and Eu), is only trivalent in oxic conditions. At a pH of 8 $NdCO_3^{2+}$ should be slightly more abundant than $Nd(CO_2)^{2-}$ (Bryne et al., 2002). FeOOH adsorbs negatively charged and neutral species like: MoO_4^{2-}, $Th(OH)_4^0$ $PbCO_3^{2-}$, and $Nd(CO_3)_2^-$ (Hein,

2013). MnO_2 adsorbs positively charged trace metals like: Cu^{2+}, Zn^{2+}, and $NdCO_3^+$ (Hein, 2013). Therefore, Nd dominantly incorporated into both, and Pb is dominantly associated with Fe oxyhyrdoxides, which is a behavior unique to the REE/Lanthanide series.

The particle reactive nature of Pb, along with its dominant eolian source generates a scavenged type water column concentration profile for Pb (Bruland et al., 2014). Pb typically has higher concentrations in the surface waters, and they decrease with depth. This process is controlled by the particle flux to the sediment, where Pb is adsorbed or "scavenged" by particles. Therefore, the decrease of Pb in the water column is faster in regions where there is high productivity (Haley et al., 2017). Nd generally has a nutrient type profile with low concentrations from scavenging at the surface and increasing concentrations with depth from dissolving particulate matter. The concentration of Nd in deep-water increases with age along the path of thermohaline circulation; therefore, the Pacific has higher concentrations at depth than the Atlantic. The difference between the elements profiles is that either Nd is released near the bottom whereas Pb stays sorbed or similarly there is a source of Nd from the bottom.

Nd and Pb both have residence times that are shorter than the nominal ocean mixing time of 1500 years (Brocker and Peng, 1982). Thus, their isotopic compositions vary within basins as well as on a basin-wide scale. The residence time of Nd (~500-1000 years; e.g., Tachikawa et al., 1999; 2003) allows deep-water provenance information to be retained. Although it is important to note that the distribution of Nd isotopes indicates a shorter residence time (< 1000 years) than the Nd concentration distribution (>10000 years; Haley et al., 2017, Goldstein and Hemming, 2003) and this is not resolved to date. The residence time of Pb is short (~50-200 years; Henderson & Maier-Reimer, 2002) in comparison. Therefore, Pb is a more sensitive indicator of changes in weathering local input and water mass mixing. The shorter residence time of Pb also

means that the dominant source of dissolved Pb to the seafloor changes more than Nd with distance from the water mass formation region.

4.4 Neodymium and Lead Isotopic Systematics

We analyzed Pb and Nd isotopes in tandem with major, trace, and REE. Examining both the isotopic and elemental forms of Pb and Nd together is a useful exercise because they have similar and yet distinct characteristics. Pb is more particle-reactive and has a shorter residence time than Nd (Tachikawa et al., 2003, Henderson and Maier-Ramier, 2002). Additionally, there are several Pb isotopes and their different decay schemes provide unique insight in to the behavior and provonanceof different rock and particulate sources (Basak and Martin, 2011). Pb isotopes can be a tracer of dissolved inputs into the ocean and sediment provenance (Grousset and Biscaye, 2005). One challenge of using Pb isotopes is that the Pb adsorbed in fish debris and foraminifera cannot be distinguished from Pb that has decayed from the U that has a relatively high concentration in carbonate and apatite, leaving limited records with which to examine long term changes in the Pb isotopic history of seawater. Additionally, the modern ocean Pb cycling is completely dominated by anthropogenic processes; thus, our ability to reconstruct past Pb cycling relies on indirect assessments of Pb biogeochemical cycling, which complicates using Pb isotopes to make interpretations in the paleo record (Goldstein and Hemming, 2002; Wilson et al., 2017 and references therein). These challenges associated with leaching Pb and interpreting Pb isotopic data in leached phases make close examination of our methods and comparisons of Pb isotopic data with trace, major and Rare Earth Element data necessary. We seek to evaluate if the use of Pb isotopes are feasible, practical and worthwhile, and we seek to establish what information the Pb isotopes contribute to this data set.

Dissolved and particulate Nd has traditionally thought to be supplied to the oceans through continental weathering and riverine input (Frank, 2002), though this paradigm has been challenged by newly discovered non-conservative inputs (Haley et al., 2017). The distribution of Nd isotope values in seawater reflects the composition of rocks surrounding the ocean basin where the water mass originates (Frank, 2002). The isotope ^{147}Sm decays to ^{143}Nd. Because of differentiation in the mantle, young arc volcanic rocks are enriched in ^{147}Sm, and thus accumulate ^{143}Nd, and old continental crust rocks are depleted in parent ^{147}Sm, and thus accumulate less daughter ^{143}Nd overtime. This means that distinct rock types impart a distinct signature when they weather into the ocean. The isotopic ratio of Nd is represented as ε_{Nd} (Where $\varepsilon_{Nd} = [(^{143}Nd/^{144}Nd_{sample})/ ^{143}Nd/^{144}Nd_{CHUR})-1]x10^4$ CHUR=0.512638).

The source of natural dissolved Pb to the ocean is a combination of local riverine inputs and eolian inputs of dust and volcanic ash (Duce et al., 1991; Henderson & Maier-Reimer, 2002; Jones et al., 2000). Seawater Pb isotopes therefore have been used both to provide information about weathering and eolian inputs. ^{238}U, ^{235}U, and ^{232}Th decay to ^{206}Pb, ^{207}Pb, and ^{208}Pb, respectively. The Pb isotopic systematics are slightly more complicated. Although distinct rocks have distinct isotopic compositions, Pb is also more mobile than other trace elements because the radioactive decay loosens the Pb in the mineral lattice. This allows for isotopic fractionation when they weather, and so Pb isotopic inputs do not match those of their rock sources (Basak and Martin, 2011).

Here we address the remaining outstanding issues precluding the use Nd isotopes as a water mass tracer, and the inclusion of Pb isotopes into our interpretations. We need to establish two things: 1) what are the controls of Nd and Pb cycling in the ocean and how do they relate to the isotopic signatures of the elements, and 2) to what extent do the physicochemical controls

(those that determine how it is adsorbed, sorbed or incorporated) on each element regulate the results of the trace metal and the REE patterns, as well as the isotopic composition of the leaches.

4.3 Methods

4.3.1 Site Selection

We selected the two study sites, ODP Site 1149 and IODP Site U1370, because they are located in distinct oceanic environments with different sediment sources and lithology. They also span the range of environments that we have used for paleoceanographic reconstructions in the Pacific (e.g. Thomas et al., 2014). ODP Site 1149 is located in the Northwestern Pacific (Modern location: 31.33, 143.35, Paleo location at 50 Ma: 24.95, -178.07). It was drilled at a water depth of 5818m and is located on the Izu-Bonin-Arc. Site 1149 contains a well-established amount of volcanic ash. There are 100 discrete ash layers in the top unit, and the clay lithology is made up of 10-30% volcanic glass according to smear slides (Plank et al., 2000; Scudder et al., 2014. Additionally, Scudder et al., (2014) used multivariate statistics to model that up to 50% of the sediment is composed of ash or altered ash). These features within Site 1149 enable us to specifically examine the influence of readily reducible ash on sequential leaching (Wilson et al., 2013). We focus our leaching evaluation on the top two units of Site 1149, as Units III-V contain progressively more indurated siliceous lithologies like chert (Plank et al., 2002). Unit I spans 0-118.2mbsf and consists of diatom and radiolarian bearing clay that is free of carbonate. There are discrete ash layers that range in thickness from a few millimeters to 5cm, chunks of pumice and dispersed ash material. Unit II spans 118.2-179.1mbsf and consists of ash bearing dark brown pelagic clay. The division between the two units was determined by the disappearance of siliceous microfossils.

IODP Site U1370 is located in the northern portion of the South Pacific Gyre. It was drilled at a water depth of 5084m (Modern Location: -41.85,-153.105, Paleo-location at 50 Ma: -55.97,-122.38). Units I and II of Site U1370 are composed of zeolotic metalliferous clay and metalliferous clay. Unit I extends from 0 to 61.9mbsf. Unit II is a short 2.9m interval of nannofossil ooze at 62mbsf. Unit III (64.6-69.4mbsf) is a very dark bown clay. There is a very slow accumulation rate at Site U1370, which makes it unique because the dissolved oxygen is persistent in the pore water to the basement (D'Hondt et al., 2015). This is significant because the oxides and oxyhydroxides where Nd and Pb are adsorbed can be readily reduced in anoxic sediments and can thus lead to porewater-derived fluxes of REE into bottom waters that can bias paleoceanographic interpretations (Abbott et al., 2015; Haley et al., 2004). Additionally, the length of exposure time at the sediment water interface is a known control on the composition of REE (Murray et al., 1991). Therefore, this provides us with an opportunity to examine the results of leaching in an environment where porewater-derived fluxes are very unlikely to have altered or influenced the elemental or isotopic composition of the oxides.

Another advantage to focusing on these sites is that there is available bulk geochemical analysis and subsequent multivariate statistical analysis of a high-resolution set of major, trace and REE at Sites 1149 and U1370 that have aided us in identifying potential end members contributing to the sediment that could also potentially influence the water column or authigenic phases (Dunlea et al., 2014; Scudder et al., 2015). In order to examine the sources of the Nd and Pb to the authigenic phases that we access via leaching we performed major, trace, and REE analysis of each step of the leaching process in order to establish a detailed picture of how elements partition across phases. We also performed Nd and Pb isotope analysis of each leaching phase in order to establish which geochemical end-members contributed to the Nd and Pb

isotopic signal in the phases accessed by leaching and examine them in the context of the elemental data.

4.3.2 Sequential Leaching and Analysis

Each sediment sample was freeze dried, powdered by hand with an agate mortar and pestle and weighed (0.75+/- 0.03 g) prior to extraction. We use a two-step sequential leaching procedure: The first leach (Leach 1) consisted of a short one-hour HH leach modified from Gutjar et al. (2007) with hydroxylamine hydrochloride in 15% acetic acid, chelated with Na-EDTA and buffered to a pH 4 with sodium acetate. 14mL of the HH mixture was added to the sediment in an acid cleaned 50ml centrifuge tube. They were placed on the shaker table for one hour before being centrifuged and transferred to a new centrifuge tube. The second leach (Leach 2) is a 24-hour HH leach (same recipe) that is designed to remove any remaining oxides from the residual component. The residual component was subsequently rinsed, dried and homogenized by hand with an agate mortar and pestle before being weighed for subsequent dissolution and analysis. The full details of the leaching procedure are outlined in Chapter II.

The supernatant from Leach 1 and Leach 2 were converted to a nitric acid matrix and diluted with MQ for analysis. A split of the dilute solution was taken for ICP-MS analysis of the trace and rare earth elements and ICP-ES analysis of the major elements and select trace elements. The residues were dissolved via flux fusion for major element analysis via ICP-ES, and via acid digestion for the trace metals and REE analysis via the ICP-MS following the methods outlined in Dunlea et al., (2015). The residue digestions, ICP-MS and ICP-ES analyses were performed at the Analytical Geochemistry Laboratory at Boston University.

A subset of samples was split and reserved for Pb and Nd isotopic analysis. The splits of Leach 1 and Leach 2 were dried and dissolved in HBr of Pb column chemistry, while the

residues were weighed and digested via HCL-HNO_3-HF closed vessel acid digestion before being converted to a HBr matrix. Two passes of standard HBr column chemistry (Lugmair & Galer, 1992) was used to isolate and purify the Pb fraction. The same process was applied to Leach 1, Leach 2 and the residue. The 0.7 N HBr washes contained the REE split and were collected in clean Teflon beakers and evaporated in preparation for Nd column chemistry. This REE split was re-dissolved in ~2 mL of concentrated HNO_3 for Eichrom Tru Spec™ cation exchange chemistry. The Nd portion subsequently was separated from the bulk REE via volumetrically calibrated Eichrom LN Spec™ Column chemistry. The Pb and Nd isotope samples were analyzed on the Thermo Triton Thermal Ionization Mass Spectrometer (TIMS) in the R. Ken Williams '45 Radiogenic Isotope Geosciences Laboratory at Texas A&M University. Pb samples were loaded onto single rhenium (Re) filaments with silica gel. In order to minimize inter-sample fractionation variability, the samples were analyzed at a constant 1251± 4°C. Nd samples were loaded onto double Re filaments with 2N HCL and analyzed as Nd^+. $\varepsilon_{Nd(t)}$ was calculated using the age models detailed in the site descriptions.

4.3.3 Q-mode Factor Analysis

Q-mode factor analysis (QFA) was performed on each of the three leached sediment phases individually, as well as a combination of the three leach phases together. We employ the same methods as used for the previously completed bulk sediment analysis (Scudder et al., 2014; Dunlea et al., 2014) using the published MATLAB scripts from Pisias et al., (2013). As is outlined in that work, factor analysis and Principal Component Analysis (PCA) are both methods for identifying relationships between variables in large sets of data, which are used in the geosciences. However, there are important differences between the two methods. While PCA

accounts for the maximum variance of all the variables in a matrix, factor analysis is based on the correlation matrix of those variables. Thus, PCA will by definition force all variables into the result while factor analysis generates unique groups (or ‘‘factors’’), each of which behaves differently from the other factors (Pisias et al 2013). Given the geochemical nature of the work, we deemed QFA as the more suitable method for the leached data. As part of the QFA routine a VARIMAX rotation is applied in order to keep the factors orthogonal to one another. This helps to make the factors more easily interpreted. This allows for the identification of the number of potential end-members contributing to the sediment and helps us to examine how the elements are grouped and their relationships within each phase. (Pisias et al., 2013).

1) The VARIMAX factor scores, which are the weight each element contributes to the discrimination of a single factor. A high-absolute value of VARIMAX factor score indicates elements that covary strongly within the factor. 2) The compositional factor score, which is the elemental composition of an individual factor. This provides a very broad idea of the compositional nature of the potential end member. 3) The factor loading which is the contribution of each factor to a single sample. This provides a map of the evolution of the importance of each factor with depth or time. QFA is an objective exploratory statistical method, designed to help identify factors (in this case elements) that vary together but its scope is limited. The compositional factor scores should not be used to identify specific sources. We use the QFA to guide our evaluation of the data, because the scope of interpretations that can be drawn from the QFA is limited.

One specific limitation of QFA is that a sufficient number of samples is required to explain the number of potential variables (i.e. the number of samples limits the number of elements we can combine at one time to determine factors) (Reimann et al., 2002). In order for

stable results we cannot enter all of the elements into factor analysis at once (Reimann et al., 2002). Viewing the whole data set (residue, leach 1, leach 2, total samples N=53) together provides us with the most samples to work with, because with more samples we can increase the number of elements we can evaluate in a group, and therefore the number of factors, which is always going to be the number of elements -1 (Reimann et al., 2002). While this may obscure the relative importance of end members that are important to only one phase, we have tried to select elements that will represent each phase well in order to limit this problem. Therefore, our approach is to identify combinations of elements that represent the entire data set well and select groups informed by understanding of the geochemistry of the systems, and then identify the factors that are consistently present within different iterations of the QFA.

We selected elements for QFA based on several geochemical criteria including their specation in seawater, and their partitioning between the phases during leaching. We selected elements with dominant positive of negative charges because of their speciation in seawater (Th, Mo, Cu, Hf, Ce, Gd, and Er) overlapping with elements with distinct distributions in lithogenic sources (Th, Hf, Zr), and we paired these elements with Mn, Fe, Pb and Nd in order to examine the behavior of elements both in the detrital portion of the sediment and that could be associated with either FeOOH or Mn2O.

In order to identify how each component of the sediment partitions across the sequential extractions we first performed factor analysis on each phase separately with combinations of four elements, similar to the approach of Ziegler et al., (2007). For example, we performed factor analysis using Ce Gd, Er and Mn with each leach phase separately in order to examine how or if the factors controlling the REE element distribution change from leach to leach, and then re repeated that processes with Ce, Gd, Er, Fe, ete. We did this iteratively with many element

combinations and then combined all three phases, added a fifth element, (I.e. Ce, Gd, Er, Fe, Mn, and eventually) a sixth element like Th, Hf, Nd, or Pb. We did this with the goal of identifying elements that consistently yield robust factors. We narrowed our element combinations for QFA via this process and eventually evaluated three representative suites of element groupings.

The first core group of elements (Th, Mo, Pb, Nd) were selected because of their dominantly negative charge in seawater, which means they are likely to be associated with FeOOH. The second group of elements (Cu, Hf, Pb, Nd) was selected because of their dominantly positive charge in seawater, which means they are likely to be associated with MnO2. The third group of elements (Ce, Gd, Er, Mn) was selected to examine how the REE elements vary with Nd, Pb, Mn and Fe, in order to create context for the REE normalized interpretations. All three groups also contain elements that are important to lithogenic compositions.

We focus here on the results from expanded element groups 1) Th, Nd, Pb, Mo, Mn and Fe, 2) Cu, Fe, Mn, Hf, Zr, and Ce and 3) Ce, Gd, Er, X, Mn, Fe. We performed factor analysis on iterations of the third group replacing the fourth element represented by X with Th, Hf, Nd, Pb and Cu in order to facilitate comparisons between the factors in groups 1, 2 and 3 more readily.

4.4 Results

4.4.1 Concentration of Major, Trace, and Rare Earth Elements in Each Fraction: Site 1149

The [Nd] and [Pb] extracted in the leaches increase with depth, which is mirrored in many trace and REE elements including P, Th, and all of the REE (refer to chapter 3 plots). From 0-109.64mbsf the average Leach 1 [Mn] is 500.10ppm (excluding the sample at 9.03), [Nd] is 12.99ppm, and [Pb] is 20.89ppm. From 136.36-170.73mbsf the average Leach 1 [Mn] is 17749.31ppm, [Nd] is 152.35ppm, and the [Pb] is 103.25ppm. From 0-109.64mbsf where the

average Leach 2 [Mn] is 1990.71ppm (excluding the sample at 9.03), [Nd] is 4.22ppm, and the [Pb] is 6.17ppm. From 136.36-170.73mbsf where the average Leach 2 [Mn] is 2583.17, the [Nd] is 28.31ppm, and the [Pb] is 11.54ppm. From 0-109.64mbsf where the average Leach 2 [Mn] is 1990.71ppm (excluding the sample at 9.03), the [Nd] is 4.22ppm, and the [Pb] is 6.17ppm. From 136.36-170.73mbsf where the average Leach 2 [Mn] is 2583.17ppm, the [Nd] is 28.31ppm, and the [Pb] is 11.54ppm. From 0-109.64mbsf where the average Residue [Mn] is 901.84ppm (excluding the sample at 9.03), [Nd] is 12.62ppm, and the [Pb] is 11.01ppm. From 136.36-170.73mbsf where the average Residue [Mn] is 508.89, [Nd] is 17.18, and the [Pb] is 12.93. While there is lower Mn in the lower portion of the residues, corresponding to where the Mn in the leaches increases, this is not the case for Fe. The average [Fe] is 38490.79ppm from 0-109.64mbsf and the average [Fe] is 43998.43ppm from 136.36-170.73mbsf.

4.4.2 Concentration of Major, Trace, and Rare Earth Elements in each fraction: Site U1370

At Site U1370, the average Leach 1 and 2 concentrations of Mn are 1257.05ppm and 14649.39ppm. The Leach 1 [Mn] exceeds the average extracted concentration of Fe (8527.42ppm). The average [Mn] extracted in Leach 2 is 1257.05ppm, and the average [Fe] extracted in Leach 2 is 2453.10ppm. The first leach contains the highest [Pb] (80.08ppm) and [Nd] (107.30ppm). The second leach contains higher on average [Nd] (90.58ppm) than the residue, however its [Pb] is 16.25 which is lower than the average residue [Pb] (18.56). The average concentration of the Nd in the residue is 13.19ppm.

There is an anomalous feature of the leached Mn profile. There is a decrease in the concentration of Mn and Fe leached at 21.65mbsf where 200.65ppm of Mn was extracted in leach 1 and 232.34ppm of Mn was extracted in Leach 2. This corresponds with a dip in Nd and Pb as well. The L1 [Nd] decreases from 120.54ppm at 20.15mbsf to 47.91ppm at 21.65mbsf and

then returns to 132.46ppm at 23.15mbsf. The L1 [Pb] decreases from 75.88ppm at 20.15mbsf to 28.81ppm at 21.65mbsf and then returns to 60.07ppm at 23.15mbsf.

4.4.3 Rare Earth Element Patterns: Site 1149

At Site 1149 the Leach 1 Ce/Ce* values average 1.06, ranging between 0.60 and 1.84. The highest Ce/Ce* values in Leach 1 are located in the top 35 meters of the core where they range from 1.26-1.84. The Leach 2 Ce/Ce* values average 1.61, ranging between 0.51 and 3.29 (Figure 4.1A). The Ce/Ce* of the residues averages very close to 1 (0.99), ranging between 0.27 and 1.23. From the downcore perspective at Site 1149 the Ce anomaly is positive in the first leach above 31.19 mbsf with a big positive excursion at 31.19mbsf then Ce/Ce* is negative until 101.1mbsf – 153.45mbsf and then resumes being negative until 170.73mbsf. All of the MREE/MREE* in Leach 1 are under 1.7 below 126.36mbsf except 101.12mbsf, which has a MREE/MREE*of 2.10. The average MREE/MREE* from 0-109.64mbsf is 2.07, the average MREE/MREE* from 126.36-170.73mbsf is 1.57 (Figure 4.1B).

The MREE/MREE* and HREE/LREE ratios of Leach 2 do not reflect the same downcore division at 126.36 as Leach 1. All of the samples except the one at 9.03 have a HREE /LREE ratio under 1.5, and the average HREE/LREE is 1.01 (Figure 4.2B). There are a few higher MREE/MREE* values ranging from 1.98-1.72 in the second leach but the overall average is 1.71. The MREE/MREE* and HREE/LREE ratios in the residue are uniform, with an average HREE/LREE of 1.01 and an average MREE/MREE* of 0.97 (Figure 4.2B). The average Ce/Ce* in the second leach is 1.61. Ce/Ce* is greater than 1 until 156.56, where the last three samples analyzed are less than 1.

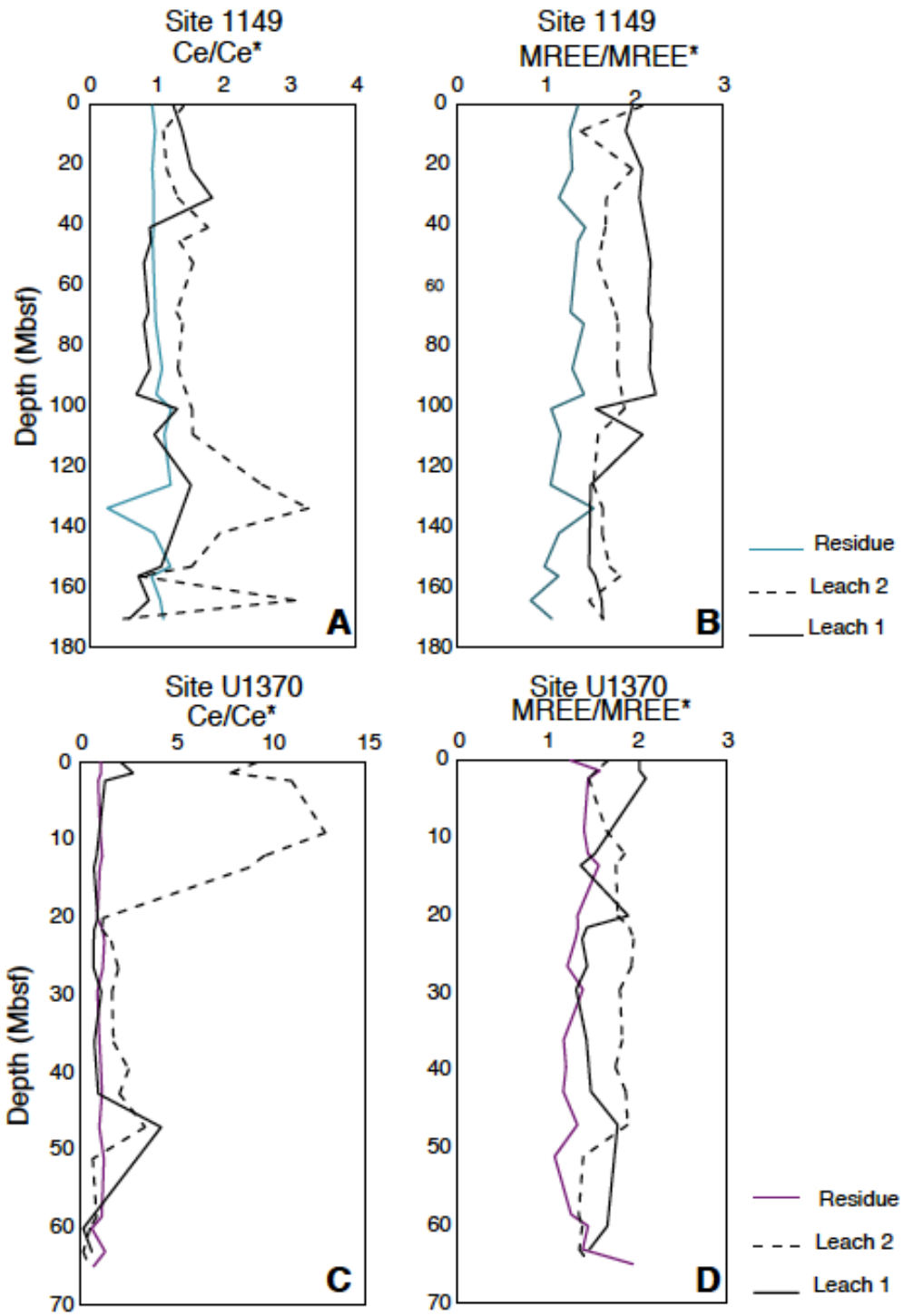

Figure 4.1 Left: The Ce anomaly of the two leach phases and corresponding residue of Site 1149 samples calculated as: Ce/Ce* = 2 x Ce_N/ (La_N + Pr_N) plotted against meters below seafloor. Right: the amount of MREE bulge calculated as: MREE/MREE*= (Eu_N+Gd_N+Tb_N+Dy_N)/((HREE+LREE)/2)), where LREE= La+Ce+Pr+Nd and HREE=Er+Tm+Yb+Lu plotted against meters below seafloor.

4.4.4 Rare Earth Element Patterns: Site U1370

The average Ce/Ce* in the first leach at Site U1370 is 1.00, ranging between 0.13 and 1.07. The top three samples (1.45, 2.45 and 9.15mbsf) have Ce/Ce* that is greater than 1. Although the average indicates a "PAAS like" flat pattern, an evaluation the individual data reveals that it actually indicates a mixture of positive and negative anomalies throughout the core. Similar to Leach 1 the top portion of Leach 2 has very high Ce/Ce* from 0.1mbsf to 13.65mbsf the Ce/Ce* values range from 7.85 to 12.85 (which is the maximum) (Figure 4.1C). The average Ce/Ce* of the second leach is 3.98, indicating that in general the second leach has a positive Ce anomaly. However, the bottom 5 samples have values that are less than 1 with a range from 0.13 (which is the overall minimum) of 0.82. The composition of the second leach at the bottom of the core is distinguished by a negative Ce anomaly. Ce/Ce* in second leach in the middle portion of the core, 20.15-47.09mbsf, ranges from a ratio of 2.52 to 1.13. The residues once again average around 1, (1.02) ranging between 0.58 and 1.28.

The MREE/MREE* and HREE/LREE values in Leach 1 display a similar pattern to the Ce/Ce* values. There are two populations within Leach 1 the first is in the top three samples of the core plus the samples at 20.15 and 47.09mbsf. These samples have high MREE/MREE* values ranging from 1.78 to 2.09, and low HREE/LREE values ranging from 0.80-1.24. The second population has relatively low MREE/MREE* values with a range from 1.32-1.63 that corresponds with the largest HREE/LREE values (1.82 at 29.65 and 1.52 at13.65) in addition to HREE/LREE values that lower and within the range of the other population. The Leach 2 samples have two populations, which essentially overlap. Overall the HREE/LREE values are very similar with a range of 0.57 to 1.16, with an average of 0.81 (Figure 4.2A).

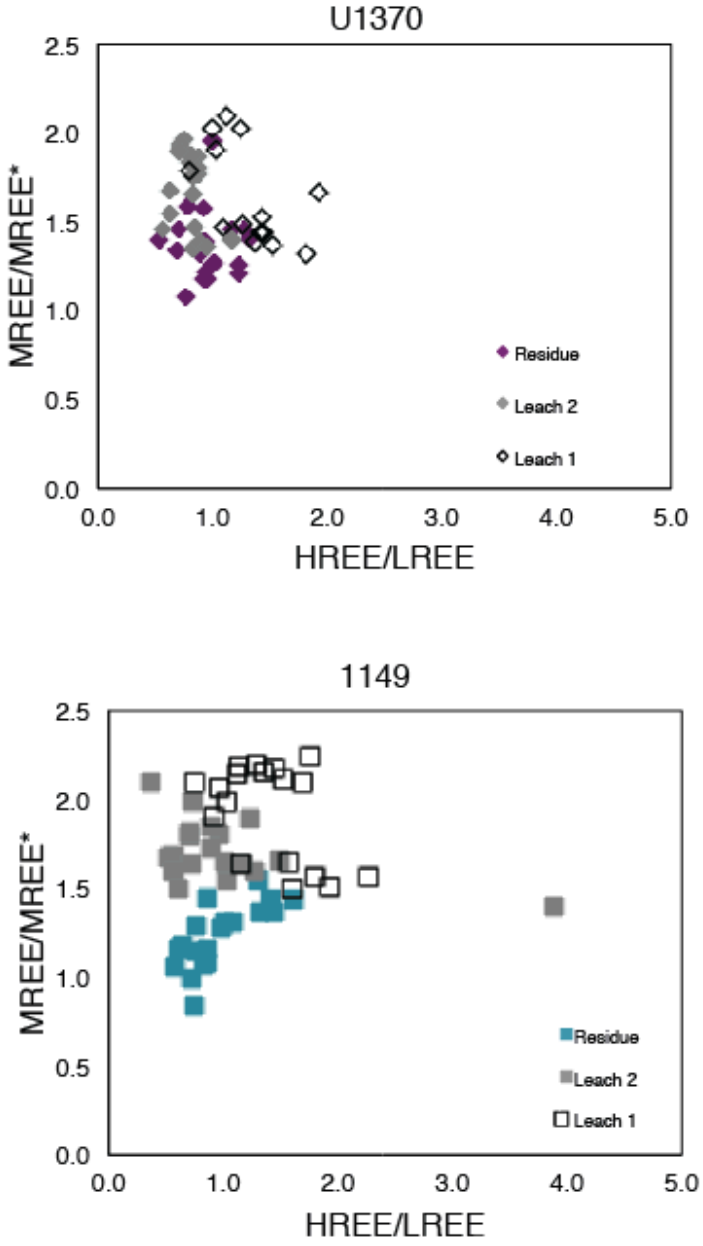

Figure 4.2 MREE/MREE* vs. HREE/LREE of Sites 1149 (a) and U1370 (b) MREE/MREE*= $(Eu_N+Gd_N+Tb_N+Dy_N)/((HREE+LREE)/2))$, and HREE/LREE where LREE= La+Ce+Pr+Nd and HREE=Er+Tm+Yb+Lu. Figure 2a. Site 1149 Figure 2b Site U1370.

The MREE/MREE* values in the top and bottom of the core are lower than those in the middle. There are four samples at the top of the core that are relatively low 1.46-1.67 from 0.1-9.15mbsf, and even lower MREE/MREE* values at the bottom of the core from 1.34-1.47 from 51.18 - 65.05mbsf (Figure 4.2A). The residues have low MREE/MREE* and low HREE/LREE values similarly to those at 1149, the MREE/MREE* the ratios range from 1.08-1.95 with an average of 1.37, and the HREE/LREE ratios range from 0.54 to 1.32 with an average of 0.95.

4.4.5 Nd and Pb Isotopes: Site1149

At Site 1149 there are clear differences in the $^{206}Pb/^{204}Pb$ distributions between the phases, with some overlap between their compositions especially in the middle of the core (Table 4.1). The residue is the most radiogenic with an average of 18.75 a minimum of 18.65 and a maximum of 18.87, is similar to the composition of the dominant aluminosilicate end member expected in the sediment (Chinese Loess $^{206}Pb/^{204}Pb$= 18.89, Figure 4.3A). The Leach 2 values are the most unradiogenic with an average of 18.57 and ranging between 18.39 and 18.68. The Leach 1 values plot between Leach 1 and the Residue with an average of 18.63 (ranging between 18.57 and 18.68). There is much less variability in the $^{207}Pb/^{204}Pb$ values. (Figure 4.3B). The values show similar distinction between phases as the $^{206}Pb/^{204}Pb$ isotopes but overlap widely in range, the overall range of the $^{207}Pb/^{204}Pb$ values across all three phases range from 15.59 to 15.71. The $^{208}Pb/^{204}Pb$ values show the same pattern as $^{206}Pb/^{204}Pb$. The residue is the most radiogenic and loess like (Chinese Loess= 39.12), with an average of 38.98 a minimum of 38.83 and a maximum of 39.21. Leach 2 is the most unradiogenic with an average of 38.69 ranging from 38.48 to 38.88 (Figure 4,3C). Leach 1 is in the middle with an average of 38.72 a minimum of 38.52 and a maximum of 38.84.

Site	Hole	Core	Core Type	Sect.	Top (cm)	Bot (cm)	Depth (mbsf)	Age (Ma)	Phase	$^{143}Nd/^{144}Nd$	Error	$\varepsilon_{Nd}(t)$	$^{206}Pb/^{204}Pb$	Error	$^{207}Pb/^{204}Pb$	Error	$^{208}Pb/^{204}Pb$	Error	Pyrometer
1149	A	1	H	1	75	77	0.75	0.03	R	-	-	-	18.69	0.0020	15.6289	0.0018	38.8615	0.0017	1246.114
1149	A	2	H	4	33	35	9.03	0.32	R	-	-	-	19.07	0.4660	15.9349	0.4815	39.6264	0.4753	1277.133
1149	A	3	H	6	46	48	21.66	0.73	R	-	-	-	-	-	-	-	-	-	-
1149	A	4	H	6	49	51	31.19	1.05	R	-	-	-	-	-	-	-	-	-	-
1149	A	5	H	6	84	86	41.04	1.42	R	-	-	-	-	-	-	-	-	-	-
1149	A	6	H	3	44	46	45.64	1.61	R	0.512103	0.1664	-10.4	18.69	0.2327	15.6354	0.2289	38.8252	0.2342	1239.689
1149	A	7	H	5	12	14	57.82	1.93	R	-	-	-	-	-	-	-	-	-	-
1149	A	8	H	6	38	40	69.08	2.85	R	0.511962	0.3352	-13.2	-	-	-	-	-	-	-
1149	A	9	H	2	71	73	72.91	3.11	R	-	-	-	-	-	-	-	-	-	-
1149	A	10	H	6	15	18	87.85	4.33	R	0.512287	0.0093	-6.8	18.75	0.7207	15.7036	0.7200	39.0575	0.7114	1244.66
1149	A	11	H	5	65	67	96.35	5.19	R	-	-	-	-	-	-	-	-	-	-
1149	A	12	H	2	44	46	101.14	5.73	R	0.512258	0.0073	-7.3	18.67	0.5831	15.6002	0.5996	38.8532	0.5856	1253.469
1149	A	13	H	1	94	96	109.64	6.81	R	-	-	-	-	-	-	-	-	-	-
1149	A	14	H	6	66	68	126.36	17.43	R	0.510789	0.0108		-	-	-	-	-	-	-
1149	A	15	H	5	37	39	134.07	22.29	R	-	-	-	-	-	-	-	-	-	-
1149	A	16	H	4	62	64	142.32	28.83	R	0.511889	0.0694	-13.9	18.83	0.4165	15.7143	0.4159	39.2087	0.4177	1290.883
1149	A	17	H	6	20	22	153.45	36.78	R	-	-	-	-	-	-	-	-	-	-
1149	A	18	H	1	36	38	156.56	39.01	R	0.510065	0.0077		18.75	0.0014	15.6410	0.0015	38.9386	0.0018	1233.504
1149	A	19	X	1	24	26	164.64	43.58	R	0.512101	0.0048	-9.4	18.87	0.4708	15.7035	0.4742	39.0376	0.4781	1252.4
1149	A	20	X	1	93	95	170.73	49.46	R	-	-	-	18.74	0.0018	15.6668	0.0018	39.0819	0.0018	1247.512
1149	A	1	H	1	75	77	0.75	0.03	L2	-	-	-	18.57	0.0080	15.6367	0.0086	38.7080	0.0082	1254.702
1149	A	2	H	4	33	35	9.03	0.32	L2	0.512356	0.0100	-5.5	18.55	0.0062	15.6072	0.0060	38.5211	0.0061	1253.429
1149	A	3	H	6	46	48	21.66	0.73	L2	0.512523	0.0017	-2.3	18.66	0.2291	15.6765	0.1926	38.8489	0.1931	1251.307
1149	A	4	H	6	49	51	31.19	1.05	L2	-	-	-	-	-	-	-	-	-	-
1149	A	5	H	6	84	86	41.04	1.42	L2	0.512493	0.0017	-2.8	-	-	-	-	-	-	-
1149	A	6	H	3	44	46	45.64	1.61	L2	-	-	-	18.56	0.0392	15.6275	0.0395	38.6471	0.0391	1256.344
1149	A	7	H	5	12	14	57.82	1.93	L2	-	-	-	-	-	-	-	-	-	-
1149	A	8	H	6	38	40	69.08	2.85	L2	0.512471	0.0018	-3.3	-	-	-	-	-	-	-
1149	A	9	H	2	71	73	72.91	3.11	L2	-	-	-	18.54	0.0367	15.6332	0.0365	38.6695	0.0366	1249.175
1149	A	10	H	6	15	18	87.85	4.33	L2	0.512452	0.0012	-3.6	-	-	-	-	-	-	-
1149	A	11	H	5	65	67	96.35	5.19	L2	-	-	-	18.65	0.0835	15.6660	0.0853	38.8642	0.0847	1025.459
1149	A	12	H	2	44	46	101.14	5.73	L2	0.51248	0.0011	-3.1	-	-	-	-	-	-	-
1149	A	13	H	1	94	96	109.64	6.81	L2	-	-	-	18.69	0.0700	15.6808	0.0704	38.8863	0.0707	1252.958

Table 4.1 .Nd and Pb isotopic data of three leached phases Leach 1 (L1), Leach 2 (L2) and Residue (R) of sediment samples from Site 1149 and Site U1370

Site	Hole	Core	Core Type	Sect.	Top (cm)	Bot (cm)	Depth (mbsf)	Age (Ma)	Phase	$^{143}Nd/^{144}Nd$	Error	$\varepsilon_{Nd}(t)$	$^{206}Pb/^{204}Pb$	Error	$^{207}Pb/^{204}Pb$	Error	$^{208}Pb/^{204}Pb$	Error	Pyrometer
1149	A	14	H	6	66	68	126.36	17.43	L2	-	-	-	-	-	-	-	-	-	-
1149	A	15	H	5	37	39	134.07	22.29	L2	-	-	-	-	-	-	-	-	-	-
1149	A	16	H	4	62	64	142.32	28.83	L2	0.51230	0.0116	-6.6	-	-	-	-	-	-	-
1149	A	17	H	6	20	22	153.45	36.78	L2	-	-	-	18.40	0.1394	15.5956	0.1395	38.4853	0.1385	1248.572
1149	A	18	H	1	36	38	156.56	39.01	L2	0.51129	0.0033	-26.3	-	-	-	-	-	-	-
1149	A	19	X	1	24	26	164.64	43.58	L2	-	-	-	18.63	0.0018	15.6175	0.0020	38.4876	0.0038	1253.377
1149	A	20	X	1	93	95	170.73	49.46	L2	0.51239	0.0005	-4.9	18.54	0.0026	15.6362	0.0026	38.7465	0.0025	1249.276
1149	A	1	H	1	75	77	0.75	0.03	L1	0.512256	0.0000	-7.5	18.61	0.0011	15.6164	0.0012	38.6325	0.0012	1250.789
1149	A	2	H	4	33	35	9.03	0.32	L1	-	-	-	18.76	0.0451	15.6368	0.0462	38.8480	0.0465	1250.119
1149	A	3	H	6	46	48	21.66	0.73	L1	0.512448	0.0006	-3.7	-	-	-	-	-	-	-
1149	A	4	H	6	49	51	31.19	1.05	L1	-	-	-	18.64	0.0154	15.6383	0.0149	38.7429	0.0156	1237.654
1149	A	5	H	6	84	86	41.04	1.42	L1	0.512249	0.0088	-7.6	18.58	0.0012	15.6205	0.0013	38.5891	0.0026	1253.291
1149	A	6	H	3	44	46	45.64	1.61	L1	0.512430	0.0015	-4.1	-	-	-	-	-	-	-
1149	A	7	H	5	12	14	57.82	1.93	L1	-	-	-	18.58	0.0029	15.6331	0.0028	38.7052	0.0030	1247.889
1149	A	8	H	6	38	40	69.08	2.85	L1	0.512432	0.0007	-4.0	-	-	-	-	-	-	-
1149	A	9	H	2	71	73	72.91	3.11	L1	-	-	-	18.63	0.0014	15.6260	0.0013	38.5209	0.0040	1250.455
1149	A	10	H	6	15	18	87.85	4.33	L1	0.505021	0.0095		-	-	-	-	-	-	-
1149	A	11	H	5	65	67	96.35	5.19	L1	-	-	-	18.67	0.0462	15.6637	0.0463	38.8483	0.0468	1263.013
1149	A	12	H	2	44	46	101.14	5.73	L1	0.512481	0.0071	-3.1	-	-	-	-	-	-	-
1149	A	13	H	1	94	96	109.64	6.81	L1	-	-	-	-	-	-	-	-	-	-
1149	A	14	H	6	66	68	126.36	17.43	L1	0.512436	0.0004	-3.9	-	-	-	-	-	-	-
1149	A	15	H	5	37	39	134.07	22.29	L1	-	-	-	18.59	0.0071	15.6303	0.0073	38.7439	0.0072	1252.873
1149	A	16	H	4	62	64	142.32	28.83	L1	0.512440	0.0037	-3.9	-	-	-	-	-	-	-
1149	A	17	H	6	20	22	153.45	36.78	L1	-	-	-	18.6543	0.0110	15.6494	0.0089	38.7884	0.0225	-
1149	A	18	H	1	36	38	156.56	39.01	L1	0.512357	0.0006	-5.5	-	-	-	-	-	-	-
1149	A	19	X	1	24	26	164.64	43.58	L1	0.512292	0.0078	-6.8	18.62	0.0383	15.6504	0.0395	38.8068	0.0385	1250.55
1149	A	20	X	1	93	95	170.73	49.46	L1	-	-	-	-	-	-	-	-	-	-
U1370	E	1	H	1	5	15	0.1	0.051	R	0.51243236	0.0808	-4.01	19.35	0.9081	15.9486	0.9254	39.7654	0.9115	1248.348
U1370	E	1	H	1	140	150	1.45	0.714	R	0.51219548	0.0020	-8.65	18.9497	0.0018	15.6279	0.0017	38.9094	0.0015	1254.301
U1370	E	1	H	2	90	100	2.45	1.194	R	0.51286339	0.1769	4.367	-	-	-	-	-	-	-
U1370	E	2	H	2	140	150	9.15	4.284	R	-	-	-	-	-	-	-	-	-	-
U1370	E	2	H	5	140	150	13.65	6.806	R	-	-	-	-	-	-	-	-	-	-

Table 4.1 continued

Site	Hole	Core	Core Type	Sect.	Top (cm)	Bot (cm)	Depth (mbsf)	Age (Ma)	Phase	$^{143}Nd/^{144}Nd$	Error	$\varepsilon_{Nd}(t)$	$^{206}Pb/^{204}Pb$	Error	$^{207}Pb/^{204}Pb$	Error	$^{208}Pb/^{204}Pb$	Error	Pyrometer
U1370	E	3	H	3	140	150	20.15	11.29	R	0.51230405	0.0097	-6.78	18.8185	0.0005	15.6378	0.0004	38.8469	0.0009	1253.538
U1370	E	3	H	4	140	150	21.65	11.29	R	-	-	-	-	-	-	-	-	-	-
U1370	E	3	H	5	140	150	23.15	11.87	R	0.51232551	0.0027	-6.39	18.635	0.0736	15.6375	0.0766	38.8693	0.0741	1243.702
U1370	E	4	H	1	140	150	26.65	13.19	R	-	-	-		0.0058		0.0058		0.0058	1249.859
U1370	E	4	H	3	140	150	29.65	14.67	R	0.51208947	0.0033	-11.1	-	-	-	-	-	-	-
U1370	E	5	H	1	140	150	36.15	19.64	R	-	-	-	18.8196	0.0017	15.6365	0.0018	38.8717	0.0018	1249.378
U1370	F	5	H	3	140	150	39.65	22.61	R	0.51220415	0.0040	-9.03	-	-	-	-	-	-	-
U1370	E	5	H	6	60	70	42.79	25.5	R	0.51218482	0.0063	-9.48	18.8166	0.0040	15.6465	0.0042	38.9210	0.0041	1253.465
U1370	E	6	H	2	134	144	47.09	30.16	R				18.8031	0.0025	15.6195	0.0026	38.8070	0.0025	1250.028
U1370	E	6	H	5	100	110	51.18	35.86	R	-	-	-	-	-	-	-	-	-	-
U1370	F	7	H	3	140	150	58.65	51.61	R	-	-	-	-	-	-	-	-	-	-
U1370	F	7	H	4	140	150	60.15	56.87	R	-	-	-	18.86	0.0063	15.6321	0.0062	38.8797	0.0065	1250.579
U1370	F	7	H	6	140	150	63.15	N/A	R	-	-	-	-	-	-	-	-	-	-
U1370	E	9	H	2	140	150	65.05	N/A	R	0.51228025	0.0041	-8.38	18.8044	0.0006	15.6265	0.0005	38.7257	0.0013	1255.769
U1370	E	1	H	1	5	15	0.1	0.051	L2	-	-	-	-	-	-	-	-	-	-
U1370	E	1	H	1	140	150	1.45	0.714	L2	0.51236096	0.0026	-5.42	18.7848	0.0513	15.6507	0.0515	38.7735	0.0516	1249.178
U1370	E	1	H	2	90	100	2.45	1.194	L2	-	-	-	-	-	-	-	-	-	-
U1370	E	2	H	2	140	150	9.15	4.284	L2	0.51235352	0.0014	-5.66	18.7004	0.0145	15.6572	0.0147	38.7482	0.0148	1223.334
U1370	E	2	H	4	140	150	12.15	5.825	L2	-	-	-	-	-	-	-	-	-	-
U1370	E	2	H	5	140	150	13.65	6.806	L2	-	-	-	-	-	-	-	-	-	-
U1370	E	3	H	3	140	150	20.15	11.29	L2	0.51221741	0.0070	-8.47	18.8769	0.0138	15.6394	0.0144	38.6668	0.0141	1251.875
U1370	E	3	H	4	140	150	21.65	11.29	L2	0.51266727	0.0016	0.288	18.6448	0.0184	15.6507	0.0188	38.6933	0.0189	1254.982
U1370	E	3	H	5	140	150	23.15	11.87	L2	0.51247726	0.0204	-3.43	18.8641	0.0407	15.6664	0.0408	38.9559	0.0405	1248.788
U1370	E	4	H	1	140	150	26.65	13.19	L2	-	-	-	-	-	-	-	-	-	-
U1370	E	4	H	3	140	150	29.65	14.67	L2	0.51241123	0.0025	-4.79	-	-	-	-	-	-	-
U1370	E	5	H	1	140	150	36.15	19.64	L2	-	-	-	-	-	-	-	-	-	-
U1370	F	5	H	3	140	150	39.65	22.61	L2	0.51247683	0.0006	-3.71	18.8591	0.0281	15.7116	0.0244	38.9939	0.0575	
U1370	E	5	H	6	60	70	42.79	25.5	L2	0.51244737	0.0017	-4.36	18.781	0.0171	15.6531	0.0170	38.8084	0.0169	1253.828
U1370	E	6	H	2	134	144	47.09	30.16	L2	-	-	-	18.817	0.0083	15.6622	0.0086	38.9205	0.0084	1251.682
U1370	E	6	H	5	100	110	51.18	35.86	L2	-	-	-	-	-	-	-	-	-	-
U1370	F	7	H	3	140	150	58.65	51.61	L2	0.51227706	0.0010	-8.34	18.7702	0.0029	15.6379	0.0029	38.7113	0.0028	1246.022
U1370	F	7	H	4	140	150	60.15	56.87	L2	-	-	-	-	-	-	-	-	-	-
U1370	E	9	H	2	140	150	65.05	N/A	L2	0.51243645	0.0081	-5.34	18.8227	0.0111	15.6777	0.0112	39.0560	0.0112	1263.359

Table 4.1 continued

Site	Hole	Core	Core Type	Sect.	Top (cm)	Bot (cm)	Depth (mbsf)	Age (Ma)	Phase	$^{143}Nd/^{144}Nd$	Error	$\varepsilon_{Nd}(t)$	$^{206}Pb/^{204}Pb$	Error	$^{207}Pb/^{204}Pb$	Error	$^{208}Pb/^{204}Pb$	Error	Pyrometer
U1370	E	1	H	1	5	15	0.1	0.051	L1	-	-	-	-	-	-	-	-	-	-
U1370	E	1	H	1	140	150	1.45	0.714	L1	0.51233971	0.0037	-5.84	18.8321	0.0004	15.6776	0.0003	38.9534	0.0008	-
U1370	E	1	H	2	90	100	2.45	1.194	L1	-	-	-	-	-	-	-	-	-	-
U1370	E	2	H	2	140	150	9.15	4.284	L1	0.512288	0.0049	-6.93	18.8021	0.0259	15.6384	0.0263	38.7927	0.0257	1254.877
U1370	E	2	H	4	140	150	12.15	5.825	L1	-	-	-	-	-	-	-	-	-	-
U1370	E	2	H	5	140	150	13.65	6.806	L1	-	-	-	-	-	-	-	-	-	-
U1370	E	3	H	3	140	150	20.15	11.29	L1	0.51224306	0.0016	-7.97	18.8175	0.1890	15.6424	0.1901	38.6014	0.1905	1254.31
U1370	E	3	H	4	140	150	21.65	11.29	L1	0.51231045	0.0006	-6.67							
U1370	E	3	H	5	140	150	23.15	11.87	L1	0.51226108	0.0016	-7.65	18.8466	0.0246	15.6589	0.0251	38.9360	0.0243	1227.468
U1370	E	4	H	1	140	150	26.65	13.19	L1	-	-	-	-	-	-	-	-	-	-
U1370	E	4	H	3	140	150	29.65	14.67	L1	0.51219184	0.0006	-9.07		0.0008	15.6295	0.0009		0.0782	1250.575
U1370	E	5	H	1	140	150	36.15	19.64	L1	-	-	-	-	-	-	-	-	-	-
U1370	F	5	H	3	140	150	39.65	22.61	L1	0.51227577	0.0007	-7.63	18.8192	0.0037	15.6770	0.0044	38.9138	0.0053	1060.013
U1370	E	5	H	6	60	70	42.79	25.5	L1	0.51227804	0.0018	-7.66	18.7737	0.0015	15.6625	0.0015	38.8361	0.0015	1250.073
U1370	E	6	H	2	134	144	47.09	30.16	L1	-	-	-	-	-	-	-	-	-	-
U1370	E	6	H	5	100	110	51.18	35.86	L1	-	-	-	-	-	-	-	-	-	-
U1370	F	7	H	3	140	150	58.65	51.61	L1	0.51240877	0.0008	-5.77	18.784	0.0593	15.6482	0.0583	38.8900	0.0599	1226.254
U1370	F	7	H	4	140	150	60.15	56.87	L1	-	-	-	-	-	-	-	-	-	-
U1370	F	7	H	6	140	150	63.15	N/A	L1	0.51233362	0.0011	-7.34	18.7517	0.0010	15.6168	0.0010	38.3427	0.0060	1254.073
U1370	E	9	H	2	140	150	65.05	N/A	L1	0.51233927	0.0006	-7.23	18.7842	0.0331	15.6517	0.0329	38.7627	0.0334	1254.924

Table 4.1 continued

The $\varepsilon_{Nd}(t)$ values of Site 1149 show the same pattern as the Pb isotopes. The residue is the least radiogenic with an average of -10. 17 $\varepsilon_{Nd}(t)$- a minimum of -13.89 and a maximum of -6.84 $\varepsilon_{Nd}(t)$ (Figure 4.4A). There are two samples that are less radiogenic than Chinese Loess ($\varepsilon_{Nd}(t)$= -10.12), which indicates there could be unconstrained components in the aluminosilicate phase of the sediment. This finding is consistent with the bulk geochemical analysis of Scudder et al., (2014). The second leach has the most radiogenic values with an average of -3.99 $\varepsilon_{Nd}(t)$- a minimum of -6.55 $\varepsilon_{Nd}(t)$- (142.3 mbsf) and a maximum of -2.25 (21.6 mbsf). The average $\varepsilon_{Nd}(t)$ of leach 1 is -4.91, with a minimum of -7.58 and a maximum of -3.06. The two values that are

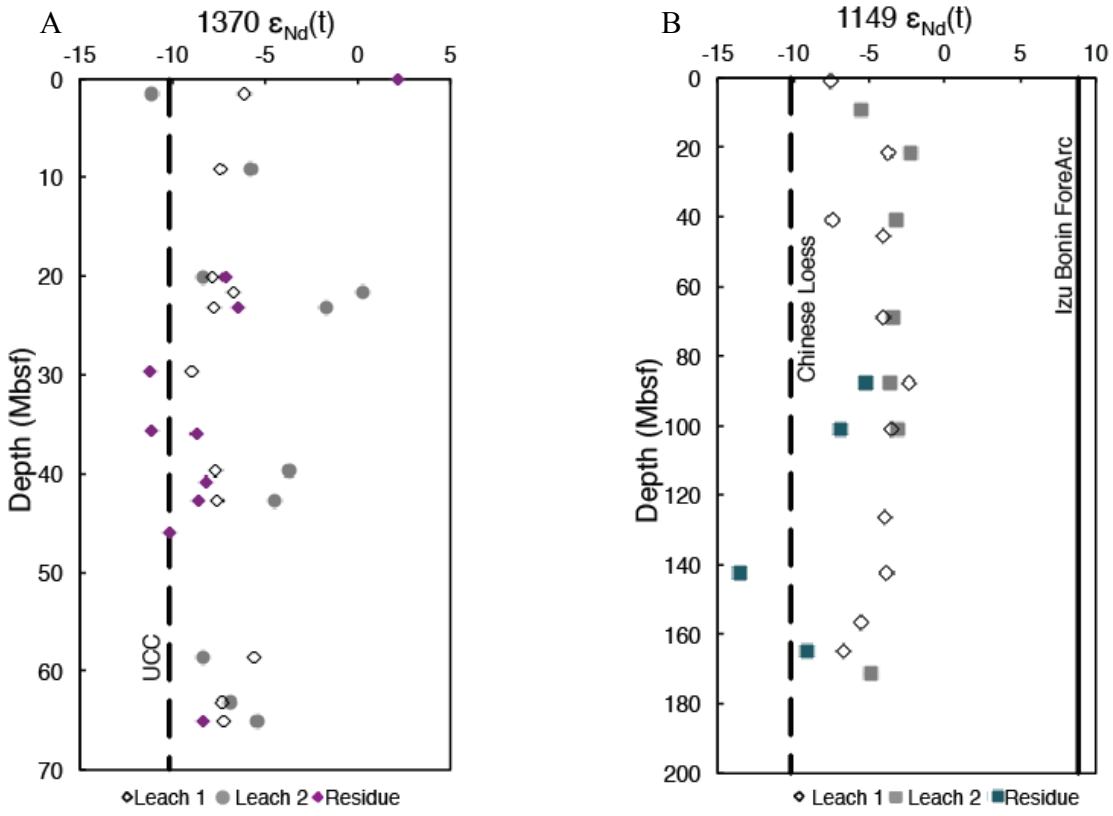

Figure 4.3 Pacific Ocean Nd isotope results data from Sites 1149 (a) and U1370 (b) plotted against depth in meters below sea floor. Error bars for individual samples are smaller than the symbol size. Open black symbols are Leach 1, closed grey symbols are Leach 2 closed symbols with color are residues.

less than -7, -7.45 at 0.75mbsf and -7.58 at 41mbsf are very anomalous for the region (4. 4A). The presence of unradiogenic values in all three phases that are out of sync with each other is puzzling.

4.4.6 Nd and Pb Isotopes: Site U1370

The range of $^{207}Pb/^{204}Pb$ in the Site U1370 residue is 15.62 to 15.65 and the range of $^{208}Pb/^{204}Pb$ is 38.73 to 38.92 (Figure 4.3E). Whereas the range of $^{206}Pb/^{204}Pb$ in the residue is 18.63 to 18.95, which is as large or larger than the range of $^{206}Pb/^{204}Pb$ for the first and second leach (Figure 4.3D). The $^{206}Pb/^{204}Pb$ ratios of Leach 2 range from 18.64 to 19.02, with an average of 18.80. $^{207}Pb/^{204}Pb$ range from 15.59 to 15.76, with an average of 15.67. The $^{208}Pb/^{204}Pb$ range from 38.24 to 39.24, with an average of 38.82. The $^{206}Pb/^{204}Pb$ range for Leach 1 is 18.75-18.89 with an average of 18.89. The $^{207}Pb/^{204}Pb$ range for Leach 1 is 15.61-15.69 with an average of 15.65. The $^{208}Pb/^{204}Pb$ range for Leach 1 is 38.22 -39.06 with an average of 38.71, this spans the full range of the residues and Leach 2. At Site U1370 all three Pb isotopes generally stay within the bounds between Average Rhyolite and PAAS, with the exception of the Leach 1 $^{208}Pb/^{204}Pb$ ratio at 29.65mbsf which is lower than the $^{208}Pb/^{204}Pb$ of Average Rhyolite (38.61). In contrast the $^{206}Pb/^{204}Pb$ ratio at 29.65 mbsf stays within the bounds of PAAS and Rhyolite and are very similar to the other isotopes measured down core. There are no clear differentiations between the phases in isotopic space. There must be another factor or several that control the distribution Pb isotopic composition of in the disparate phases of the sediment.

At Site U1370 the Nd isotopes show more differentiation between the phases, with distinct but slightly overlapping signatures for each phase. At the top of the core there are some values that are more radiogenic, the upper most sample has a Nd IC of -4.01. From -4.02 the

residue then rapidly decreases to -8.65, and subsequently shifts back up to $\varepsilon_{Nd}(t)$ -6.78 and -6.39. Below 14mbsf the residue ranges between -8.34 and -11.06 (Figure 4.4B). The Leach 1 Nd values range between -9.07 and -5.76 with an average of -7.25. Leach 2 ranges between -8.47 and +0.29 with an average of -5.09. Leach 1 and the residue seem to co-vary at 29.67mbsf, where Leach 1 is at its minimum ($\varepsilon_{Nd}(t)$= -9.07) and where the residue has its minimum ($\varepsilon_{Nd}(t)$= -11.06). Leach 2 also decreases at the same interval from +0.29 at ~20mbsf to -4 at 29.67 mbsf. In general, the residues are unradiogenic and plot near the Nd isotopic composition of UCC (-10). The residue containing an isotopic signature that is unradiogenic and upper continental crust-like is what we would expect, given that the origin of the residue is generally interpreted as the "detrital" or lithogenic component upon which the other phases are sorbed/adsorbed. This indicates that the same process is controlling the Nd isotopic composition of both the residue and the oxide coatings, which is not what we would expect if the Nd and Pb in the oxide coating originate from seawater.

4.5 Discussion

4.5.1 Q-mode Factor Analysis: Identification of End Members

Examining both Sites 1149 and 1370 we identified 5 factors, which were generally consistent across the two sites (Figures 4.5 and 4.6). Together these five factors explain 99% of the variability in the data at each site. As with any coefficient of determination, that these factors explain 99% of the variability in the data is statistically significant signifying that, aside from some reasonable geochemical and stastical error, with these factors alone we can account for all of the sources across the leach phases.

The pattern of elements with high factor scores, explaining each factor for the five factors are similar at both sites, and consistent across the different element iterations (Th, Nd, Pb,

Mo, Mn and Fe, Cu, Fe, Mn, Hf, Zr, and Ce, and 3) Ce, Gd, Er, X, Mn, and Fe). On a large scale this indicates that the result of five factors is robust, and that through iterations of elements with the limited number of variables we have identified the broad factors that describe the components in the system. This indicates that the elements behave consistently in their sorption from site to site, and/or the leach procedure has consistent control over the reduction processes. We have identified similar factors with similar behaviors within unique groups of elements so even though they do not look exactly the same from element group to element group we outline their characteristics and explain why we conclude they represent the same factors below.

Based on the modeled elemental covariance and composition, the four main factors we identify that explain the data across the three leach phases are interpreted as a lithogenic factor, an adsorbed factor, a factor we call "Ce" (because Ce has a high factor score indicating Ce explains most of the variability in the factor), and a factor we call "Mn" (because Mn has a high factor score). The 5th factor we identify is similar between the sites with high individual VARIMAX factors of individual elements that covary negatively with Fe and Mn. We call this factor "quasi-lithogenic" at Site 1149 and identify it as hydrothermal at Site U1370. These categorizations are intentionally broad and are not intended to be definitive sources, rather they are the best interpretation based on the available data.

The lithogenic factor has a Fe VARIMAX factor score near 1, and covaries with Cu, Zr and Hf where they are included in element groups (Figure 4. 5 & 4.6). The adsorbed factor has high factor scores for Er, Gd, Ce (generally in the order of importance) and covaries positively with Pb, Mo, Th, Mn or Nd where they are included. In the element groups without Er, Gd and Ce, the Pb, Mo and Nd seem to be dominant. The Ce factor has a high Ce VARIMAX factor near one and covaries positively with Hf and Zr and negatively with Hd, Er, and Th where they are

included. The Mn factor has a Mn factor score near 1 for Mn. The fifth factor which, we tentatively argue is hydrothermal at Site U1370 and is a second lithogenic component at Site 1149 is characterized by a combination of strongly covarying Th, Pb, Cu or Hf negatively covarying with Fe and Mn. Where Th is included in the element suite the overall importance of the hydrothermal factor in the whole data set increases. This factor is the most different between the two sites. The Site U1370 hydrothermal factor is identifiable by the increase of individual factor loadings down core across each of the element iterations. We call the 5th factor at Site 1149 "quasi-lithogenic" because, although it has broadly the same element patterns within factors as the 5th Site U1370 factor, it explains more of the data at Site 1149 than the hydrothermal factor does at Site U1370. There is no hydrothermal component identified at Site 1149 (Scudder et al., 2014).

4.5.2 Site 1149 Factor Analysis

The lithogenic factor at Site 1149 explains between 35.25 and 38.19% of the total combined data. The phase with the highest factor loading per sample for the lithogenic factor is the residue with an average factor loading of 81.81%. Please note that for simplicity we report the average factor loadings for the element group Ce, Gd, Er, Cu, Fe, and Mn, which represents well the overall trends identified by all of the iterations of element groups. Sample loading is determined on a sample by sample basis so we view the average sample loadings for each phase individually. The average factor loading for the lithogenic factor for Leach 2 is 10.52% and the average factor loading for Leach 1 is 5.98% (Table 4.2, Figure 4.7B). A large portion of the second leach is not explained by the lithogenic factor. This indicates that the composition of the residues is distinct from the leaches and contributes minimally to their composition.

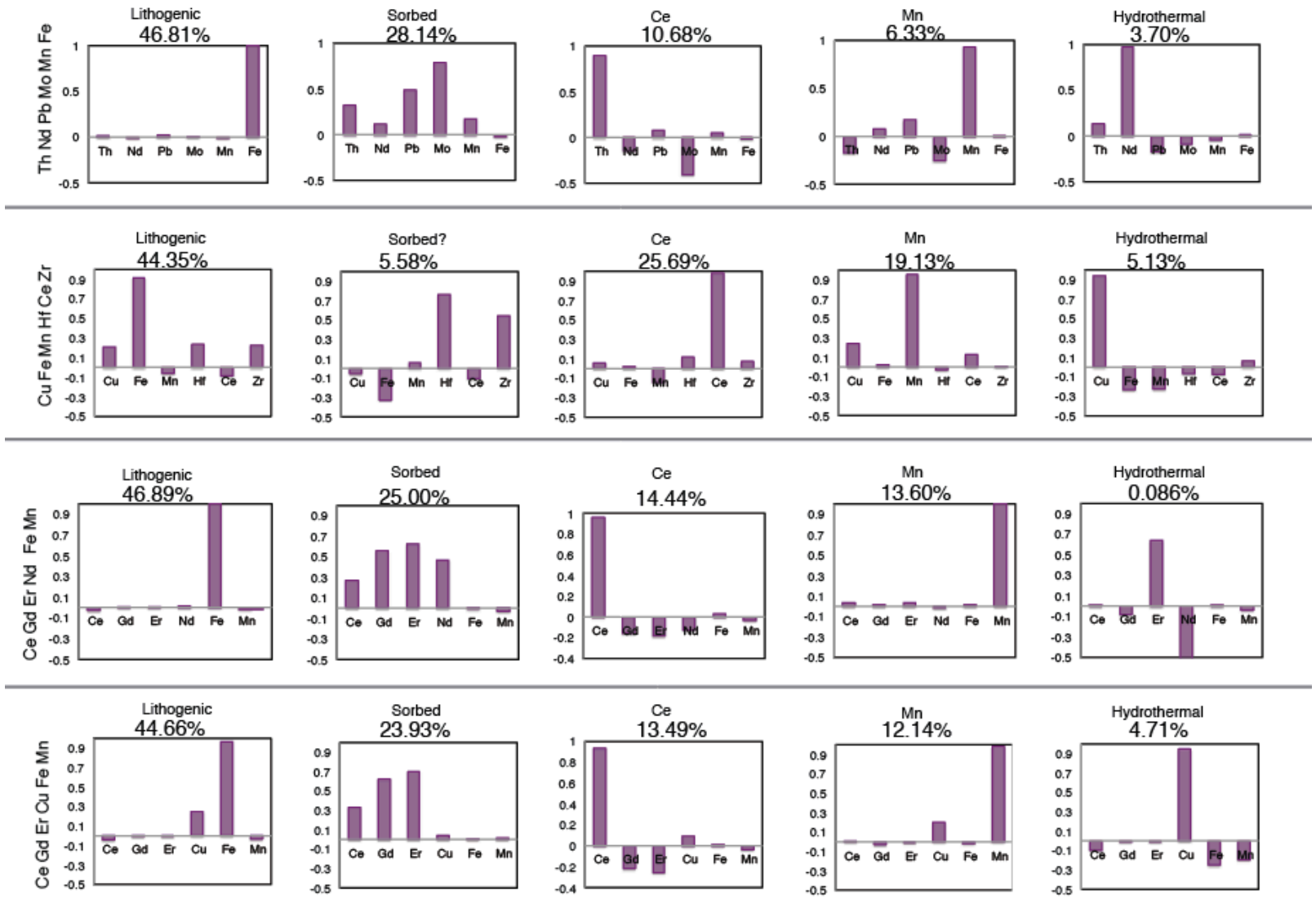

Figure 4.4 Varimax rotated factor scores for Site U1370 produced by Q-mode factor analysis (n=53). The rows are grouped by element groups used to perform factor analysis and the columns are grouped by identified factors.

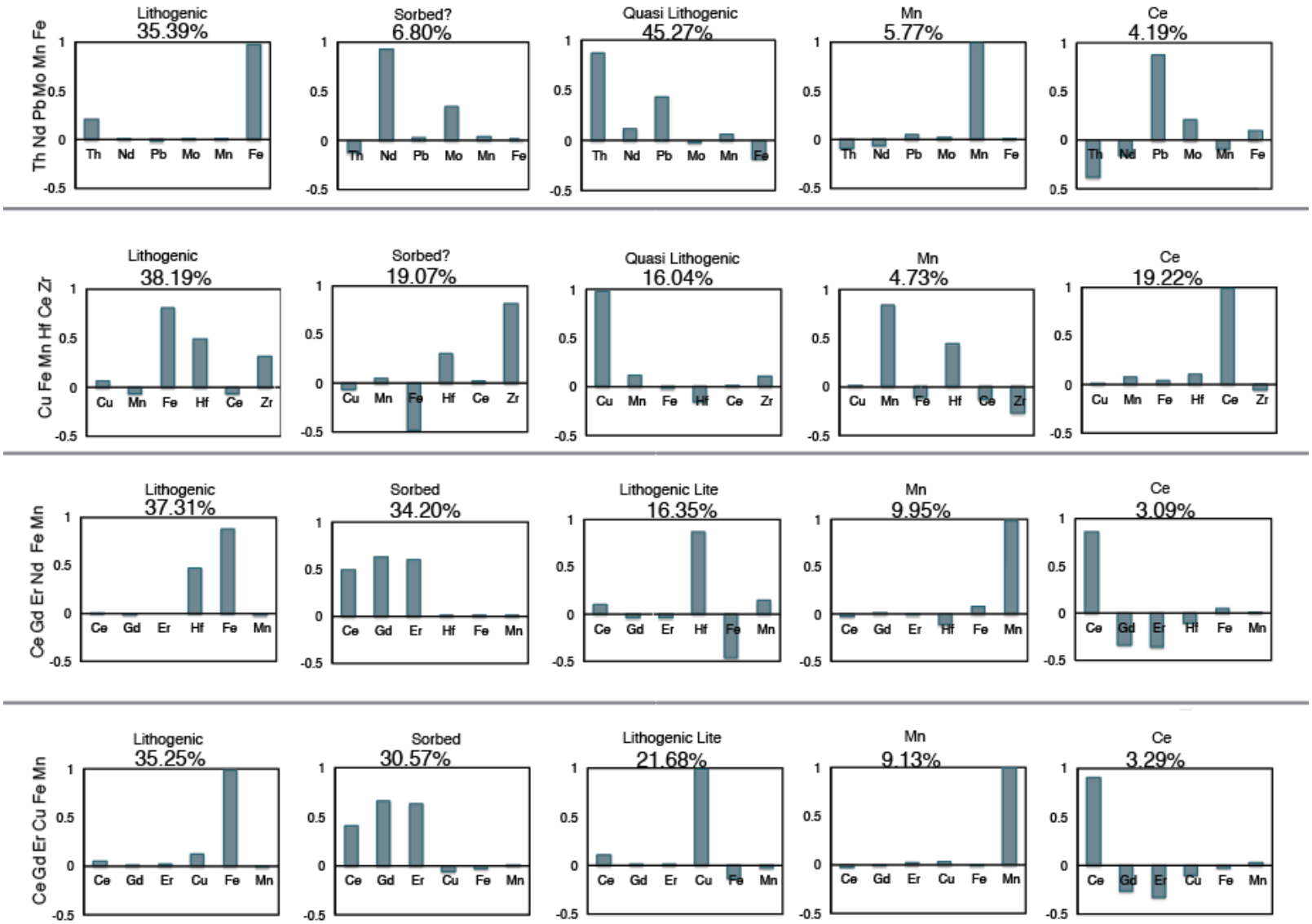

Figure 4.5 Varimax rotated factor scores for Site U1370 produced by Q-mode factor analysis (n=53). The rows are grouped by element groups used to perform factor analysis and the columns are grouped by identified factors.

This corroborates a unique source in the second leach which is also indicated by the contrast between unradiogenic isotopic signature found in the residues and the radiogenic isotopic values found in Leach 2.

Quasi-lithogenic explains a large portion of the first and second leach at Site 1149; when Th is included in the element suite, quasi-lithogenic explains 45.27%. Overall it explains a large present of the total data explained because it explains such a large portion of both Leach 1

Site	Phase	Average Precent Factor Loading					
		Lithogenic	Sorbed	Ce	Mn	Quasi Lithogenic	Hydrothermal
1149	Total Percent Explained	35.25	30.57	3.29	9.13	21.68	N/A
1149	Leach 1	5.98	53.93	7.09	7.02	25.96	N/A
1149	Leach 2	10.52	25.1	10.98	22.59	30.29	N/A
1149	Residue	81.81	4.88	1.77	2.49	9.02	N/A
U1370	Total Percent Explained	44.66	23.93	13.49	12.14	N/A	4.71
U1370	Leach 1	7.99	38.36	12.07	30.32	N/A	10.61
U1370	Leach 2	19.71	30.23	26.68	13.55	N/A	19.83
U1370	Residue	76.34	4.45	4.85	4.71	N/A	9.64

Table 4.2 The average factor loadings for the element group Ce, Gd, Er, Cu, Fe, and Mn, which represents well the overall trends identified by all of the iterations of element groups. Sample loading are determined on a sample by sample basis and the average sample loadings for each phase is presented in this table.

(22.96%) and Leach 2 (30.39%) individually. The factor loading patterns of Leach 1 and Leach 2 of quasi-lithogenic are very similar at Site 1149, indicating that they both contain a large portion of this factor in contrast with the residue, where the Leach 1 and Leach 2 factor loadings are lower. The quasi-lithogenic factor at Site 1149 is similar to the hydrothermal component at Site U1370 (detailed below), however it does not seem geologically reasonable for there to be a hydrothermal influence in the middle of the core, and the factor loadings do not confirm that they are the same factor.

The adsorbed component explains between 6.80 and 42.40% of the total combined data depending on the element group. The results of the Ce, Ge, Er, Nd, Fe, and Mn element suite display the highest percentage of the data explained by the adsorbed factor. This suite is useful for examining the behavior of Nd, Mn, and Fe in the context of the other REEs. However, like at Site U1370 four factors explain 99.97% of the data with this element combination and there is not a discernable 5th factor. The other factors explain or "absorb" more of the variability in the data. This is a good illustration of the importance of iterative evaluation of elements in order to identify the best explanation of the factors in the data. The lowest percent explained by the adsorbed factor is modeled with the Th, Nd, Pm, Mn and Fe element suites. The presence of Th increases the importance of the quasi-lithogenic factor, and this results in a decrease in the percent explained by the other factors. Like with the lithogenic factor there is much less differentiation between the factor loadings of the adsorbed factor in the first and second leach.

The Ce factor explains a small portion of the data between 1.65% to 19.22% All three phases show similar interwoven factor loadings with sharp perturbations across all of the element models, especially in the second leach, at 126.36 and 164.64mbsf. The Mn factor explains a similar portion of the data ranging between 4.18% and 15.85% of the total data explained. It represents a relatively variable portion of all three phases with an average of 7.02, 22.59 and 2.49% of the individual factor loadings residue, Leach 2 and Leach 1 respectively. The high Mn ash sample at 9.03mbsf is clearly resolved in this factor. The increases in factor loadings in all three phases of the Mn factor at 9.03 correspond to decreases in factor loadings in both of the lithogenic factors. The high factor loading in the second leach, and the resolution of the high ash sample indicates that this factor may not solely represent leached Mn but may also or alternatively represent a readily-reducible ash component.

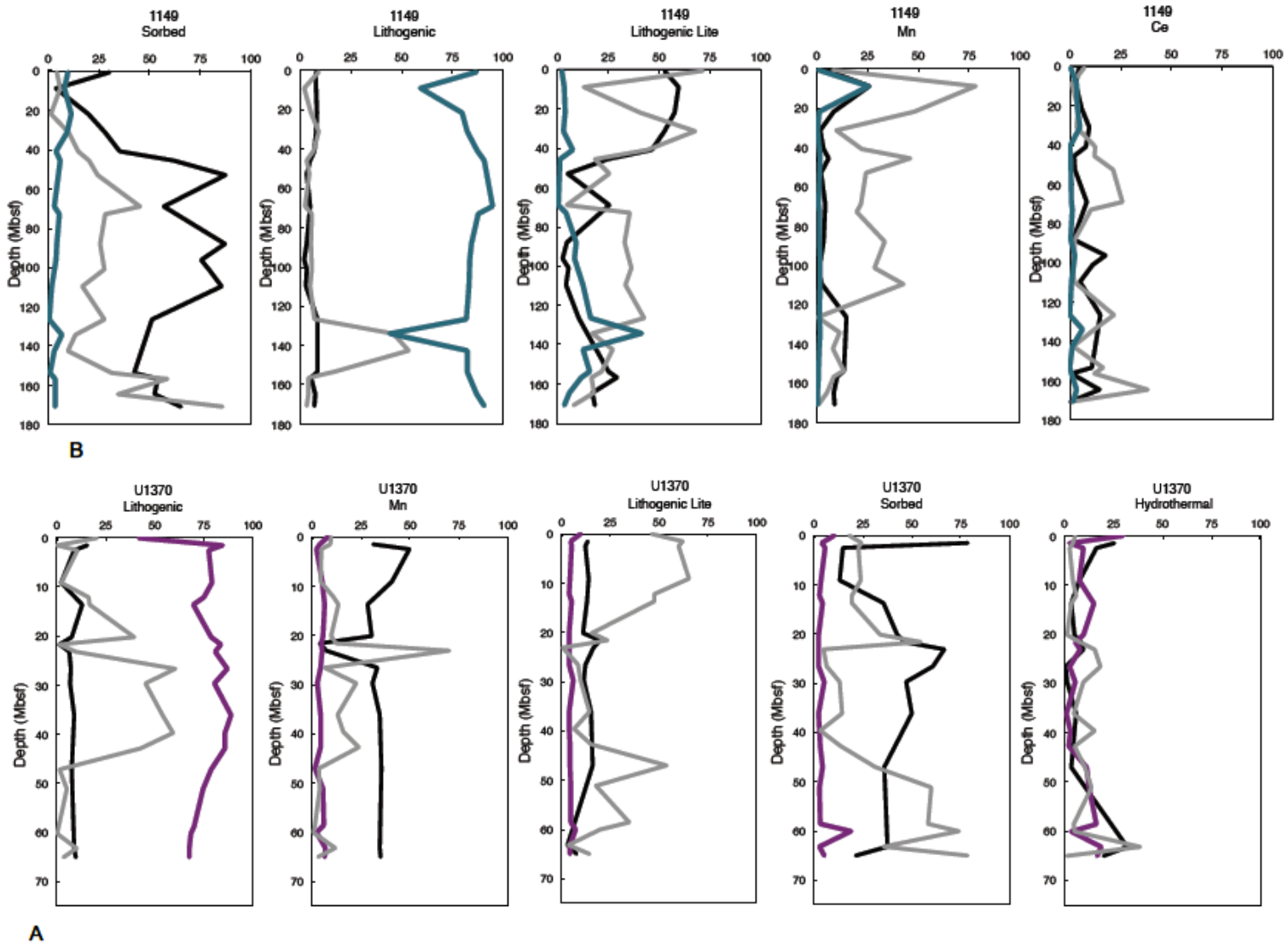

Figure 4.6 Factor down core plots: Varimax factor loadings for each factor, produced by Q-mode factor analysis from the Ce, Gd, Er, Cu, Fe, Mn grouping, plotted down core for each phase. The percentage of each sample explained by each factor, plotted against depth.

4.5.3 Site U1370 Factor Analysis

The lithogenic factor explains between 43.05 and 46.86% of the data within each element grouping. The importance of the lithogenic factor increases from Leach 1 where the average lithogenic factor loading on a sample is 7.99%, to an average lithogenic factor loading of 19.71 for Leach 2. For simplicity we report the average factor loadings for the element group Ce, Gd, Er, Cu, Fe, and Mn. The highest factor loadings for the Ce, Gd, Er, Zr, Fe, Mn iteration of the lithogenic factor are in residue samples with an average factor loading of 76.34%. The systematic differentiation between the three phases is an important result because it displays the lithogenic influence on the first and second leaches, and that the lithogenic factor has the least influence on leach 1, the shortest leach. It also makes clear that the residue is not comprised of one single component.

The sorbed factor explains a range between 5.58 and 28.14% of the total data set (all three phases modeled together), depending on the element suite. The highest individual sample factor loadings are in Leach 1 where the average factor loading for the Ce, Gd, Er, Cu, Fe, Mn iteration of the sorbed factor is 38.36%. The importance of the sorbed factor is lower in Leach 2 (30.23%) but increases with depth. After the sorbed and lithogenic fractions the relative importance of factor from element suite to element suite are more variable depending on the elements employed. The next factor we will examine is the Ce factor although it is not consistently the third most important factor. The Ce factor is characterized by high Ce VARIMAX factor score which positively covaries with Hf and negatively covaries with Th. Therefore, we tentatively include the high Th factor from the Th, Nd, Pb, Mo, Mn, Fe element group where Ce is not included. The high Th factor also has a similar down core factor loading pattern as the Ce factors that are well modeled with the other element groups This is a good

example of the importance of iterations because the Th, Nd, Pb, Mo, Mn, Fe model only explains 97.6% of the data, and we have found that Ce is required in the model to explain 99% of the data. The Ce factor explains between 10.68 and 25.69% of the data and is highest in the second leach with an average individual factor loading of 26.68% (Figure 4.7A).

The Mn factor explains a small portion of the data ranging from 6.33-19.13%. Where the Mn factor accounts for a high portion of the data there is not a discernable 5th factor (this occurs in the elemental suite Ce, Gd, Er, Nd, Fe and Mn where, because Nd behaves cohesively with the other REEs, the quasi-lithogenic factor is very weak. The factor loadings on individual samples are highest in the first leach with an average of 30.31% of the individual factor loadings. This indicates that the Mn factor and the sorbed factors are associated. It is possible that they represent the Mn2O we extract, and the elements that are sorbed to it, respectively.

The hydrothermal factor at Site U1370 is characterized by a high VARIMAX factor on an individual element (Nd, Cu, Hf, Zr, Th), which negatively covaries with Fe and Mn. An argument could be made that this factor represents a second lithogenic component because of the high concentration of Hf and Th in dust and ash sources. Hf is one of few elements Dunlea et al. (2015) identified as a dominantly terriginous component that is above detection limit in the leach phases where elements like Cs and Rb are below detection limit in all of the phases save the residue. We have identified this factor both because of its element scores, but it also seems coherently one factor because of the consistent increase in individual factor loading for Leach 2 samples below 50mbsf. This combined with the increase in sorbed factor loading over the same allows us to conclude this factor represents a hydrothermal source and possibly confirms the increase of hydrothermal influence with depth. The individual factor loadings for the hydrothermal factor are similar between the three leach phases, 10.61% for Leach 1, 9.83% of

Leach 2 and 9.64% for the residue. The hydrothermal component explains between 0 (in the Ce, Ge, Er. Nd, Fe. Mn element group as described above) and 8.99%.

While we have identified similar factors at both sites, the distribution between the factors in the phases at Site 1149 is very different from the distributions at Site U1370. We are not arguing that this factor analysis indicates the same sources influence the composition of Sites 1149 and U1370. The goal is to understand the processes and elemental groupings that result from the leaches.

4.5.4 Comparison of the Three Sets of Analyses: Site 1149

In order to evaluate the association between the potential sources to each phase and potential source, their elemental compositions, their isotopic compositions and how all of these factors vary down core, we employ QFA, and compare it here to the elemental and isotopic data. The increase in leached Fe below 126.36mbsf follows the increase in Fe and Mn concentration with depth measured in the bulk, and the increase in the calculated Fe and Mn excess identified in chapter III. Comparing Leach 1 to the Residue and Leach 2 provide some context for the two sections of Site 1149 that we have investigated. The HREE/LREE of the top portion of Leach 1 is high in comparison to the other phases (1.33), and the bottom portion is even higher (1.62; Figure 4.2B). This indicates that the HREE elements in Leach 1 are enriched with respect to the LREE elements, and that the lower portion of the core has a pattern that looks more like seawater than the top portion. While there is wide variation in the REE pattern of each sample in Leach 1 the overall the majority of the samples have a pattern that indicates it is derived from seawater.

The MREE/MREE* in Leach 1 also has a clear differentiation at the 126.36mbsf boundary where the Mn concentration in Leach 1 increases. The Ce anomaly stays below 1 above 100mbsf, which occurs above the increase in calculated excess Fe. This pattern is

consistent with other major, trace and REE patterns that show a differentiation between the composition of the top and bottom of Site 1149. Where there is a positive Ce anomaly there is a greater distinction between both leach phases and the residue (Figure 4.2A).

4.5.5 Comparison of the Three Sets of Analyses: Site U1370

At Site U1370 the factors show clear divisions in the compositions between phases and confirm our assessment of the fidelity of the leach in chapter III. However, they also highlight the overlap between factors in each phase. This is especially clear in the heterogeneous nature of Leach 2 and its high lithogenic factor loadings in addition to sorbed components. The isotopic data mirrors this finding with three phases that are distinct from each other, but where Leach 2 has a unique radiogenic signature that cannot be explained through mixing of the compositions of Leach 1 and the Residue. While there is not a clear pattern of the second leaching dominated by a single factor at Site U1370, the Ce factor does have high factor loadings at the top and bottom of the core. It is possible that this factor is responsible for the radiogenic signatures in the second leach. It is also possible that this difference is created by one source with a very radiogenic component with a disproportionately large impact on the total composition because of the unradiogenic nature of the South Pacific. There are individual samples that have unique MREE/MREE* and HREE/LREE patterns, but overall the analyzed values are consistent throughout the section. We attribute the isolated unique values in shallower burial depths to changes in burial rate and or terrigenous inputs. The bottom of the core has a very low Ce anomaly indicative of hydrothermal inputs (Murray et al., 1991), which are corroborated by the factor analysis, although to not have a unique signature in isotopic space.

The results of the isotopic analysis indicate that some portion of each leach fraction analysis is controlled by the composition of the sediment sources identified in the residue and by some

portion of elements that are controlled by the physiochemical interactions that occur in seawater. There is a finite limit of control each source exerts on each phase. 4.5.6 Consideration of the Origin of the Regional Lithogenic Signature

The observation that on average the Leach 2 values are more radiogenic in both Nd and Pb space confirms that the second leach contains a unique source and is not only composed of remaining Fe-Mn oxyhydroxides. It is possible that this phase reflects a reducible volcanic ash like that observed by Wilson et al. (2013). If this is the case, there is no evidence in the major and trace metal data that an ash is completely leached in the second leach (i.e. we do not leach Si or Al above detection limit, nor do we leach nearly any Ti).

The Nd isotopic differences between the residue, Leach 1, and Leach 2 analyses is clear at Site U1370. This indicates that there is a distinct source contributing to the second leach that becomes reduced. However, the Pb isotope analyses indicate only a small amount of variability among the three sets of analyses (Figure 4.8). The ternary diagrams of element groups informed by the results of factor analysis indicate clear differentiation between each phase. Here we refer to the distributions of the populations of elements previously described. Both Site U1370 plots Ce, Mn, Cu (Figure 4.9A) and Pb, Nd, Zr (Figure 4.9B) indicate that the first leach has the lowest contribution from elements representing a lithogenic source (Cu and Zr), and that the influence of Cu and Zr increase in the second leach, and finally the residue is dominated by the Cu and Zr. In the Ce, Mn, Cu plot there is a clear mixing line of the residue samples between the composition of dust like sources like PAAS, and UCC and high Mg ash (Figure 4.8). The second leach samples plot around Average Rhyolite, UCC and PAAS in the Ce, Mn Cu plot, and around Rhyolite and PAAS is the Pb, Nd Zr plot (Figure 4.8). This confirms that the second leach's composition is dominated by lithogenic components.

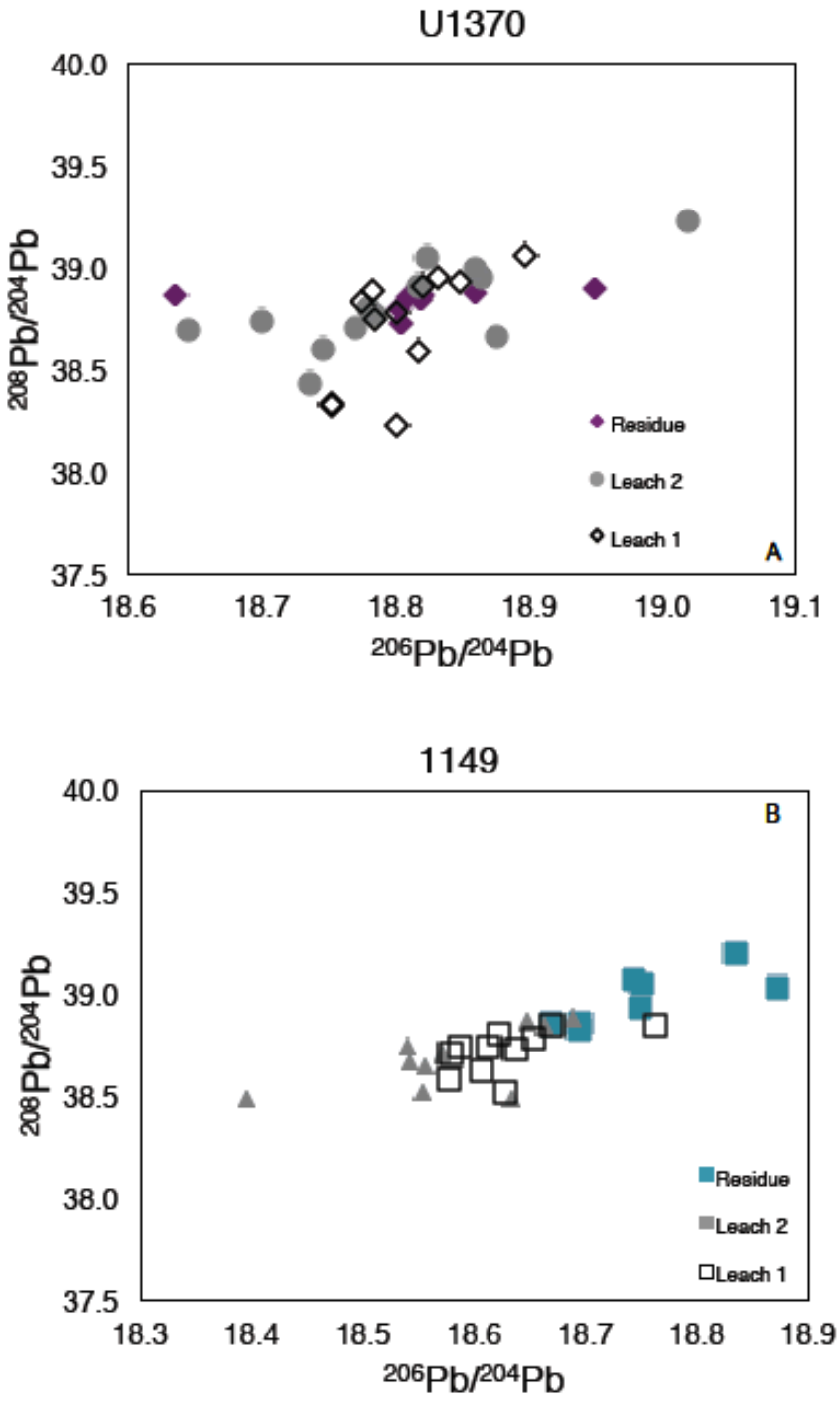

Figure 4.7 $^{206}Pb/^{204}Pb$ vs. $^{208}Pb/^{204}Pb$ isotopic ratios of each leach phase, (A: Site U1370, B: Site 1149)

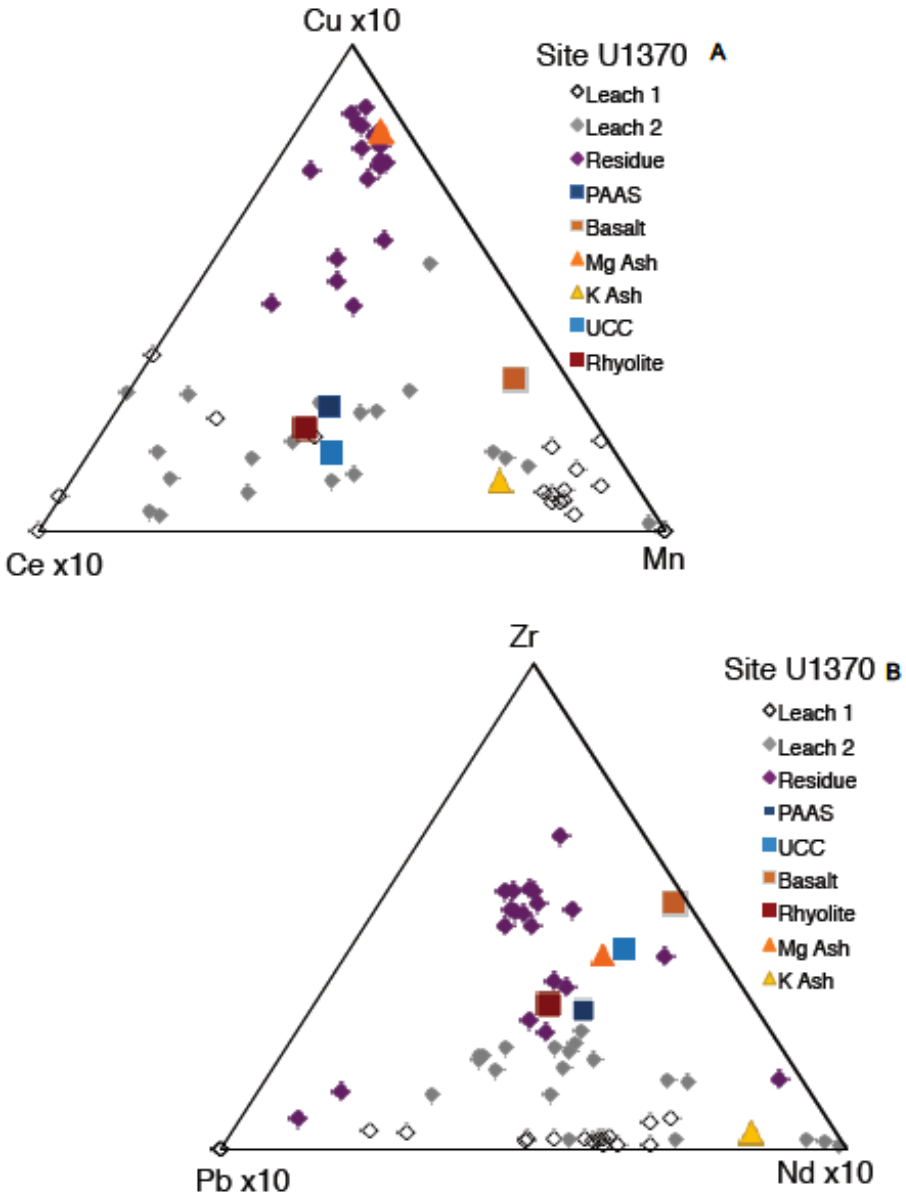

Figure 4.8 Site U1370 samples from the three leach phases plotted on ternary diagrams with end-member compositions. The element concentrations were scaled, in the plot and then normalized so the three element concentrations sum to a constant, in order for the elements to be of comparable magnitude with each other

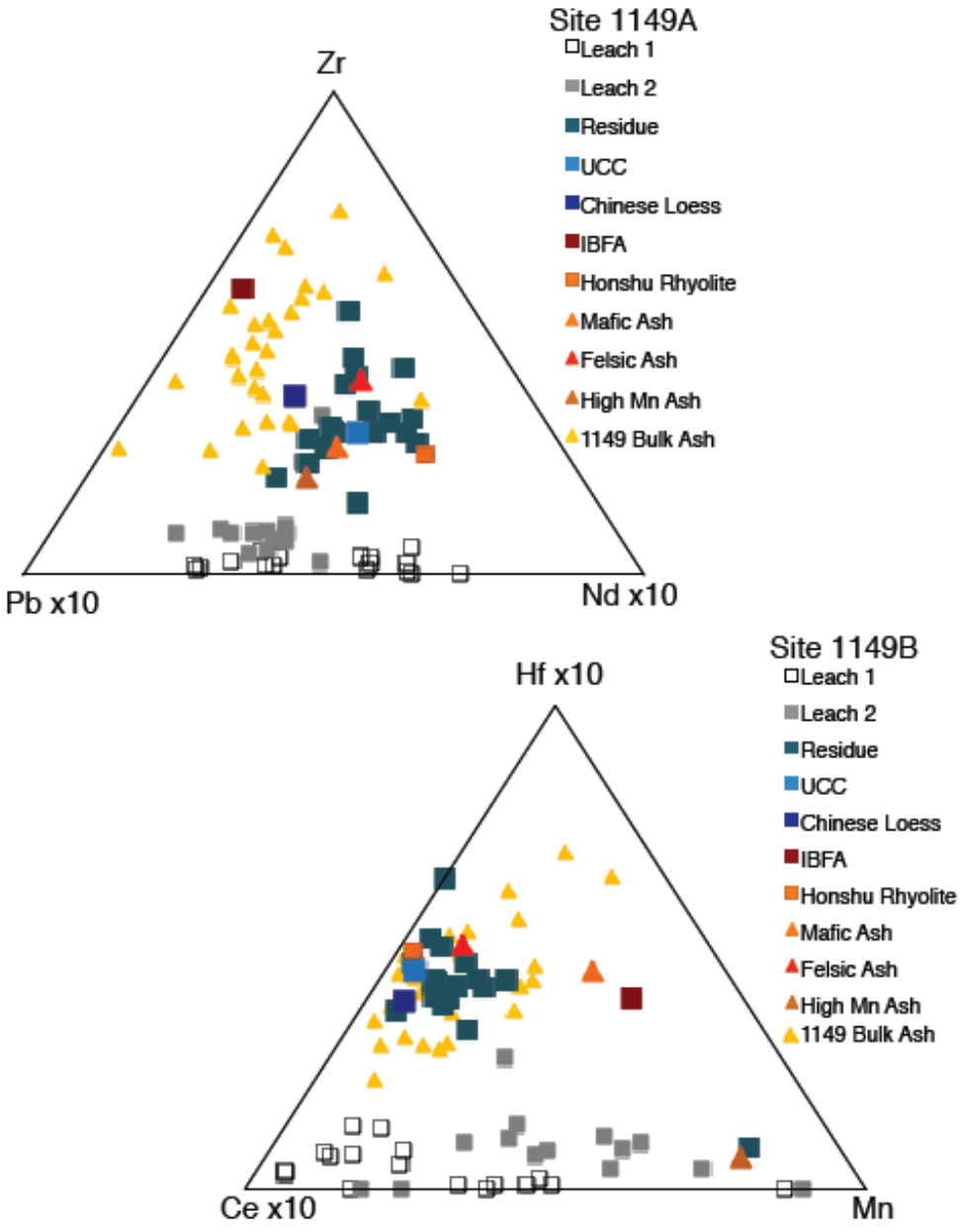

Figure 4.9 Site 1149 samples from the three leach phases plotted on ternary diagrams with end-member compositions. The element concentrations were scaled, in the plot and then normalized so the three element concentrations sum to a constant, in order for the elements to be of comparable magnitude with each other

The Site 1149 ternary diagrams show less differentiation between each phase then the Site U1370 diagrams. There is a similar pattern of increasingly lithogenic influence moving toward Hf and Zr, in the Ce, Mn, Hf (Figure 4.10A) and Pb, Nd and Zr (Figure 4.10B) plots, respectively. The Leach 1 samples plot very near Ce and Mn, and Nd and Pb. No sources plot with the Leach 1 population. We have also not identified the end member that best represents quasi-lithogenic. It is possible that it is an ash signature although we would expect an ash rich factor to have higher factor loadings in the top of the core where the most ash layers and dispersed ash occur. Although we cannot identify the source of the factor at this time it is a necessary component to fully explain the data.

The radiogenic to unradiogenic pattern is very clear in $^{206}Pb/^{204}Pb$ vs. $^{208}Pb/^{204}Pb$ space at Site 1149. This suggests that we are removing some radiogenic end member from the residue in the second leach, or that there is fractionation occurring. The same plot also highlights a second population of Leach 2 samples besides the dominate one with $^{206}Pb/^{204}Pb$ values that are more radiogenic than the Leach 1 samples. The second Leach 2 population overlaps with the intersection of Leach 1 and Residue values at ~18.65 (at 9.03, 87.85 and 101.14 mbsf). These three relatively radiogenic Leach 2 values do not have any REE patterns in common. However, they all are in the upper portion in the core where the $^{206}Pb/^{204}Pb$ values are also relatively low ranging from 18.65 to 18.75. Thus, it is likely that this population represents a source that is more radiogenic contributing to the residue and Leach 2 at this interval. This interpretation is consistent with increased ash accumulation in the upper portion of the core (Plank et al., 2000; Scudder et al., 2014). Overall, a radiogenic source, likely represented by "quasi-lithogenic" which is the dominant factor in Leach 2 and controls the isotopic composition in the second leach. The factor loadings of quasi-lithogenic are higher at the top of the core and decrease with

depth. This pattern supports our conclusion that the second leach is dominated by readily reducible volcanic ash source. The clear differentiation between phases in isotopic space echoes the findings of the sources contribute to each phase.

4.5.7 Implications for the proxy

The results of this comprehensive elemental and isotopic analysis of the leach phases and their elemental composition supports the influence of lithogenic-like components in the leach that previously have been interpreted as a water-mass signature. The analyses of the second leach indicate the presence of sources that are not evident from analysis of the fish debris oxide coatings and residues (chapter II). It is clear that these previously unconstrained sources are present in both sites to varying extents but with more significant influence at Site 1149, especially in the top portion of the core. Although it is likely that labile ash is responsible for the radiogenic signatures at both sites we cannot be prescriptive about the pathway of this "contamination." It is difficult to assign a pathway because it does not seem to be associated with aluminosilicate elements that would indicate aggressive over-leaching (chapter III). This signature must therefore originate from a reduction and porewater flux from within the sediment, or as from overprinting via reversible scavenging. This could be clarified via examining the REE patterns of related fish debris.

The extent to which the isotopic composition of water mass is overprinted depends on the 1) amount of time it is exposed to the additional inputs (i.e. the water mass flux determines the effect of the benthic flux on the provenance signature), 2) the concentration of the overprinting material in comparison to that of the bottom water, and 3) the difference in isotopic composition between the benthic flux and the original signature. Nd and Pb isotopic reconstructions must be informed and constrained by the lithology of the sediment and additional input sources that to the

water column. Regardless of the quantified overprinting the isotopic composition and corresponding REE patterns still convey primary provenance information about the circulation of water masses at that time.

4.6 Conclusions

Examining the leached phases from the perspective of elemental distributions, REE patterns, factor analysis and isotopic composition has allowed us to gain insight into the controls on elemental distributions in marine sediments at Sites 1149 and U1370. We identify five factors that explain 99% of the data at both sites and provide context for the distributions of REE patterns and the distribution of isotopic compositions. Overall the factor analysis for Site 1149 indicates a much more complicated separation of factors across the phases. At Site 1149 the first and second leach are explained in large part by the quasi-lithogenic factor but explained to a much smaller extent by the lithogenic factor. The most striking result is the radiogenic signature in the second leach, which at Site 1149 is controlled by the quasi-lithogenic factor which likely composed of volcanic ash.

Site U1370 has a similar isotopic composition distribution with a radiogenic second leach, which indicates there lithogenic component that is not as well resolved in the factor analysis as it is at Site 1149 contributing to the second leach. This portion of the sediment is not associated with elements found in aluminosilicate rocks, which means its origins must either be from a lithogenic composition in the bottom water either released via pore water flux or reverse scavenging of sinking particulates, or it is a component that has been altered with time, allowing the trace and REE elements to become disassociated with their aluminosilicate carriers.

However, at Site U1370 there is clear separation between the factors that control each phase, i.e. the lithogenic phases make up a very small portion of the first leach, and the portion of

the data explained by lithogenic influence increases in the second leach, and again in the residue which is dominated by lithogenic factors. In summary the Site U1370 evaluation indicated that analysis of the Nd and Pb isotopes of the leached oxide coatings from this site, and sites with similar compositions, are likely to isolate a seawater component that reflects quasi conservative mixing. However, the results of Site 1149 only raise more questions about the material extracted by the leach in a location with so much ash, and so many different sediment components. While these results limit the interpretations that we can make from sites like Site 1149 where there is consistent evidence of overprinting in the first leach, as long as the extent of overprinting is still controlled by exposure time Nd and Pb can potential be used to constrain changes in circulation in these regions.

4.8 References

Basak, Chandranath, and Ellen E Martin. 2013. "Antarctic weathering and carbonate compensation at the Eocene-Oligocene transition." *Nature Geoscience* 6 (2):121-124.

Broecker, WS, and TH Peng. 1982. "Tracers in the Sea, 690 pp." *Lamont-Doherty Geological Observatory, Palisades, NY*.

Bruland, K. W., R. Middag, and M. C. Lohan. 2014. "8.2 - Controls of Trace Metals in Seawater A2 - Holland, Heinrich D." In *Treatise on Geochemistry (Second Edition)*, edited by Karl K. Turekian, 19-51. Oxford: Elsevier.

Byrne, Robert H. 2002. "Inorganic speciation of dissolved elements in seawater: the influence of pH on concentration ratios." *Geochemical Transactions* 3:11-11. doi: 10.1186/1467-4866-3-11.

D'Hondt, Steven, Fumio Inagaki, Carlos Alvarez Zarikian, Nathalie Dubois, Tim Engelhardt, Helen Evans, Timothy Ferdelman, Britta Gribsholt, Robert N. Harris, Bryce W. Hoppie, Jung-Ho Hyun, Jens Kallmeyer, Jinwook Kim, Jill E. Lynch, Satoshi Mitsunobu, Yuki Morono, Richard W. Murray, Takaya Shimono, Fumito Shiraishi, Davic C. Smith, Christopher E. Smith-Duque, Arthur J. Spivack, Bjorn Olav Steinsbu, Yohei Suzuki, Michal Szpak, Laurent Toffin, Goichiro Uramoto, Yasuhiko T. Yamaguchi, Guo-Liang Zhang, Xiao-Hua Zhang, and Wiebke Ziebis. 2013. "IODP Expedition 329; Life and habitability beneath the seafloor of the South Pacific Gyre." *Scientific Drilling* 15:4.

Duce, Robert A., and Neil W. Tindale. 1991. "Atmospheric transport of iron and its deposition in the ocean." *Limnology and Oceanography* 36 (8):1715-1726. doi: doi:10.4319/lo.1991.36.8.1715.

Dunlea, Ann G., Richard W. Murray, Justine Sauvage, Robert A. Pockalny, Arthur J. Spivack, Robert N. Harris, and Steven D'Hondt. 2015. "Cobalt-based age models of pelagic clay in the South Pacific Gyre." *Geochemistry, Geophysics, Geosystems* 16 (8):2694-2710. doi: doi:10.1002/2015GC005892.

Dunlea, Ann G, Richard W Murray, Justine Sauvage, Arthur J Spivack, Robert N Harris, and Steven D'Hondt. 2015. "Dust, volcanic ash, and the evolution of the South Pacific Gyre through the Cenozoic." *Paleoceanography* 30 (8):1078-1099.

Frank, Martin. 2002. "Radiogenic isotopes: tracers of past ocean circulation and erosional input." *Reviews of geophysics* 40 (1).

Goldstein, S. L., and S. R. Hemming. 2003. "6.17 - Long-lived Isotopic Tracers in Oceanography, Paleoceanography, and Ice-sheet Dynamics A2 - Holland, Heinrich D." In *Treatise on Geochemistry*, edited by Karl K. Turekian, 453-489. Oxford: Pergamon.

Grousset, Francis E., and Pierre E. Biscaye. 2005. "Tracing dust sources and transport patterns using Sr, Nd and Pb isotopes." *Chemical Geology* 222 (3):149-167. doi: https://doi.org/10.1016/j.chemgeo.2005.05.006.

Gutjahr, Marcus, Martin Frank, Claudine H. Stirling, Veronika Klemm, Tina van de Flierdt, and Alex N. Halliday. 2007. "Reliable extraction of a deepwater trace metal isotope signal from Fe–Mn oxyhydroxide coatings of marine sediments." *Chemical Geology* 242 (3):351-370. doi: https://doi.org/10.1016/j.chemgeo.2007.03.021.

Haley, Brian A., Jianghui Du, April N. Abbott, and James McManus. 2017. "The Impact of Benthic Processes on Rare Earth Element and Neodymium Isotope Distributions in the Oceans." *Frontiers in Marine Science* 4 (426). doi: 10.3389/fmars.2017.00426.

Haley, Brian A., Gary P. Klinkhammer, and James McManus. 2004. "Rare earth elements in pore waters of marine sediments." *Geochimica et Cosmochimica Acta* 68 (6):1265-1279. doi: https://doi.org/10.1016/j.gca.2003.09.012.

Hein, James R., Kira Mizell, Andrea Koschinsky, and Tracey A. Conrad. 2013. "Deep-ocean mineral deposits as a source of critical metals for high- and green-technology applications: Comparison with land-based resources." *Ore Geology Reviews* 51:1-14. doi: https://doi.org/10.1016/j.oregeorev.2012.12.001.

Henderson, Gideon M., and Ernst Maier-Reimer. 2002. "Advection and removal of 210Pb and stable Pb isotopes in the oceans: a general circulation model study." *Geochimica et Cosmochimica Acta* 66 (2):257-272. doi: 10.1016/s0016-7037(01)00779-7.

Jones, Charles E., Alex N. Halliday, David K. Rea, and Robert M. Owen. 1994. "Neodymium isotopic variations in North Pacific modern silicate sediment and the insignificance of detrital REE contributions to seawater." *Earth and Planetary Science Letters* 127 (1):55-66. doi: https://doi.org/10.1016/0012-821X(94)90197-X.

Jones, Charles E., Alex N. Halliday, David K. Rea, and Robert M. Owen. 2000. "Eolian inputs of lead to the North Pacific." *Geochimica et Cosmochimica Acta* 64 (8):1405-1416. doi: https://doi.org/10.1016/S0016-7037(99)00439-1.

Koschinsky, Andrea, and James Hein. 2003. *Uptake of elements from seawater by ferromanganese crusts: Solid-phase associations and seawater speciation*. Vol. 198.

Lugmair, GW, and SJG Galer. 1992. "Age and isotopic relationships among the angrites Lewis Cliff 86010 and Angra dos Reis." *Geochimica et Cosmochimica Acta* 56 (4):1673-1694.

Martin, E. E., and B. A. Haley. 2000. "Fossil fish teeth as proxies for seawater Sr and Nd isotopes." *Geochimica et Cosmochimica Acta* 64 (5):835-847. doi: https://doi.org/10.1016/S0016-7037(99)00376-2.

Murray, Richard W., Marilyn R. Buchholtz Ten Brink, David C. Gerlach, G. Price Russ, and David L. Jones. 1991. "Rare earth, major, and trace elements in chert from the Franciscan Complex and Monterey Group, California: Assessing REE sources to fine-grained marine sediments." *Geochimica et Cosmochimica Acta* 55 (7):1875-1895. doi: https://doi.org/10.1016/0016-7037(91)90030-9.

Pisias, Nicklas G., Richard W. Murray, and Rachel P. Scudder. 2013. "Multivariate statistical analysis and partitioning of sedimentary geochemical data sets: General principles and specific MATLAB scripts." *Geochemistry, Geophysics, Geosystems* 14 (10):4015-4020. doi: doi:10.1002/ggge.20247.

Plank, Terry, John N. Ludden, Carlota Escutia, Lewis Abrams, Jeffrey C. Alt, Robin N. Armstrong, Samantha Barr, Annachiara Bartolini, Graeme Cairns, Martin R. Fisk, Gilles Guèrin, Shelley A. Haveman, Tetsuro Hirono, José Honnorez, Katherine A. Kelley, Roger L. Larson, Francesca M. Lozar, Richard W. Murray, Thomas K. Pletsch, Robert A. Pockalny, Olivier Rouxel, Angelika Schmidt, David C. Smith, Arthur J. Spivack, Hubert Staudigel, Maureen B. Steiner, and Robert B. Valentine. 2000. "Leg 185 summary; inputs to the Izu-Mariana subduction system." *Proceedings of the Ocean Drilling Program, initial reports, Izu-Mariana Margin; covering Leg 185 of the cruises of the drilling vessel JOIDES Resolution, Hong Kong, People's Republic of China, to Yokohama, Japan, sites 801 and 1149, 12 April-14 June 1999* 185:1.

Plank, Terry, John N. Ludden, Carlota Escutia, Lewis Abrams, Jeffrey C. Alt, Robin N. Armstrong, Samantha Barr, Annachiara Bartolini, Graeme Cairns, Martin R. Fisk, Gilles Guèrin, Shelley A. Haveman, Tetsuro Hirono, José Honnorez, Katherine A. Kelley, Roger L. Larson, Francesca M. Lozar, Richard W. Murray, Thomas K. Pletsch, Robert A. Pockalny, Olivier Rouxel, Angelika Schmidt, David C. Smith, Arthur J. Spivack, Hubert

Staudigel, Maureen B. Steiner, and Robert B. Valentine. 2000. "Site 1149." *Proceedings of the Ocean Drilling Program, initial reports, Izu-Mariana Margin; covering Leg 185 of the cruises of the drilling vessel JOIDES Resolution, Hong Kong, People's Republic of China, to Yokohama, Japan, sites 801 and 1149, 12 April-14 June 1999* 185:190.

Scudder, Rachel P., Richard W. Murray, Julie C. Schindlbeck, Steffen Kutterolf, Folkmar Hauff, and Claire C. McKinley. 2014. "Regional-scale input of dispersed and discrete volcanic ash to the Izu-Bonin and Mariana subduction zones." *Geochemistry, Geophysics, Geosystems* 15 (11):4369-4379. doi: 10.1002/2014GC005561.

Tachikawa, K., V. Athias, and C. Jeandel. 2003. "Neodymium budget in the modern ocean and paleo-oceanographic implications." *Journal of Geophysical Research: Oceans* 108 (C8):n/a-n/a. doi: 10.1029/1999JC000285.

Thomas, Deborah J, Robert Korty, Matthew Huber, Jessica A Schubert, and Brian Haines. 2014. "Nd isotopic structure of the Pacific Ocean 70–30 Ma and numerical evidence for vigorous ocean circulation and ocean heat transport in a greenhouse world." *Paleoceanography* 29 (5):454-469.

Wilson, David J, Alexander M Piotrowski, Albert Galy, and Josephine A Clegg. 2013. "Reactivity of neodymium carriers in deep sea sediments: Implications for boundary exchange and paleoceanography." *Geochimica et Cosmochimica Acta* 109:197-221.

Wilson, David J., Tina van de Flierdt, and Jess F. Adkins. 2017. "Lead isotopes in deep-sea coral skeletons: Ground-truthing and a first deglacial Southern Ocean record." *Geochimica et Cosmochimica Acta* 204:350-374. doi: https://doi.org/10.1016/j.gca.2017.01.052.

5. CONCLUSIONS

The goal of this dissertation is to assess the foundation of using Pb and Nd as radiogenic isotope tracers: 1) The dominant source of dissolved Nd and Pb to the oceans is presumed to be fluvial inputs; 2) Other sources of Nd and Pb to the oceans have been presumed negligible; 3) The isotopic composition of the fluvial inputs reflects the regional geology drained by those fluvial systems – hence there is a relationship to provenance; 4) Both have short residence times in the oceans; 5) Several sedimentary phases record and retain the composition of the dissolved Nd and Pb at the seafloor. In the introduction we identified the recent advances in the knowledge of Nd and Pb systematics, and how we hoped to use our study to further the state of the understanding of Nd as a proxy.

Chapter II presented the interpretation of new Nd isotope data suggesting that the Nd isotopic composition of the South Pacific evolved very little over the time interval 70 to 15ma. The new data confirmed a southern source of deep-water recorded in the Pacific sector of the Southern Ocean prior to the opening of the Drake Passage (40Ma). The new data also identified an increase in the isotopic composition in the North Pacific from 35 to 25Ma. We interpret the higher (more radiogenic) isotopic composition as a diminished rate of water-mass movement in the region. However, this interpretation is not unique and the potential contributions of other sources of Nd to the dissolved inventory highlight the problem with the premises 1 and 4 outlined above. These questions about Nd at the seafloor inspired the next study.

Chapter III explored the reproducibility of the leaching method in order to establish the reliability of the leaching procedure. We identified the reproducibility of the elemental and isotopic analysis generated with sequential leaching of a standard reference material USGS

MAG-1, and INTL-STD-A, which is an in-house internal standard from the Atlantic Ocean. The first leach of MAG-1 has the lowest overall reproducibility for both elemental and isotopic data. This is consistent with the findings in Kyrc et al., (2006), who identified MAG-1 as the best standard for evaluation of leaching procedures. MAG-1 is a clayey mud with low carbonate content; therefore, this finding bodes well for the use of our leaching procedure on pelagic clay for paleoreconstructions.

We also explored the fidelity of the leaching procedure by analyzing the major, trace and rare earth elements of Sites 1149 and U1370 in order to identify potential phases within the seafloor sediments might contribute dissolved Nd to the seafloor or the pore waters, and to evaluate premise 5. We identified rare earth patterns depleted with respect to PAAS in the top 100 meters of Site 1149, and sporadically within Site U1370. This raises questions about the source of this lithogenic pattern because there is no evidence from the major elements often associated with aluminosilicates, like dust or ash, were extracted into the leach phases. This raises questions about the source of this lithogenic pattern because there is no evidence from the major elements often associated with aluminosilicates like dust or ash was extracted into the leach phases.

Chapter IV explored the remaining outstanding question of what could have imparted the PAAS depleted REE patterns without corresponding aluminosilicate elements. Substantial inputs of either in the form of a “benthic flux” or leach “contamination” would challenge the presumption of characteristics 1,2, and 4 listed above, and impact the viability of Nd (and Pb) as tracers of ancient water mass composition. We examined the elemental concentration and isotopic analyses of the two leaches and residual detritus from Sites 1149 and U1370 to identify potential sources and controls on the dissolved Nd and Pb recorded at the two sites. In order to

constrain the origin of the PAAS depleted REE patterns we examine the chemical populations indicated by the major, trace and REE, as well as the results of the Q-mode Factor analysis. We identified that there is a source to the leaches, especially in the second leach, which is not an intermediate between the residue and seawater composition. The second leach has the most radiogenic signature, indicating that it is composed of a source that is distinct. We identify five factors in each site that explain 99% of the data. The factor analysis reveals that the sources that explain the data are present in each of the three phases and confirms the influence of a second lithogenic signature at Site 1149, specifically one that dominates in the top 100mbsf.

A continuing theme of this work is the presence of a radiogenic source to the North Pacific that influences the REE distribution and isotopic composition of the leaches. There is a readily reducible source in the Northwest Pacific that is an important portion of the sediment that must be accounted for in paleoceanographic interpretations from the region. The geochemical results from the South Pacific indicate that the Nd, Pb and the REE elements in the region represent a signature dominantly and consistently derived from seawater. We establish that there are locations and circumstances in which either the sedimentary phases do not record and retain the composition of the dissolved Nd and Pb at the seafloor or that the dominant source of dissolved Nd and Pb to the oceans is not fluvial inputs. However, we also establish that there are locations and circumstances where the conditions of Nd and Pb to function as tracers are met, and paleoceanographic interpretations are possible.

APENDIX A:

SITE DESCRIPTIONS AND AGE MODELS

Site 464

Deep Sea Drilling Program (DSDP) Site 464 was drilled on the Northern Hess Rise (Modern Location: 39.8607, 173.889 (Paleo-location at 50 Ma: 27.88, -149.24) at a water depth of 4670 m and a paleo-water depth ~4000m. The study interval was recovered in cores 5 and 6 (45.4-36.0 mbsf) and consists of siliceous clay at the very top (until 36.1 mbsf) and transitions to brown clay for the rest of the interval. Unfortunately, the entire section lacks biostratigraphic age control (*Thide et al*., 1981). Three age datums have previously been identified and employed to constrain the ages on samples from Site 464: The shipboard party assigned age of 75 Ma at the base of the brown clay at the bottom of Core 10, 89.00 mbsf (Thiede et al., 1981), an intermediate point based on the most precisely identified icthyolith age available (55.80 Ma, 50.00 mbsf), and the last occurrence (LO) of *S. pentas* (2.8 Ma, 32.0 mbsf) (*Hague et al*., 2012). A constant sedimentation rate of .38 m/my is assumed between 9.05 Ma and 55.96 Ma, and 2.04 m/my between 55.96 and 75.00 Ma. These accumulation rates yield ages that are consistent with the qualitative ichtyolith ages provided by *Doyle & Riedel* (1981)

Site 1209

ODP Site 1209, is in the Northwest Pacific in the central part of the southern high of Shatsky Rise (Modern Location: 32.65, 158.5 Paleo-location at 50 Ma: 23.24,-164.71) at a water depth of 2398.3 m and a paleo-water depth of ~2000 m. The study interval was recovered in cores 12 and 13 (104.9-114.44 mbsf). The cores consist of clayey nannofossil ooze and nannofossil ooze with clay until 111.2 mbsf (within section 12-6). At this interval there is a major lower Miocene/upper Oligocene unconformity, which is marked by a transition to

primarily nannofossil ooze. The ages detailed in *Bralower* (2005) have been updated with numerical ages from *Gradstein et al.* (2012). 2

Site 596

DSDP Site 596 is in the Southwest Pacific Ocean (Modern Location: -23.85,-167.65 Paleo-location at 50 Ma: -37.35,-138.72) at a water depth of 5614 m, and a paleo-water depth of ~5000m. The study interval was recovered in core 2 (5.9 – 14.0 mbsf) and consists of a reddish zeolitic clay until 10.2 mbsf and transitions to a metalliferous pelagic clay. The entire section lacks biostratigraphically useful microfossils (*Winfrey et al*., 1987). A "constant" Co accumulation age model is applied to assign numeric ages to the sediment intervals (*Zhou & Kyte*, 1992). As the age model is tied to the iridium peak at the K/T boundary, we updated the numeric ages by adjusting the K/T age to the new GTS 2012 value.

Site U1370

IODP Site U1370, is in the South Pacific Ocean (Modern Location: -41.85,-153.105, Paleo-location at 50 Ma: -55.97,-122.38) at a water depth of 5084.7 m and a paleo-water depth of ~5000 m. The study interval was recovered in cores 2-4 (~10-30 mbsf) and consists of metalliferous zeolitic pelagic clay and metalliferous clay. There is a short interval (2.9 m) of nannofossil ooze at 62 mbsf which contains planktonic foraminifers and calcareous nannofossils. A Co based age model, with a lower age constraint at the K-Pg boundary is used to model ages (Dunlea et al., 2015).